Glass-Ceramic Sealant Reinforcement for High-Temperature Applications

Beatriz Cela Greven

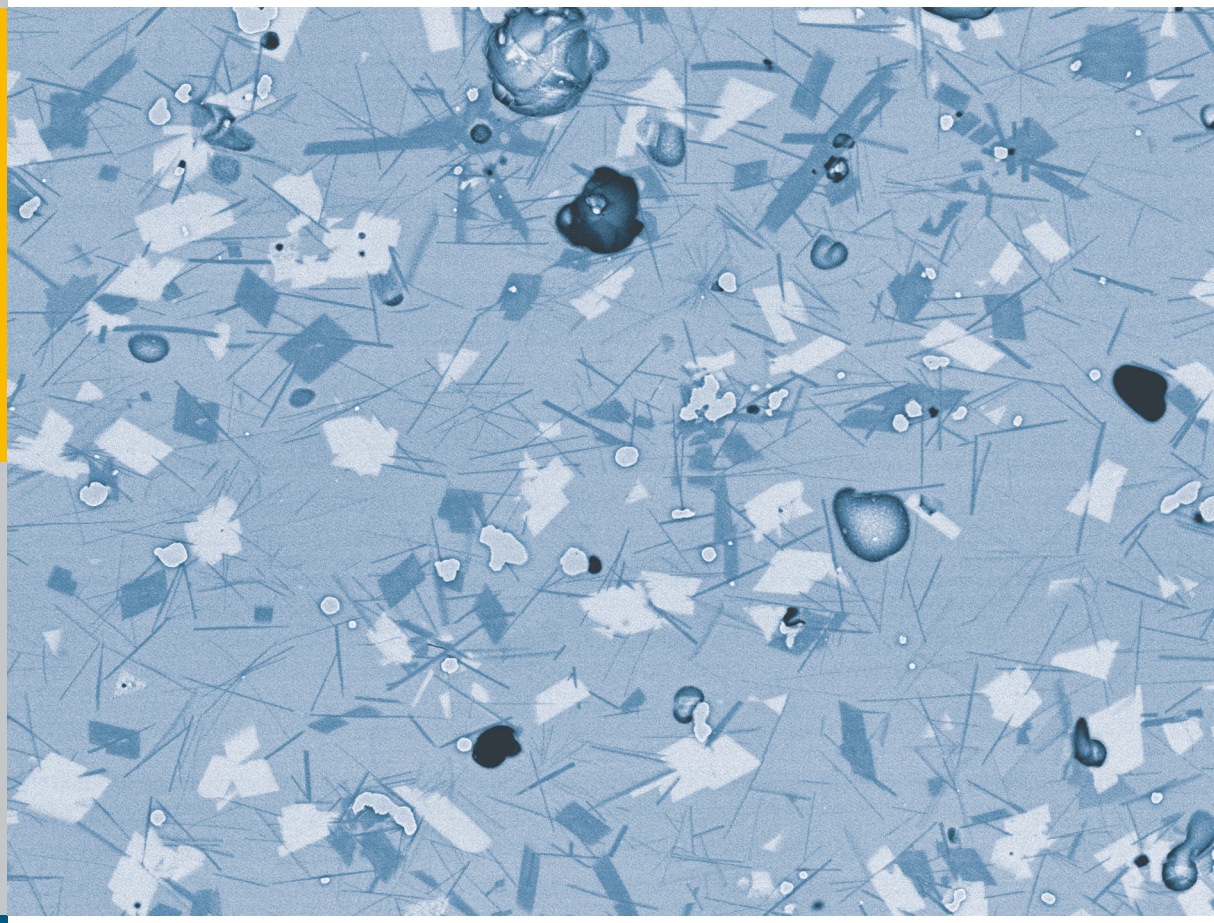

Energie & Umwelt / Energy & Environment
Band / Volume 255
ISBN 978-3-95806-042-5

JÜLICH
FORSCHUNGSZENTRUM

Schriften des Forschungszentrums Jülich
Reihe Energie & Umwelt / Energy & Environment Band / Volume 255

Forschungszentrum Jülich GmbH
Central Institute for Engineering, Electronics and Analytics (ZEA)
Engineering and Technology (ZEA-1)

Glass-Ceramic Sealant Reinforcement for High-Temperature Applications

Beatriz Cela Greven

Schriften des Forschungszentrums Jülich
Reihe Energie & Umwelt / Energy & Environment Band / Volume 255

ISSN 1866-1793 ISBN 978-3-95806-042-5

Bibliografische Information der Deutschen Nationalbibliothek.
Die Deutsche Nationalbibliothek verzeichnet diese Publikation in der
Deutschen Nationalbibliografie; detaillierte Bibliografische Daten
sind im Internet über http://dnb.d-nb.de abrufbar.

Herausgeber und Vertrieb:	Forschungszentrum Jülich GmbH Zentralbibliothek, Verlag 52425 Jülich Tel.: +49 2461 61-5368 Fax: +49 2461 61-6103 E-Mail: zb-publikation@fz-juelich.de www.fz-juelich.de/zb
Umschlaggestaltung:	Grafische Medien, Forschungszentrum Jülich GmbH
Druck:	Grafische Medien, Forschungszentrum Jülich GmbH
Copyright:	Forschungszentrum Jülich 2015

Schriften des Forschungszentrums Jülich
Reihe Energie & Umwelt / Energy & Environment, Band / Volume 255

D 82 (Diss. RWTH Aachen University, 2014)

ISSN 1866-1793
ISBN 978-3-95806-042-5

The complete volume is freely available on the Internet on the Jülicher Open Access Server (JuSER)
at www.fz-juelich.de/zb/openaccess.

Acknowledgement

Apart from the efforts of myself, the success of any project depends largely on the encouragement and guidelines of many others. I take this opportunity to express my gratitude to the people who have been instrumental in the successful completion of this PhD thesis. I would like to express my thanks to my advisor Professor Dr. Reinhard Conradt, who encouraged me on this research and supported my ideas. I would also like to thank Professor Dr. Uwe Reisgen for all the corrections and suggestions that he gave on my thesis. I would especially like to thank Dr. Sonja Groß-Barsnick for being my supervisor at the Forschungszentrum Jülich, whose selfless time and care were sometimes all that kept me going. Without her encouragement and guidance this PhD work would not have materialized. The guidance and support received from all the colleagues from the Central Institute for Engineering, Electronics and Analytics (ZEA-1) at Forschungszentrum Jülich in special my colleagues Arnold Cramer, Dr. Dietrich Faidel, Matthias Bellartz, Ruth Göddertz, Klaus Watermeyer, Kai Fisher, Thomas Koppitz, Dirk Federmann, Dr. Peter Batfasky, Dr. Wilfried Behr, and Dr. Joseph Remmel, whose contribution were vital for the success of this work. I am grateful for their constant support and help. An extra thank for Dr. Dietrich Faidel that made my life much easier giving me a ride nearly every day to work during 3 years.

My sincere appreciation and thank to Dr. Federico Smeacetto, Dr. Andrea Ventrella and Professor Dr. Monica Ferraris from the Politecnico di Torino in Italy, who collaborated with knowledge and time performing important experiments which the results were used in this work.

A special thanks to my parents Cesar Miguel Cela and Vânia V. B. Cela, and my sisters Mariana Cela and Jéssica Cela, who let me go in the direction of my dreams. Their motivation inspired me to never give up. Thank you for all the support and help even from far away and for the recreating summer vacations we spent together during my doctorate time. I would like to express my appreciation for all the help given by my parents-in-law Ingrid and Kurt Greven, who many times made me feel a little bit less homesick. And last but not least I would also like to thank my beloved husband Andreas Greven who spent sleepless nights with me and was always my support in the moments when there was no one to answer my queries.

Abstract

In the development of solid oxide fuel cells, the components most in need of improvement are still the sealants. Over the last decade, several types of sealants have been investigated for use under high temperatures, such as compressive, compliant, and rigidly bonded seals. Of these three types, rigidly bonded glass-ceramic seals are the most promising. Their properties can be tailored to match the requirements of SOFC sealants. These include the coefficient of thermal expansion, joining temperature, crystallization behavior, electrical insulation, and gas-tightness. Nevertheless, in the past, the developed sealant compositions failed to demonstrate sufficient mechanical strength. This property is extremely important to avoid catastrophic failure of the rigid seals during SOFC operation. Additionally, there is a lack of standardized methods to characterize the mechanical strength of joined components in the research community. This makes it difficult to rely on the results of the state of art measurements, to reproduce them, and indeed to compare them.

In order to improve the mechanical strength of glass-ceramic sealants, this work proposes reinforcing the glass-ceramic sealant with different metallic and ceramic particles. A new concept of laminate sealant, known as a multilayer design, was developed in an attempt to combine the properties of two types of composites in one joint. In addition, three possible methods for mechanical strength characterization were developed.

The reinforcement concept is mainly based on adding fillers to the glass matrix named “87”, which is a composition from the system BaO-CaO-SiO_2. The chosen fillers were metallic particles including nickel (Ni), nickel-chromium (NiCr) (80-20), copper (Cu), and silver (Ag), as well as ceramic fillers such as gadolinium-doped ceria (CGO) particles and yttrium-stabilized zirconia (YSZ) particles or fibers. These materials were tested in different weight concentrations in the glass matrix to form the composites. This approach showed that adding filler materials (metallic or ceramic) improved the mechanical strength values. The multilayer design was also proven to be effective in combining the properties of two different composite layers in one joint. Electrically insulating samples with sufficient mechanical strength were produced with single layers of reinforced sealant as well as with the multilayer approach.

In developing the mechanical strength test, three types of measurements were investigated: tensile test, shear bond test, and torsion test. The first two tests were developed in-house and the third test was performed within a bilateral cooperation with Politecnico di Torino in Italy. The torsion test obtained the most reliable and reproducible results for the joined samples. The values for shear strength obtained by this method were close to what was expected according to theory and computer simulations. The torsion test method was therefore deemed the most appropriate mechanical strength test for this purpose.

The analysis performed in this work indicated that the combination glass 87 and 20 wt.-% Ni fulfilled the requirements for SOFC sealants. The samples made with this composite sealant exhibited the highest shear strength values, and they remained gas-tight and electrically insulating after 500 h at 800 °C.

Kurzfassung

In der Entwicklung von Hochtemperatur-Feststoffbrennstoffzellen sind die Dichtungen nach wie vor jene Komponenten, die der meisten Verbesserungen bedürfen. Verschiedene Arten von Dichtungen wurden im vergangenen Jahrzehnt untersucht, so auch druckfeste, nachgiebige und starre Dichtungen. Die starr verbundenen Glaskeramik-Dichtungen erwiesen sich als die Vielversprechendste der drei Varianten. Deren Eigenschaften können kontrolliert an die Anforderungen für Feststoffbrennstoffzellen-Dichtungen angepasst werden. Explizit gemeint ist die thermische Ausdehnung, die Fügetemperatur, die Kristallisationsverhalten, die elektrische Isolation und die Gasdichtigkeit. Dennoch haben die bis heute entwickelten Zusammensetzungen der Dichtmittel keine ausreichend gute mechanische Festigkeit. Diese Eigenschaft ist von hoher großer Bedeutung um das fatale Versagen der starren Dichtungen während des Betriebs der Feststoffbrennstoffzelle zu vermeiden. Zusätzlich mangelt es an standardisierten Verfahren, die mechanische Festigkeit von Verbindungen zu charakterisieren. Dadurch ist es schwierig, sich auf vergleichbare Resultate der aktuellen Technik zuverlässig zu stützen, diese zu reproduzieren oder zu vergleichen.

Es konnte gezeigt werden, dass durch verschiedene metallische und keramische Füllstoffe die glaskeramische Dichtung im Hinblick auf die mechanische Festigkeit verstärkt werden konnte. Ein neues Konzept einer laminar aufgebauten Dichtung, welche hier als Mehrschicht-Design bezeichnet wird, wurde als konzeptioneller Ansatz entwickelt, um die Eigenschaften von zwei verschiedenen Verbundwerkstoffen in einer Verbindung zu kombinieren. Zusätzlich wurden drei mögliche Verfahren entwickelt, die mechanische Festigkeit zu charakterisieren und zu bewerten. Alle erwiesen sich als eine neue und verbesserte Methodik zum Test von Materialverbunden.

Das Konzept zur Verstärkung von Glasloten basiert im Wesentlichen auf dem Hinzufügen von Füllstoffen in eine Glasmatrix „87“ aus dem System $BaO\text{-}CaO\text{-}SiO_2$. Die ausgewählten Füllstoffe waren die metallischen Partikel Nickel (Ni), Nickel-Chrom (NiCr) (80-20), Kupfer (Cu) und Silber (Ag), sowie die keramischen Füllstoffe Gadolinium-dotiertes Ceroxid (CGO) und Yttrium-stabilisierte Zirkoniumdioxid (YSZ) als Partikel oder Fasern. Diese Materialien wurden in verschiedenen Anteilen der Glasmatrix zugesetzt. Es konnte gezeigt werden, dass durch die Zugabe von

metallischen oder keramischen Füllstoffen die mechanischen Festigkeiten verbessert werden konnten. Das mehrschichtige Design hat sich ebenso als effektiv erwiesen, um die Eigenschaften von zwei verschiedenen Kompositen in einer Fügeverbindung zu kombinieren. Elektrisch isolierende Materialproben mit ausreichend mechanischer Festigkeit konnten sowohl durch die einschichtige Dichtung als auch durch das mehrschichtige Design produziert werden.

Im Rahmen der Entwicklung von Testverfahren zur mechanischen Festigkeit wurden Zugbelastung, Scherhaftung und Torsionsbelastung geprüft. Die ersten beiden Verfahren konnten hausintern untersucht werden, das dritte Verfahren war durch eine bilaterale Kooperation mit der Politecnico di Torino möglich. Der Torsionstest erwies sich als die zuverlässigste und reproduzierbarste Methode im Vergleich zu den anderen geprüften Verfahren. Die auf diese Weise ermittelten Werte kamen denjenigen am nächsten, welche theoretisch zu erwarten waren oder aus Computersimulationen für Scherfestigkeit hervorgingen. Der Torisonstest zeigt sich zu diesem Zeitpunkt als das am besten geeignete Verfahren zur Prüfung der mechanischen Festigkeit für diesen Verwendungszweck.

Die in dieser Arbeit erstellte Analyse bezeugt, dass die Kombination aus Glassmatrix 87 und 20 wt.-% Ni alle Anforderungen als Dichtmittel für Feststoffbrennstoffzellen erfüllt. Die mit diesem zusammengesetzten Glaslot erstellten Proben zeigten die höchsten Scherfestigkeit-Werte und verblieben auch nach 500 h gasdicht und elektrisch isolierend.

Contents

1. Introduction 1
2. State of art of sealants for high-temperature applications 4
2.1. Sealants for high-temperature applications 6
2.2. Sealing materials for solid oxide fuel cells 8
3. Strength of sealing materials 13
4. Reinforcement of glass-ceramic sealants by filler materials 16
4.1. Filler material influence on viscosity and CTE of sealant 21
4.2. Composite sealants for SOFC applications 22
4.3. State of art of strength evaluation of glass sealants 23
4.3.1. Testing of shear strength 29
4.3.2. Micro-mechanical testing 32
4.3.3. Bending test 33
4.3.4. Creep test 34
4.3.5. Testing of tensile strength 35
5. Experimental 39
5.1. Chemical analysis 40
5.2. Measurement of viscous behaviour by hot stage microscopy (HSM) 41
5.3. Dilatometry 45
5.4. Joining tests 46
5.5. Gas tightness test 47
5.6. Four-point electrical resistance measurement 48
5.7. Glass paste and application methods 50
5.7.1. Rheological testing 52
5.8. Glass-ceramic sealant reinforcement 53
5.9. Multilayer concept 55
5.10. Strength measurements 56
5.10.1. Tensile strength 56
5.10.2. In-house shear test set-up development 58
5.10.3. Torsion test developed by Politecnico di Torino 59
6. Results and discussion 62

6.1. Alternative filler reinforcement evaluation 62
6.1.1. Feasibility investigation 62
6.2. Joining test 76
6.3. Electrical resistance measurements of composites 76
6.4. Strength evaluation 78
6.4.1. Tensile strength 79
6.4.2. In-house developed shear test 81
6.4.3. Torsion test 83
6.5. Multilayer sealant design 86
6.5.1. Joining tests 87
6.5.2. Electrical resistance measurement 95
6.5.3. Tensile strength 96
6.5.4. Glass 104 97
7. Summary 102
8. Appendices 104
9. References 105

List of symbols and abbreviations

A	Area ..... m²
ASR	Area specific resistance ..... Ω·cm²
BCS	Barium calcium silicate, $BaO\text{-}CaO\text{-}SiO_2$
CGO	Gadolinium-doped ceria
CSR	Controlled shear rate
CTE	Coefficient of thermal expansion ..... ppm/K
DISMIC	Dep. of Material Science and Chem. Engineering, Politecnico di Torino
E	Elastic modulus ..... G·Pa
EDS	Energy dispersive spectroscopy
EOM	Emulsion over mesh
F	Force ..... N
F10	FZJ SOFC stack design with 100 cm² area cells
FZJ	Forschungszentrum Jülich GmbH
GHI	Institut für Gesteinshüttenkunde, RWTH-Aachen
H	Hardness ..... G·Pa
HSM	Hot Stage Microscopy
I	Electrical current ..... A
ICP-OES	Inductively coupled plasma - optical emission spectrometry
ID	Identity
IEK-1	Institut for energy and climate research at Forschungszentrum Jülich
IWM	Fraunhofer-Institut für Werkstoffmechanik Freiburg
K*i*	Bulk compression modulus of the component *i* of a composite
K_{IC}	Fracture toughness ..... $MPa \cdot m^{0.5}$
mol %	Mol percent
NAS	Sodium aluminosilicate system
P	Power ..... W
p	Pressure or pressure variation ..... mbar
PO	Pre-oxidation treatment
q_L	Leakage rate ..... $mbar \cdot l \cdot s^{-1}$
R	Electrical resistance ..... Ω·cm²

RT	Room temperature
RWTH	Rheinisch-Westfälische Technische Hochschule
SEM	Scanning electronic microscopy
SOFC	Solid Oxide Fuel Cell
T_{DF}	Deformation temperature ….....°C
T_F	Flow temperature …….....°C
T_{FS}	First shrinkage temperature …..... °C
Tg	Glass transition temperature ..... °C, K
T_{HB}	Temperature at half ball …….....°C
T_{MS}	Maximum shrinkage temperature ..... °C
T_S	Temperature at sphere …….....°C
U	Voltage V
V	Volume or volume variation l
vol.%	Volume percent
wt.-%	Weight percent
yi	Weight fraction of the component *i* of a composite ..... g
YSZ	Yttrium-stabilized Zirconia
ZEA-1	Central institute of engineering and technology at FZJ
ZEA-3	Institute for Analytics at FZJ
α_{comp}	Calculated CTE of the composite by the simple mixing rules
α_{glass}	CTE of a glass ..... ppm/K
αi	CTE of the component *i* of a composite ..... ppm/K
α_{Ni}	CTE of nickel ..... ppm/K
Δt	Time period ..... s
ΔT	Temperature interval
ρi	Density of the component *i* of a composite ..... kg/m³
η	Viscosity ..... dPa·s

List of Figures

Fig. 1 Schematic presentation of a repeating unit of a planar SOFC with a rigid glass-ceramic seal [Buc 2010] 1

Fig. 2 The evolution of engineering materials with time [Ash 1992] 5

Fig. 3 Overview of the current sealing types for high-temperature applications [Buc 2010] 7

Fig. 4 Fracture surface of as-received Crofer22APU sealed with a glass. (A) Low magnification and (B) high magnification of the circled area in (A) show the microcracked chromate [Cho 2010] 11

Fig. 5 Typical maximum strength of glasses 13

Fig. 6 Comparison of leakage rates of dummy and real stack tests performed with gas flow resulted in sealant failure [Blu 2010] 15

Fig. 7 Ashby charts of strength vs. toughness of materials [http://www-materials.eng.cam.ac.uk/mpsite/interactive_charts/strength-toughness/NS6Chart.html] 16

Fig. 8 Ashby charts of fracture toughness vs. Young's modulus [http://grantadesign.com/ashbycharts.htm] 18

Fig. 9 Ashby charts of thermal expansion vs. thermal conductivity [http://grantadesign.com/ashbycharts.htm] 19

Fig. 10 Simple shear test specimen [Sch 2002b] 29

Fig. 11 Special shear specimen developed for the testing of glass sealants [Mal 2007] 30

Fig. 12 Work principle of shear test with: a) laser joined test sample; b) furnace joined sample [Fai 2012] 31

Fig. 13 Joint specimen for shear test, dimensions in mm [Lin 2012] 32

Fig. 14 Head-to-head specimen geometry [Mal 2012b] 34

Fig. 15 Sample tested at 800 °C with 43 % strain in comparison with a non-tested sample [Liu 2011] 35

Fig. 16 Joined samples in the tensile strength measurement set-up [Sch 2002b] 36

Fig. 17 Tensile strength measurement set-ups used by different groups to evaluate the glass sealants for SOFC [Sme 2008b]; [Lin 2012]; [Cho 2008a].....38

Fig. 18 Geometric shape corresponding to each fixed viscosity point [Pas 2001]; [Pas 2005]; [DIN 1984]; [DIN 1998].....43

Fig. 19 Preparation of the samples for dilatometry measurement: a) pressed samples sintered in waved platinum foil; b) after sintering the glass bar is deformed; c) to obtain a precise measurement the sintered bars need to be reshaped by cutting and polishing to obtain 25 mm length, 6 mm diameter and parallel extremities 45

Fig. 20 a) Sandwich sample formed of two Crofer22APU plates of 50 x 50 mm^2 dimension joined by glass-ceramic sealant. b) Schematic view of a sandwich sample open with the applied sealant.....47

Fig. 21 Schematic drawing of sandwich sample prepared for the four-point electrical resistance measurement with spot welded platinum wires 48

Fig. 22 Sintered bar sample prepared with silver paste and platinum wires for the four-point electrical resistance measurement.....48

Fig. 23 Diagram of an electrical circuit of one solid oxide cell.....49

Fig. 24 Glass sealant application methods: a) robot dispenser; b) screen printing 51

Fig. 25 Schematic draw of plate-plate viscosity measuring system. R is the radius of the measuring plate and h is the gap between the upper and lower measuring plate 52

Fig. 26 Thermal expansion coefficient of CeO_2, GDC10 (CGO with 10 mol% Gd) and GDC20 (CGO with 20 mol% Gd) [Hay 2000] 54

Fig. 27 Multilayer sealant designs.....55

Fig. 28 Tensile strength test: a) measurement set-up with adaptors and specimen assembled in universal machine; b) tested butt-joint open sample.....57

Fig. 29 Principle of shear test: a) Schematic draw from joint shear test; b) Shear test machine in the start of a measurement, wedge touching the sample to be measured.....58

Fig. 30 Torsion machine set up: a) general view; b) details on the sample holder [Fer 2012a] 59

Fig. 31 Samples holder and printed miniature hourglass shaped samples. a) templates, samples holder and joining pieces; b) lower part of the samples holder with printed half-samples.....61

Fig. 32 First feasibility investigation analyzing the interface between sintered pressed pellets of the composites and Crofer22APU substrates.....62

Fig. 33 SEM image of: a) pure glass 87; and b) glass 87 with 5 wt.-% Cu 63

Fig. 34 Glass 87 with 25 wt.-% Cu filler a) microstructure overview; and b) detailed microstructure showing different crystalline phases, marked points analysed by EDS 63

Fig. 35 Microstructure of glass 87-Ni composites as joined. Filler in wt.-% from a to f: 0, 1, 5, 25, 50 and 75.....65

Fig. 36 a) Thickness of oxide layer formed around the nickel particles in the 5 wt.-% Ni composite; measured by EDS line scan 66

Fig. 36 b) Thickness of oxide layer formed around the nickel particles in the 25 wt.-% Ni composite; measured by EDS line scan 67

Fig. 36 c) Thickness of oxide layer formed around the nickel particles in the 50 wt.-% Ni composite; measured by EDS line scan 68

Fig. 37 SEM image of glass 87 with 20 wt.-% NiCr added to glass 87 matrix: a) bulk sealant in the center of the sample cross section; b) outer part of the sealant, interface with air, with the formation of barium chromate (light gray).....69

Fig. 38 SEM image of highly crystallized composite sample thermally treated at 850 °C for 10 h, composed of glass 87 with 20 wt.-% Montmorillonite 70

Fig. 39 Good dispersion of 20 wt.-% CGO particles in glass matrix 87. No interface or reaction zone formed between the filler and glass.....71

Fig. 40 Shadow images at 850 °C of pure gass 87 and glass matrix 87 with the corresponding filler additions in Crofer22APU substrate.....74

Fig. 41 Hot-stage microscopy results of area transformation and sintering ΔT of each composite: a) pure glass 87 and composites of glass 87 with ceramic fillers; b) pure glass 87 and composites of glass 87 with metallic fillers 75

Fig. 42 Four-point electrical resistance measured in bar-shaped samples. Similar conductivity behavior was found for the samples containing nickel and the annealed pure glass matrix 77

Fig. 43 Butt-joint samples with increased metal thickness led to better significant strength results due to decreased bending during the test 80

Fig. 44 Shear test of joined samples: a) four samples joined in the same 50 x 50 mm² plate; b) single sample set-up 82

Fig. 45 Shear strength results attained with the first sample concept (Fig. 44a). The variation in shear strength could be the result of pre-damage caused by sample A to sample B, C, or D 83

Fig. 46 Shear strength low-high-close chart of as-joined composite-to-steel torsion test. Composites made of glass 87 and filler additives in wt.-% 85

Fig. 47 Shear strength low-high-close chart of annealed composite-to-steel torsion test. Composites made of glass 87 and filler additives in wt.-% 86

Fig. 48 Double-layered sandwich samples as joined: a) upper layer filled with YSZ fibers (low porosity) and lower layer with Ag particles; b) upper layer filled with Ag particles and lower layer with YSZ particles (high porosity).....88

Fig. 49 Triple-layered sandwich samples with inner layer reinforced with silver particles, and outer layers filled with: a) YSZ fibers; b) YSZ particles (high porosity); c) pure glass 89

Fig. 50 Triple-layered sandwich samples with outer layers reinforced with silver particles, and inner layer filled with: a) YSZ fibers; b) YSZ particles; c) pure glass 90

Fig. 51 Nanoparticles of silver were encountered in a layer of pure glass in the multilayer design of pure glass/glass with 20 wt.-% Ag/pure glass. The Ag particles migrated from the silver-containing inner layer to the other layers 91

Fig. 52 Cross section of the glass 87 (H) with 13 wt.-% YSZ fibers sintered in silver foil 92

Fig. 53 EDS line scan showing the presence of a silver particle in the middle of the glass ceramic pellet of Fig. 51 93

Fig. 54 Ellingham diagram for the oxides stability [Con 2010] 94

Fig. 55 Strength comparison of single-layer and multilayer composites 97

Fig. 56 Hot stage microscopy of glass 87 and glass 104, pure and with YSZ fibers, showing the change in area corresponding to an increase in temperature and the ΔT during sintering of each composition 98

Fig. 57 Joint microstructures of sandwich samples composed of Crofer22APU and sealant based on matrix glass 104 and filler from a to c: 0 wt.-% YSZ, 13 wt.-% YSZ fibers, and 20 wt.-% Ag 100

Fig. 58 Diffusion test with glass sealant pellet on pure silver foil sintered at 850 °C for 10 h: a) pure glass 104, b) glass 104 with 13 wt.-% YSZ fibers 101

Fig. 59 Fracture of hour-glass samples after the torsion test measearument. All the composite sealants showed similar fracture patterns. 104

List of Tables

Table 1 Coefficients of thermal expansion of crystalline phases commonly formed in glass-ceramic sealants [Bah 1972]; [Ban 1991]; [Wei 2004]; [Fer 2005]; [Mah 2010b]; [Buc 2010] 12

Table 2 Literature results of mechanical characterization of glass sealants for SOFC 25

Table 3 Literature results of joint room temperature tensile strength with glass ceramic sealants 37

Table 4 Chemical composition of glass 87 used in this study 39

Table 5 Chemical composition of glass 104 used in this study 40

Table 6 Comparison of fixed viscosity points attained by HSM 44

Table 7 Comparison of the filler materials properties [Ben 1979]; [Mor 2010]; [Sig 2012]; [Nan 2012]; [Mat 2012]; [Thy 2013]; [Wsj 2013]; [Tax 2013]; [Fue 2013] 54

Table 8 The multilayer possibilities 56

Table 9 EDS point analysis of composite with 25 wt.-% Cu particles shown in Fig. 35. Results in atom% 63

Table 10 Measured technical alpha and softening point of the composites as-sintered and technical alpha of annealed samples 72

Table 11 Characteristic fixed-point temperature for the pure glass matrix and the composites, correlated with the estimated viscosity level at those points 73

Table 12 Four-point electrical resistance measurements results for as-joined and annealed samples 78

Table 13 Comparison of the maximum and average tensile strengths for the different sample geometries at breaking force calculated by simulation 81

Table 14 Results of four-point electrical resistance measurements of the multilayer sandwich samples as-joined, annealed, and thermally cycled. Calculated current losses through the sealant based on 100 cm² cells in the Jülich stack design (F10) 95

Table 15 Technical alpha of the glass 104 and composites 98

Table 16 Four-point electrical resistance measurements results for as joined and annealed samples.....104

1. Introduction

Seals and sealing processes are an important part of the construction process for complex devices. Seals are the most challenging component for high-temperature applications. Highly challenging examples include sealing SiC/SiC parts in thermonuclear fusion reactors, in separation membrane reactors, and planar solid oxide fuel cell (SOFC) stacks, where seals need to fulfill several requirements.

SOFCs are electrochemical devices in which a fuel, i.e. hydrogen or even methane, reacts with oxygen ions at an anode to produce electrical energy [Ner 1899]. These fuel cells operate with high energy conversion efficiency and very low air pollutant emission rates. However, a single cell unit usually generates a relatively small voltage; thus, to achieve higher voltage output, individual cells are connected together in series to form a stack [Ste 2001]; [Blu 2005].

In planar SOFCs, fuel gas and air must be kept separate from each other to prevent a decrease in the efficiency of the production of electrical energy as well as direct combustion and local overheating of the components. Therefore, gas-tight sealing is essential along the edges of the electrodes, electrolyte, and interconnect as well as between individual cells to bond the cell stacks, preventing the gases from mixing in the anode or the cathode, and providing electrical insulation to avoid shunting. The sealant must seal the adjacent cell components and must be stable during long-term cell operation [Mah 2010].

In the stack design used at Forschungszentrum Jülich (FZJ), three layers of glass ceramic are used. They seal the metal frame to the anode side of the interconnect plate, the metal frame to the cathode side of the interconnect plate, and the cell outer rim to the interconnect plate, as shown in Fig. 1 [Blu 2011]; [Buc 2010].

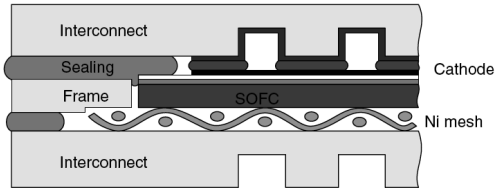

Fig. 1 Schematic presentation of a repeating unit of a planar SOFC with a rigid glass-ceramic seal [Buc 2010]

Several physical and chemical properties should be obtained simultaneously for a sealing material to allow proper SOFC operation. The most important are high-temperature stability (between 750–900 °C), electrical insulation (> 2 $k\Omega \cdot cm^2$), gas-tightness, sufficient adaptation of the coefficient of thermal expansion (CTE) to the other components of the SOFC (CTE of anode substrate ~ $12 \cdot 10^{-6}$ K^{-1}, ferritic steel ~ $10 \cdot 10^{-6}$ K^{-1}), good adhesion to steel and the electrolyte, chemical stability in oxidizing and (humid) reducing atmospheres, plasticity at the joining temperature ($\eta \sim 10^5 - 10^6$ Pa·s), and sufficient strength to withstand thermal stresses [Mah 2010]; [Wei 2006]; [Zha 2009].

A great number of materials and approaches have been investigated as sealants for planar-type SOFC stacks, such as glass sealants, glass-ceramic sealants, glass-ceramic composite sealants, and cement sealants [Les 2007]. The best of these approaches successfully seal the cells with acceptable leakage rates. Presently, glasses or glass-ceramics are widely used as sealing materials for several joining partners (glass, ceramic, and metal) because they easily form hermetic seals in useful shapes. They provide electrical insulation and are also chemically stable under corrosive or oxidizing environments. Moreover, they can be applied to the components by inexpensive processes like screen printing or extruding [Sch 2002a]. However, significant problems appear with these seals during long-term operation. This is due to corrosion effects or cracking associated with multiple thermal cycles.

Currently, the strength of the glass-ceramic composite sealant is considered a very important characteristic [Gro 2011]. The sealant must withstand temperature cycling and reducing-oxidizing cycling during operation, as well as pressure from the gas flow, the weight of the other repeating units and the dead load of the stack. Therefore, new reinforcement strategies need to be elaborated with the use of filler materials controlling the plasticity at joining temperatures [Blu 2011]. The use of filler materials in an established glass sealant matrix leads to new glass-ceramic composites that require detailed investigation of the influence of filler materials on the strength of the joints. Remarkable development has taken place in this field, as reported in the literature [Gro 2011]; [Blu 2011]; [Gro 2006]; [Wan 2007]; [Gro 2007]; [ZHa 2011]; [Bea 2005].

Over the last decade, Forschungszentrum Jülich GmbH (FZJ) in cooperation with the Instut für Gesteinshüttenkunde, RWTH-Aachen (GHI) has developed and improved glass and glass-ceramics sealants to fulfil the requirements of planar SOFC stacks [Lah

2000]; [Sch 2002a]; [Haa 2005]; [Gro 2006]; [Wan 2007]; [Gro 2007]; [ZHa 2011]; [Gro 2011]. One of the glasses developed at FZJ, known as glass 87 and also referred to in the literature as glass H, presented excellent joining properties and has been used in several stacks [Blu 2005]; [Blu 2011]; [Blu 2012]. Nevertheless, this glass does not yet present sufficient strength under operation conditions. Therefore, this study focused on the reinforcing the glass matrix 87 with several filler additions and using an alternative sealant design, which were then tested and characterized. Mechanical characterization methods are discussed and a new methodology is proposed for the shear stress analysis of joined samples.

2. State of art of sealants for high-temperature applications

The search for materials with enhanced properties is producing new discoveries at a faster rate than ever before. Several types of materials have been in focus at different periods of time. Asheby described the dominance of various material types in a graph shown in Fig. 2. It demonstrates how the choice of materials used has changed with time [Ash 1992]. The evolution of materials also altered the dominance of natural materials to metals, and nowadays a nearly equal distribution can be seen between the ceramics and glasses, composites, polymers, and metals.

Today, efforts concentrate on improving performance under extreme conditions. Materials now need to be designed for high-temperature and high-stress applications. The microstructure, composition, and processing of modern materials are therefore more complex. Together with the appearance of new materials, more elaborate structures designs are also being developed for the new applications. With the production of larger and highly complex structures, joining is still unavoidable when processing by a basic route [Mes 1995]. Furthermore, the requirements imposed by the new applications are often not covered by a single material type. Instead, the devices are usually composed of several different types of materials, such as metal alloys, glasses, ceramics, polymers, and composites, which need to be united.

Joining dissimilar materials represents the greatest challenge for a materials engineer. Differences in physical properties, such as melting points and CTEs, and undesirable metallurgical interactions, such as the formation of brittle intermetallic phases, can essentially preclude the joining of many dissimilar materials [Eag 1994]. Unfortunately, advances in joining techniques are slower than the evolution of materials [Hla 1996]. Consequently, it is common that the major restriction for the use of advanced materials is the lack of suitable techniques for joining them to each other or to other types of materials [Hla 1996]. In order to develop better joining techniques for conventional and new materials, it is necessary to improve our understanding of the relationships between the microstructure and the mechanical properties of the bonded or welded joints.

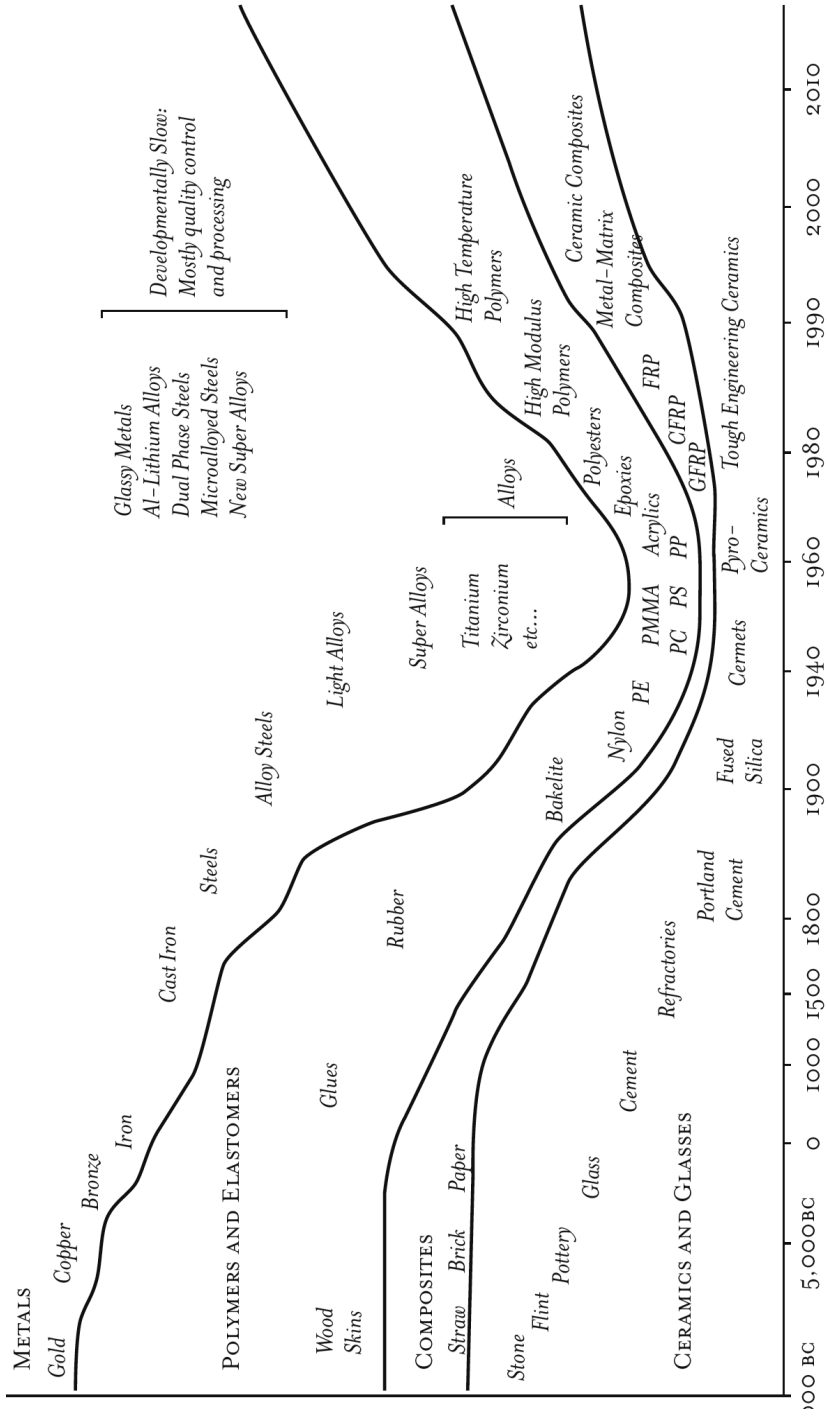

Fig. 2 The evolution of engineering materials with time [Ash 1992]

2.1. Sealants for high-temperature applications

Sealants for high-temperature applications have been developed with a focus on electrochemical devices such as SOFCs and high-temperature separation membrane reactors for oxygen separation and purification. In both cases, the sealants are responsible for gas-tightness and electrical insulation [Hat 2010].

Oxygen ionic or proton-conducting ceramic membranes are technologically important in high-temperature gas separation and membrane reactor processes. The operating temperatures of these membranes are typically between 600 °C and 1000 °C. For practical applications of these ceramic membranes, the membrane must be sealed to a dense ceramic or metal support tube [Hat 2010]; [Qi 2001].

The joining of machined SiC/SiC composites for thermonuclear fusion reactors is another interesting application, demanding sealants that withstand high temperatures [Fer 2008]; [Ric 2004]. The parts made of SiC/SiC composites can be produced as half-finished products and in simple shapes only. Therefore, one of the leading technological issues is the development of a suitable joining technique for the fusion environment. Several joining techniques have been proposed, but most of them involve adhesion by pre-ceramic polymers, reaction bonding, and brazing processes. Each of these techniques has potential advantages and disadvantages, and different mechanical performances have been reported. Moreover, the irradiation degradation of such joints has yet to be assessed [Ric 2004]. The thermo-mechanical stability of the joining up to 1000 °C (1270 K) should be comparable to the SiC/SiC composite and ideally the joint should have a composite structure that is just as damage tolerant as the base material itself [Fer 1994].

The high operating temperature (650–1000 °C) considerably limits the variety of sealing options; in principle, no organic or polymer seal can be employed. Fig. 3 provides an overview of conventional high-temperature seals [Buc 2010]. Alternatively, inorganic materials with high melting points can be used to seal the ceramic membranes at high temperatures above 600 °C [Hat 2010]; [Qi 2001].

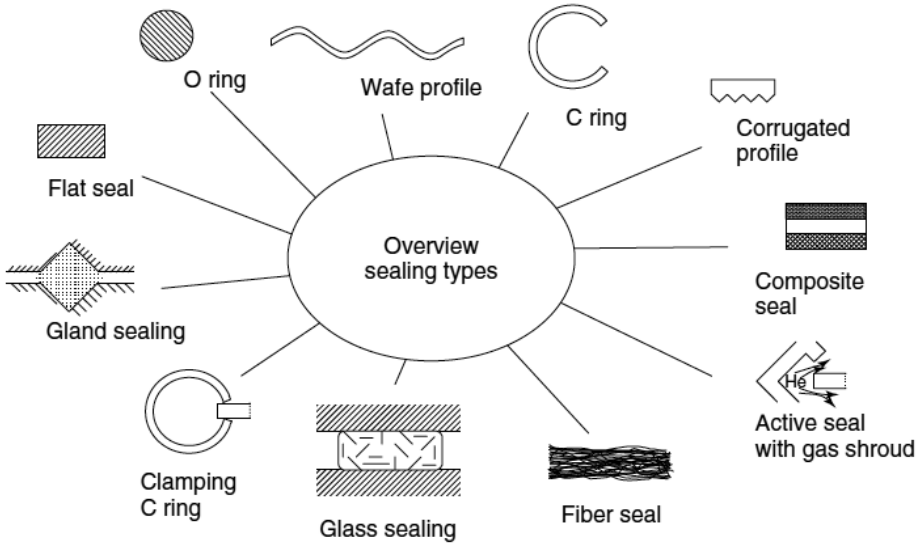

Fig. 3 Overview of the current sealing types for high-temperature applications [Buc 2010]

Choosing the sealing materials for those high-temperature applications can be very challenging. Several requirements need to be respected in order to achieve a successful combination. These include good thermal and chemical compatibility, good wettability, specific viscosity, matched CTEs, and an adequate bonding strength with the other components, which can be metal or ceramic parts. Noble ductile metals, for example silver and gold, pure glass, or ceramic are among the possible materials that can be used as high-temperature seals. Nevertheless, none of them meet all of the desired parameters. Metal seals usually have higher CTEs than the joining partners, and the pure glass seals can easily react with the joining surfaces provoking failure at the interface. Ceramic-glass composite seals perform better than pure metal, glass, or ceramic seals because the properties of the composite seal can be tailored to match those of the joining partner's materials [Qi 2001].

2.2. Sealing materials for solid oxide fuel cells

Among the components of a SOFC stack, the sealant is still the component most in need of development. There is still no standard or fully tested and understood sealing material due to the large number of possible candidates. Within the last decade, many papers have been published reporting significant research and development progress for the sealants. Research groups from around the world established several potential candidates as sealants for SOFCs. Three different types of seals are currently being researched: the compressive seal, the compliant seal, and the rigidly bonded seal. In the last few years, several review articles dedicated to this topic have been published [Don 1993]; [Don 2000]; [Fer 2005]; [Wei 2006]; [Les 2007]; [Don 2008]; [Mah 2010b]; [Mah 2010a].

Compressive seals use deformable materials that do not bond to the planar SOFC components but serve as gaskets instead. The material is compressed by external forces applied to the fuel cell stack and the sealing is a result of the pressure. The sealing surfaces can slide past one another without disrupting gas-tightness, and the individual stack components can expand and contract during thermal cycling. The matching of CTE values is not as important as for a rigid seal, like a glass-ceramic seal, for example. The main advantage of this technique is the option of stack mid-term repair by releasing the compressive load, disassembling the stack, and replacing the damaged components. However, the addition of a load frame makes the operation more complex, increases the weight and thermal mass as well as the cost of the SOFC, and seriously limits the use of compressive seals in mobile applications [Wei 2006]; [Les 2007].

Improvements on mica-based seals were made by Chou et al. in several studies that reported on compressive mica single layers, multilayer mica seals or hybrid mica with a glass interlayer, and infiltrated mica with wetting or melt-forming agents such as $Bi(NO_3)_3$ or H_3BO_3 [Cho 2002]; [Cho 2003a]; [Cho 2003b]; [Cho 2003c]; [Cho 2004]; [Chou 2005]; [Cho 2006]. However, both infiltrated mica and hybrid mica presented problems during aging combined with cycling processes. The infiltrated mica B_2O_3 volatilization provoked an increased leakage rate, and the hybrid mica was dissolved by the glass, changing the composition of the glass layer. Le et al. criticized the use of a glass interlayer in a hybrid mica seal, because it makes it impossible to repair the stack by replacing the malfunctioning sealant layer, thus eliminating the biggest advantage of this type of sealants [Le 2006]. A non-glass compressive seal made of alumina-silica

fiber paper and fumed silica dispersions performed better than the conventional mica and results were comparable with the hybrid mica [Le 2007].

Glasses are considered the best candidate materials for a number of applications due to their specific properties. They have a lower density than the majority of structural metals and alloys, and are hard and highly resistant to compressive stresses. Their electrical and thermal insulating properties as well as their chemical stability are additional favorable characteristics [Dlo 1997]. Two types of sealants were developed with glasses: compliant seals and rigidly bonded seals.

Compliant seals are glasses that are intended to remain vitreous without any substantial crystallization, thereby retaining their softening or compliant behavior after the sealing process. As a result, this non-rigid seal reduces residual stresses and has self-healing properties [Cho 2012]. Of the compositions already developed and tested, the compliant seals have not been as successful as rigid glass-ceramics, because some of the compliant glasses are electrically instable, have poor oxidation resistance, and react with other components of the SOFC stack [Buc 2010]; [Mah 2010a]; [Mah 2010b].

Most of the compliant glass-seal compositions contain alkalis, i.e. sodium and potassium, which are commonly added in glass-making to lower the melting temperatures. However, under an external electrical field, mobile ions tend to move towards the electrode (referred to as electrode polarization). It is possible that the alkalis may accumulate near the electrode (the interconnect steel plates), resulting in a different composition to the bulk glass matrix. The localized higher concentration of alkalis could reduce the glass viscosity, and hence may lead to enhanced corrosion along the interfaces [Uhl 1983]; [Sch 1990]; [Vog 1992]. The presence of alkali oxide in glass sealants has been shown to promote evaporation of Cr from the interconnect [Dur 2000]. The evaporation of Cr from the interconnect can poison the functional ceramic parts of the solid oxide fuel cell, limiting its operation lifetime. Furthermore, some highly volatile oxides such as P_2O_5, B_2O_3, and PbO should be avoided or minimized [Gea 2003].

Other research groups are engaged in producing sealants containing alkalis, for example at the Politecnico di Torino [Sme 2008a]; [Sme 2010]; [Sme 2008b]. Labeled as SACN, the barium and boron-free glass was composed of 50-55 wt.-% SiO_2, 10-12 wt.-% Al_2O_3, 20-23 wt.-% CaO, and 10-12 wt.-% Na_2O, showing partial crystallization during joining. Joining tests performed with Crofer22APU for 400 h exposure in air at

800 °C showed that using a pre-oxidized Crofer22APU substrate can prevent Cr diffusion through the glass seal [Sme 2008a].

Rigidly bonded seals are glass-ceramics or glass-ceramic composites. Much research has concentrated on these materials due to their manifold advantages, such as the possibility of tailoring performance depending on composition design, high electrical resistivity, hermetic sealing, and their suitability for stationary and mobile applications with an easy and flexible fabrication process [Gea 2001]; [Gro 2006]; [Gro 2007]. The most important parameter for the selection of a glass sealant material is the glass transition temperature, T_g. For the initial stage of the joining process, sufficient flow of the sealing material is essential. Afterwards, the glass should partly or fully crystallize and form a rigid joint. However, the crystalline phases improve the mechanical strength of the joints. If the sealing glass does not crystallize, the joint with the parent glass would be much more brittle and would be unable to withstand thermal stresses that occur during stack operation due to the CTE mismatches of the sealant and stack components. Viscous creep may release the stresses. The CTE can be adjusted by the choice of glass composition or by using a composite with filler materials added to a glass matrix.

Furthermore the CTE of a sealing glass can significantly change during the initial thermal treatment. Thermal treatment can affect the CTE for two reasons: 1) structural rearrangement of the amorphous glass and 2) formation of devitrified phases with different CTE values [Mah 2010]. In a BaO–MgO–borosilicate glass, for example, the devitrified phases are $BaSiO_3$, $BaSi_2O_5$, Ba_2SiO_4, $MgSiO_3$, and $BaMgSiO_4$ [Pas 2007]. Many of these phases are already well characterized and have precisely measured CTE values (see Table 1).

Under typical SOFC stack operating conditions, the glass matrix tends to crystallize depending on the glass composition. Here, a glass matrix based on the system of BaO-CaO-SiO_2 (BCS) is used as an example. Considering that during glass crystallization, diverse barium silicates can be formed, the high CTE of the silicates containing high levels of barium could change the initial CTE of the amorphous sealant. This property could be useful in a controlled way, e.g. when adding the barium silicate in crystalline phases as a filler to reinforce a low-expansion glass composition.

The changes in crystallinity also need to be controlled at the interface between the sealant and interconnect materials. Undesired phases can form due to reactions between the joining partners. When using barium-rich glasses, i.e. from the BaO-CaO-

Al_2O_3-SiO_2 system, and ferritic Cr-containing steel as interconnects, $BaCrO_4$ often forms at the interface. The barium chromate phase has a high CTE which provokes a mismatch between the $BaCrO_4$ phase, the interconnector, and the glass seal [Mah 2010]. Thermal stress arises, and pores and cracks are formed at the interface, as shown in Fig. 4 [Cho 2010].

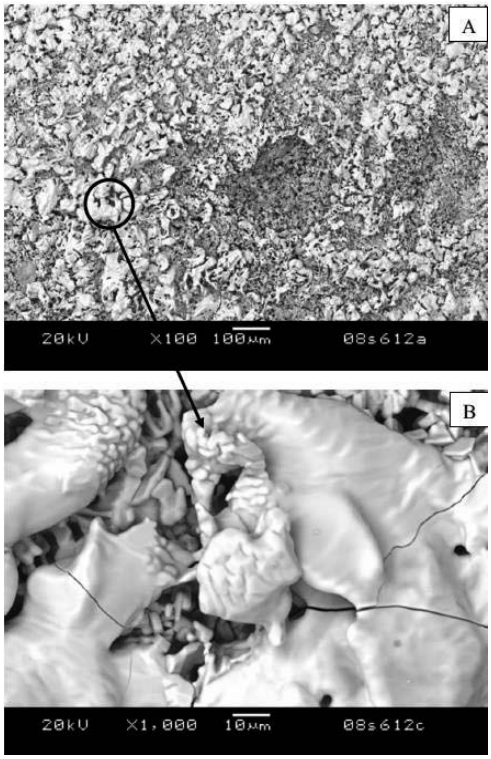

Fig. 4 Fracture surface of as-received Crofer22APU sealed with a glass. (A) Low magnification and (B) high magnification of the circled area in (A) show the microcracked chromate [Cho 2010]

Table 1 Coefficients of thermal expansion of crystalline phases commonly formed in glass-ceramic sealants [Bah 1972]; [Ban 1991]; [Wei 2004]; [Fer 2005]; [Mah 2010b]; [Buc 2010]

Phase	**CTE (10^{-6}/K) at 20 °C**
SiO_2	α_{II} = 7.9 $\alpha^{\perp}$ = 13.3
$MgSiO_3$ (Enstatite)	9.0-12.0
$MgSiO_3$ (Clinoenstatite)	7.8-13.5
$MgSiO_3$ (Protoenstatite)	9.8
Mg_2SiO_3 (Forsterite)	9.4
$CaSiO_3$ (Wollastonite)	9.4
Ca_2SiO_4 (Calcium orthosilicate)	10.8-14.4
$BaSiO_3$ (Barium silicate)	9-13
$BaSi_2O_5$ (Barium disilicate)	14.1
$Ba_2Si_3O_8$ (Barium silicate)	12.6
$Ba_3CaSi_2O_8$	12-14
$BaZrO_3$ (Barium zirconate)	7.9
BaB_2O_4 (Barium borate)	α_a = 4.0 α_c = 36.0
$BaAl_2Si_2O_8$ (Hexacelsian)	7-8
$BaAl_2Si_2O_8$ (Monocelsian)	2-3
$BaAl_2Si_2O_8$ (Orthocelsian)	5-7
$Mg_2Al_4Si_4O_{18}$ (Cordierite)	2

3. Strength of sealing materials

Glasses have high intrinsic strength. Estimating the strength of the O-Si-O bond using its thermodynamic data, i.e. heat of formation, molar volume and density, leads to a theoretical value of 20,000 MPa for soda lime glasses, based on a calculation of the glass strength by its structure. Highest glass strength values achieved in practical was for fibers, which can be up to 5,000 MPa. The lower actual strength of most glasses is due to surface defects, and inclusions [Con 2010]. Fig. 5 shows the theoretical strength according to glass structure calculations and the maximum strength reached by different glass types.

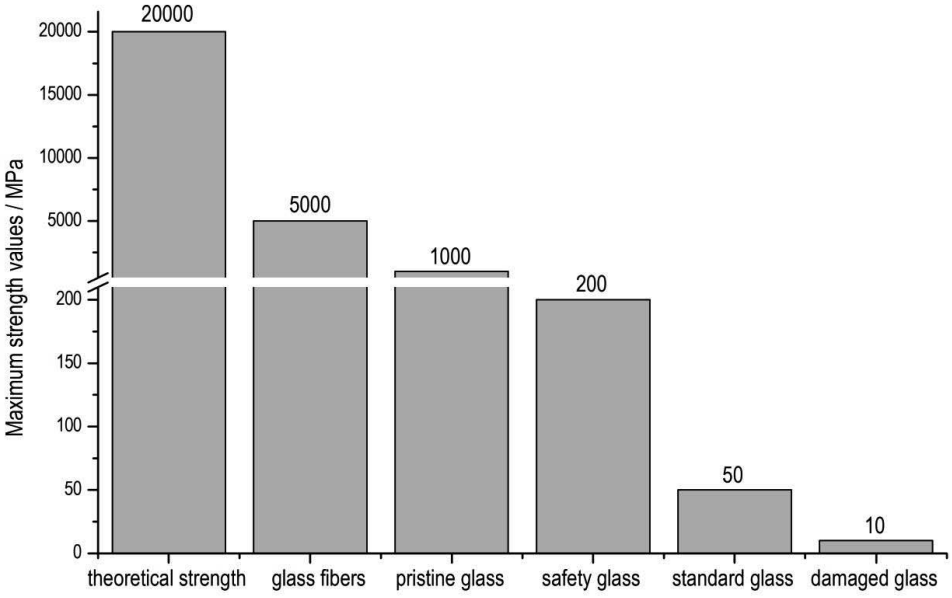

Fig. 5 Typical maximum strength of glasses

Blum et al. [Blu 2010] recently demonstrate that the glass-ceramic sealant materials tested by FZJ are relatively low in mechanical strength, resulting in failure under stack relevant conditions. Dummy tests presented low leakage rates, while tests with corresponding stacks had increasing leakage rate. The only difference between the dummy and stack tests was gas flow applied after the joining process for stack commissioning. Therefore comparable gas flow was applied during dummy tests and

these presented the same high leakage rates seem in the stack tests, as shown in Fig. 6. Through thermo-mechanical analyses based on modeling and experimental data, it was found that the failure of glass sealant happens exactly where the associated stresses are maximal. A complex temperature distribution an increase of stresses is provoked at certain points of the components.

Reducing the gas flow, stack design adaptation, or exchanging the glass sealant composition could diminish or avoid the gas leakage failure. The easiest and safest solution is to substitute the glass sealant for one with higher mechanical strength to withstand the stresses. The sealant material need to be developed and design concepts can be used for the components that allow accommodation of higher mechanical stress [Blu 2012].

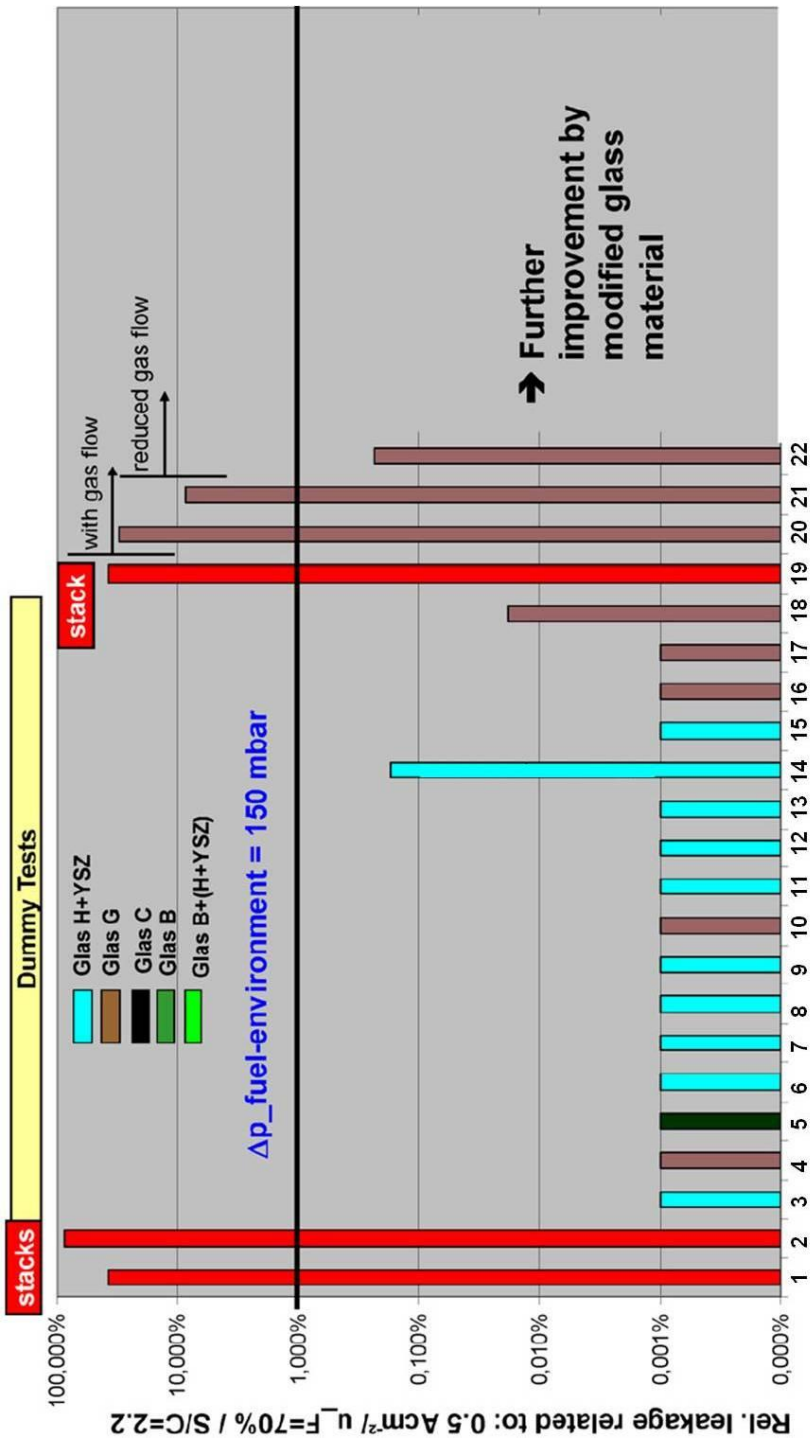

Fig. 6 Comparison of leakage rates of dummy and real stack tests performed with gas flow resulted in sealant failure [Blu 2010]

4. Reinforcement of glass-ceramic sealants by filler materials

Sealant toughness can be increased by addition of selected filler materials. In the selection process is important to observe several important material properties. The Ashby material selection method is an appropriate tool for the optimal choice of filler material for a specific application. Fig.7 shows Ashby chart for strength related to the toughness.

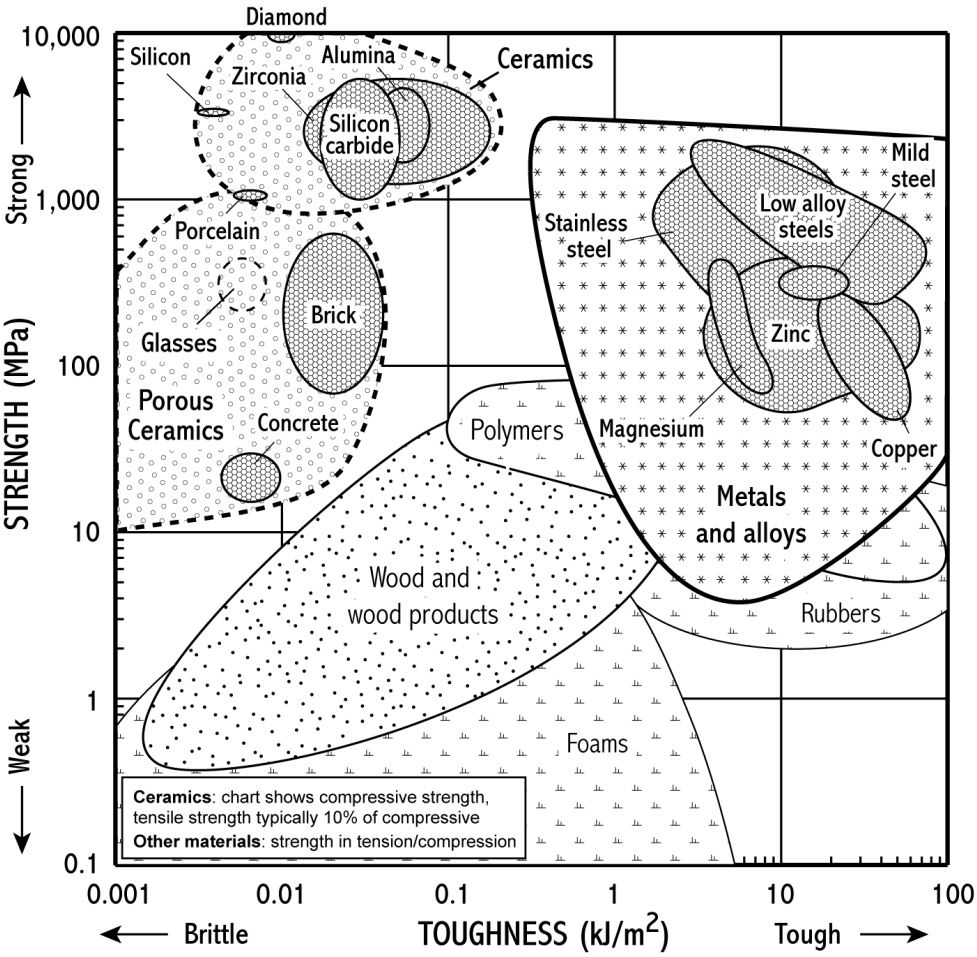

Fig. 7 Ashby charts of strength vs. toughness of materials [http://www-materials.eng.cam.ac.uk/mpsite/interactive_charts/strength-toughness/NS6Chart.html]

Furthermore the analyses of Ashby charts of fracture toughness and Young's modulus, Fig. 8, and thermal expansion with thermal conductivity, Fig. 9, can indicate which classes of materials are the most indicated for an specific application, i.e. to be used as filler materials in a glass-ceramic sealants. According to the Ashby charts glass material has usually lower strength and fracture toughness than ceramics, i.e. zirconia, and metals, i.e. nickel or copper. Technical ceramics and metals are found in a region of higher thermal expansion than certain glasses.

Enhance toughness of brittle materials by adding particles have been investigated by several research groups. Metallic dispersion toughening of glasses was topic of several studies since the early 1970's [Ste 1968]; [Bis 1980]; [Krs 1981]. The first glass matrix composites were reinforced by Ni and W particles, followed then by extensive work with Al. Other metallic particles and alloys, i.e. Mo, V, Cu, and Fe–Ni–Co were investigated for filling glass compositions at the end of last century [Ber 2004]; [Ban 1997].

The particle/matrix interface quality becomes of great importance because it strongly influences the particle deformation pattern. Failure models for composite materials suggest that the toughness enhancing mechanisms are associated with inclusions. The particles act as inclusions and decrease crack growth driving force by deflecting the cracks, either by enhancing energy dissipative processes or by decreasing stresses ahead of the crack. Simultaneously, the plastic deformation fracture or interfacial de-bonding of the filler phase in the wake of a crack further increases the energy required for specimen failure [Lip 1994].

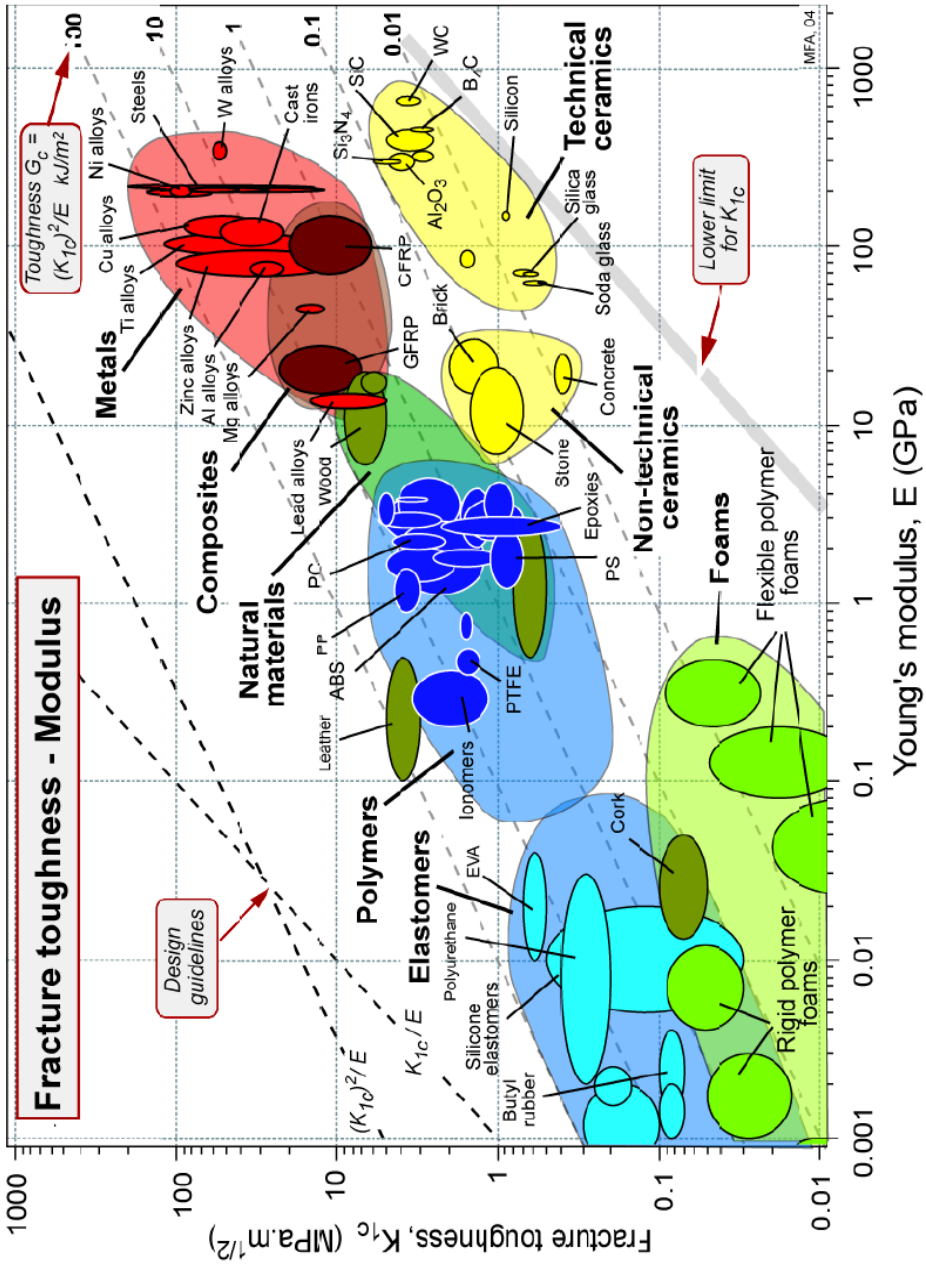

Fig. 8 Ashby charts of fracture toughness vs. Young's modulus [http://grantadesign.com/ashbycharts.htm]

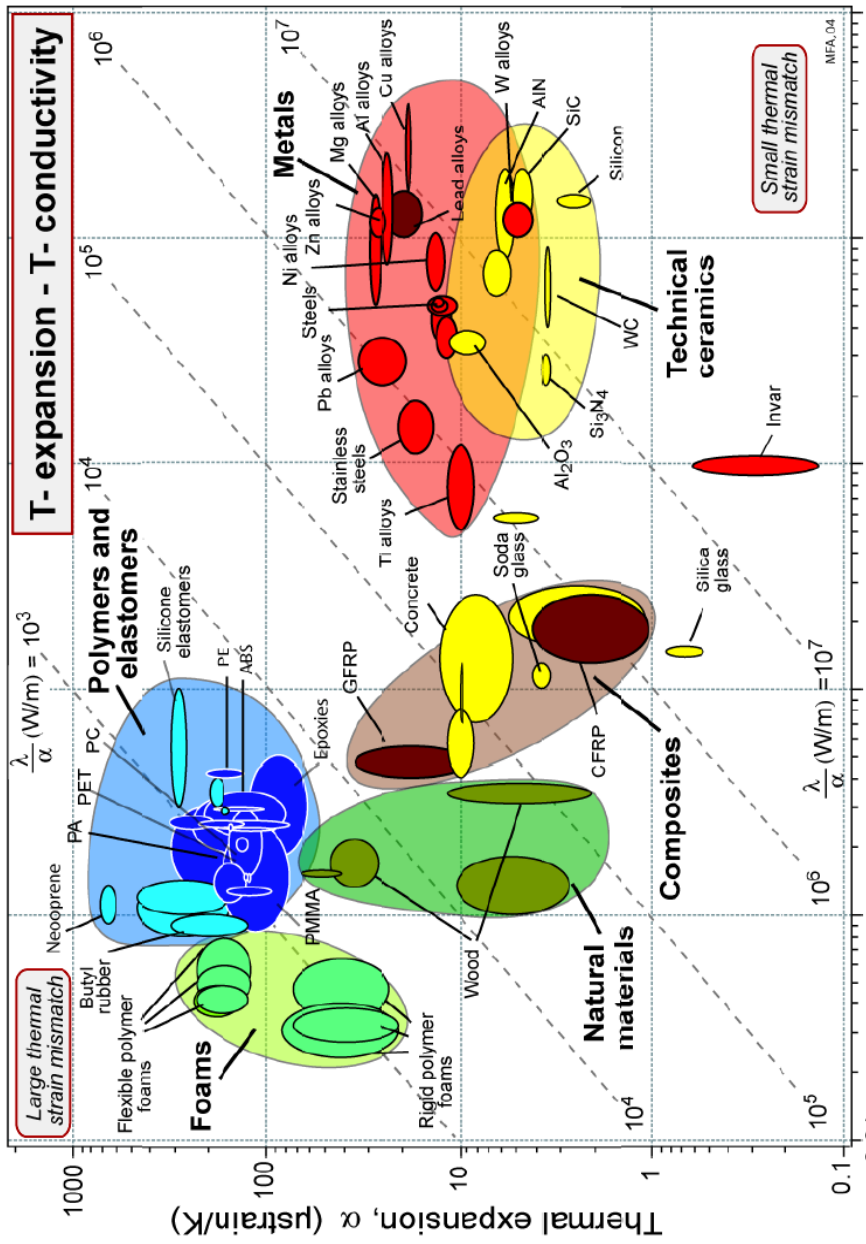

Fig. 9 Ashby charts of thermal expansion vs. thermal conductivity [http://grantadesign.com/ashbycharts.htm]

Adding ceramic fillers to the glass matrix proportionate mainly crack deflection as toughening mechanism. Deflection toughening arises whenever interactions between the advancing crack front and particle cause planarity deviation of the crack. The consequence of such interaction is the reduction in the stress-intensity factor at the crack tip. Deflection processes can occur in polycrystalline bodies, where an amorphous grain-boundary phase gives rise to a weakened interface between particles [Qui 1991]; [Lip 1995].

The ductile metal particles can absorb the crack energy and increase the strength of the composite by bridging the crack [Qui 1991]. It is essential for the effectiveness of the crack bridging mechanism that the particles are well-bonded to the matrix and that the advancing crack tip is drawn through the particles [Hut 1989]. The toughening increment should increase with the volume fraction of metal particles. There is, however, a limit to the amount of metal phase that can be added if the particles are to remain isolated from each other and hence contribute effectively to the toughening. Further, interconnected metallic particles are likely to lead to adverse changes in some properties, such as electrical insulation, corrosion resistance, and creep performance. For example, it has been observed that particle contents over 20 vol. %, which in wt.-% depends on the densities of the materials, can lead to substantial increase in the electrical conductivity of the composite [Hus 2003]. The toughening increment should increase with the yield strength of the metal and with the size of the inclusion. However, if the inclusion becomes too large, then the difference in the coefficients of thermal expansion of the metal and the ceramic matrix is likely to result in cracking, which may lead to an advancing crack being able to by-pass the particle [Yeo 2008].

Composites formed by glass and Ni particles have been studied since many decades. At the end of the 60's Sett and Fulrath [Set 1968], and Hasselman and Fulrath [Has 1970] in two complementing publications used glasses with CTE lower than, higher than, and matching the one of nickel. The bond between filler and matrix was developed by the migration of oxide at the sintering temperature and the resultant saturation of the glass with the oxide near the nickel. Results show that glass lower expansion presented porosity, weakening the composite. Strengthening improvements were observed in the composites with no CTE mismatch, as well as with the ones containing glass with higher CTE. The reason for that is the mechanical contraction of glass around the nickel during cooling [Krs 1981].

Moore and Kunz researched on the Kovar (Fe-Ni-Co) alloy particle-toughened borosilicate sealing glass [Moo 1987]. They proposed that surface treatment such as controlled oxidation or chemical etching of the reinforcement particles could improve the glass-to-metal bonding resulting in higher strength than with the untreated particles. Substantial improvement of 2.5 times of the fracture toughness was found when the etched Kovar particles reinforced the glass in comparison to the values obtained for the pure glass. The acid etching generates extensive, uniform surface roughness and results in mechanical interlocking of the particle/glass interface [Moo 1987].

4.1. Filler material influence on viscosity and CTE of sealant

Filler materials can also take influence on the viscous behaviour and the coefficient of thermal expansion of the sealant. This is an important aspect that should be considered during the choice of filler material type and amount to be added. The joining thermal treatment can be optimized after evaluation of the specific viscosity of curve of the composites. For example Hot Stage Microscopy (HSM) can be used to characterize the composite materials.

As part of the evaluation mixing rules can be used for estimate the coefficient of thermal expansion of the composites. By using these equations, and by controlling material composition and formulation, it is possible to approach the specifically desired values. The promising range of weight ratios of glassy matrix to mineral admixture to reach a desired value α_{comp} (CTE of the composite) may be estimated by simple mixing rules such as shown in Eq. (1)

$$\alpha_{\text{comp}} \approx \frac{\sum \alpha_i \cdot y_i / \rho_i}{\sum y_i / \rho_i} \qquad \alpha_{\text{comp}} \approx \frac{\sum \alpha_i \cdot K_i \cdot y_i / \rho_i}{\sum K_i \cdot y_i / \rho_i} \qquad \text{Eq. (1)}$$

where αi, yi, ρi, and Ki denote the thermal expansion coefficient, weight fraction, density, and bulk compression modulus, respectively of the component i. A potential shortcoming of the latter approach lies in the fact that many mineral admixtures are easily dissolved in a liquid oxide glass matrix or are converted to other phases. In a

more recent approach, the nature of mineral admixtures is restricted to constitutional phases of the glass-forming system only. Such phases coexist with the rest of the system. They can be added at arbitrary amounts without any risk of change of their identity by a chemical reaction [Buc 2010].

4.2. Composite sealants for SOFC applications

Glass-composite sealants for SOFC have being recently reported in literature. These materials are comprised of a low viscous glass and a dispersed filler material, which in most of the cases have higher CTE than the glass matrix. Both ceramic and metallic particles can be added to a glass matrix to improve the CTE compatibility, as well as to control the viscosity during the joining process and to enhance the joint mechanical properties. Fillers should promote a controlled crystallization of the glass matrix, which after joining ideally stays unaffected during the life-time of the stack. Moreover the reinforcement of the glass-ceramic sealant used in SOFC should not impair the other matched properties. Most specifically electrical insulation should be preserved, as well as a good adhesion, coefficient of thermal expansion (CTE) compatibility, and other requisites of this application.

Chou et al. studied the effect of nickel oxide particles filler in a glass sealant for SOFC applications. It was demonstrated that the addition of 5, 10 and 15 vol. % of NiO in a glass based in the system SrO-B_2O_3-Y_2O_3-SiO_2-CaO could linearly increase the sealant CTEs in agreement with Turner's equation for the rule of mixture. Improvement in mechanical properties happened with the increase of filler amount until a certain point. The sealant strength decreased with addition of 15 vol. % NiO. Overall, the composite glass with NiO demonstrated a viable way to tailor thermal and mechanical properties [Cho 2007].

Glass-silver composites for SOFC sealant first results were published in 2005 by Beatty [Bea 2005]. Borosilicate frits produced by Ferro Corporation, composed by SiO_2, B_2O_3, Al_2O_3, CaO, K_2O and Na_2O, were mixed with several amounts of silver in vol. %. The research has shown by joining tests that this composite sealant was hermetically tight and possibly would withstand better thermal cycling and ageing. Electrical data and metallographic cross-sections indicated that the seal surface was electrically insulating

across a wide range of compositions, and the embedded Ag domains had substantial connectivity down to silver volume fractions of approximately 10 vol. % [Bea 2005].

Further investigation concerning the use of Ag in SOFC glass sealant were done by Corral et al. [Cor 2008] and Gross et al. [Gro 2011]. Corral et al. evaluated that the use of particulate filler, independent of being Ag or ZrO_2 particles, caused an increase in the viscosity on that specific glass composition. The observed increase in viscosity was compatible with the calculated by using classical suspension rheology models [Cor 2008]. The research group at Forschungszentrum Jülich added 20 wt.-% of silver particles, 20 wt.-% of YSZ particles, or 13 wt.-% YSZ fibers in a Barium-Calcium-Silicate glass matrix (glass H) and performed tensile strength tests. The silver reinforced composite presented the best tensile strength result in comparison with the ceramic reinforced sealants [Gro 2011].

The use of MgO particles as filler in a sodium aluminosilicate (NAS) glass matrix was reported to increase the CTE of the composite to close to 12 ppm/K, providing better match with the other components and less thermal stresses during thermal cycling. Bonding strength and interface reactivity between metal and glass could be better controlled. Nevertheless part of the MgO particles reacted with the glass and were dissolved in the glass composition [Nie 2007].

Investigation showed the potential benefit of adding thermodynamically stable crystalline phases to a specific glass system. This concept was tested in two silicate systems. The first glass matrix was based on $CaO\text{-}MgO\text{-}Al_2O_3\text{-}SiO_2$ system. Barium silicate crystalline phases were added to the glass matrix and phase transformation was observed in some cases. Crystalline phases that can coexist with the glass composition could avoid the undesirable filler phase transformation. Same experiments were performed with a glass based on $BaO\text{-}MgO\text{-}SiO_2$ system. This could confirm that the concept of using a coexisting phase is a good alternative to tailor the properties of a glass sealant [Gro 2005]; [Wan 2010].

4.3. State of art of strength evaluation of glass sealants

Mechanical properties are the key features for the development of a SOFC sealant. Several approaches were investigated to improve the fracture resistance of the glass sealants. Reinforcement increases the toughness of the brittle matrix, for example

by dispersing fillers in the glass matrix it is possible to dissipate the crack energy by bridging and/or deflection. Many new possibilities of glass and glass-ceramic composites can be investigated for being used as SOFC sealant. Nevertheless it is still a nowadays problem to quantitatively evaluate the mechanical strength of a joined steel-sealant-steel sample. At this moment there is no standardised method to test the mechanical strength of joined ceramics and composites. Measuring the shear or tensile strength of the same joining material with different test methods will lead to different results.

Many studies have reported mechanical properties of brazes and glass solders for different applications. Nevertheless, most of the studies were done in bulk material for analysis such as tensile, in the absence of constraint effects present in the real joint configuration [Rhe 2003]; [ZHa 2011]; [Lui 2011]; [Mal 2012a]; [Lin 2012]; [Cho 2010]; [Gro 2011]. A relatively wide variety of specimen configurations have been devised to test strength of brazed and solders joints and even more specifically glass sealants for SOFC.. There are specific advantages and disadvantages to each of the existent specimen and test designs, and the choice made in each individual study is generally motivated by a compromise between ease of brazing and lack of ambiguity in mechanical test data [Rou 1999]. A common method is to test braze joints under shear loading which is frequently a representative loading state for real brazed joints [Rou 1999]; [Kim 2005]. Due to the thermal mismatch of the ceramic and metallic materials in the SOFC stack, the seals experience predominantly shear stresses and therefore, similarly to the brazed joint, it should also be tested under shear loading.

At Forschungszentrum Jülich the glass-ceramics of the BaO-CaO-Al_2O_3-SiO_2 system were used in the SOFC stack assembling during the last years. The mechanical properties of this sealant were investigated and discussed in a number of publications [Mal 2007b]; [Mal 2009]; [ZHa 2011]; [Mal 2012a]; [Mal 2012b]; [Gro 2006]; [Gro 2011]; [Fai 2011]. Different approaches were tested in order to obtain an evaluation of the mechanical behaviour. Among many methodologies the FZJ research group used shear test, tensile strength test, micro-hardness and four points bending.

Many research groups have developed their own methodologies for mechanical characterization of the glass sealants. Several types of glass sealants compositions were tested using the distinct methods for mechanical evaluation. An overview of the literature results until the present moment are represented in the Table 2.

Table 2 Literature results of mechanical characterization of glass sealants for SOFC

Glass sealant	Joining partner	Joining conditions	Test type	Result	Reference
Glass 58 BaO-CaO-Al_2O_3-SiO_2	1.4742 steel	as joined	Shear test RT[1]	Shear stress 8.6 - 10.5 MPa	[Sch 2002b]
	1.4742 steel[2]		Tensile strength RT[1]	3.6 – 15.2 MPa	
Glass 73 BaO-CaO-B_2O_3-SiO_2	HNA[2]	as joined		32.9 – 38.1 MPa	
	1.4742 steel[2]	as joined		8.9 – 35.9 MPa	
Glass S25 BaO-CaO-Al_2O_3-SiO_2	HNA[2]	as joined		21.2 – 27.7 MPa	
	1.4742 steel[2]	as joined		10.5 – 424 MPa	
NAS Na_2O-Al_2O_3-SiO_2 addition of 30 vol. % MgO as filler	Crofer22APU coated	Various	Shear test RT[1]	0.92 - 2.09 MPa	[Nie 2008]
	Sandvik experimental batch	Various	Shear test RT[1]	1.21 – 2.36 MPa	
SiO_2-CaO-BaO	Crofer22APU	as joined	Shear test at 800°C	Critical shear stress 3 MPa; Shear modulus 1 GPa	[Mal 2007]
		Annealed	Shear test at 800°C	Critical shear stress 4 MPa; Shear modulus 15 GPa	[Mal 2007]
YSO75 (SrO,CaO)-Y_2O_3-B_2O_3-SiO_2	Crofer22APU	as joined	Tensile strength RT[1]	6.3 ± 0.9 MPa	[Chou 2008a]
YSO75 (SrO,CaO)-Y_2O_3-B_2O_3-SiO_2	Crofer22APU	as joined	Tensile strength RT[1]	6.3 ± 0.9 MPa	[Chou 2008a]
BaO-SiO_2-Al_2O_3-CaO-B_2O_3	Sintered cylinders 10 mm length, 5 mm diameter	as joined	Creep test under compression load	Creep strain of 43% at 800 °C with 58.5 kg load	[Liu 2011]
SACN SiO_2-Al_2O_3-CaO-Na_2O	Crofer22APU	as joined	Tensile strength RT[1]	6 MPa	[Sme 2008]

Glass sealant	Joining partner	Joining conditions	Test type	Result	Reference
Glass 87 BaO-CaO-SiO_2	Crofer22H	as joined	Tensile strength RT[1]	3.8 ± 0.03 MPa	[Gro 2011]
	Sintered bars	as joined	Microhardness RT[1]	E = 72 ± 5 GPa; H = 5.6 ± 0.7 GPa; K_{IC} 0.99 Mpa · $m^{0.5}$	[ZHa 2011]
		Annealed		E = 80 ± 9 GPa; H = 5.5 ± 1.3 GPa; K_{IC} 1.12 Mpa · $m^{0.5}$	
	Crofer22APU	Laser joined	Shear test RT[1]	Shear stress ~ 12 MPa	[Fai 2012]
	Crofer22APU	as joined	Four-point bending test RT[1]	Fracture stress 52 ± 1 MPa	[Mal 2012a]
			Four-point bending test 800 °C	Fracture stress ~ 1 MPa	
	Sintered bars		Four-point bending test RT[1]	Fracture stress 55 ± 7 MPa	
			Four-point bending test 800 °C	Fracture stress 10 ± 2 MPa	
Glass 48 BaO-CaO-SiO_2	Sintered bars	as joined	Microhardness RT[1]	E = 77 ± 3 GPa; H = 5.5 ± 1.3 GPa; K_{IC} 0.64 Mpa · $m^{0.5}$	[ZHa 2011]
		Annealed		E = 77 ± 3 GPa; H = 7.5 ± 0.5 GPa; K_{IC} 0.69 MPa $m^{0.5}$	
	Sintered bars	as joined	4 point bending test RT[1] 4 point bending test 800 °C	Fracture stress 91 ± 12 MPa	[Mal 2012a]
		Annealed		Fracture stress ~ 90 MPa	
GC-9 BaO-B_2O_3-Al_2O_3-SiO_2	Crofer22H	as joined	Tensile strength RT[1]	16.7 – 23 MPa	[Lin 2012]
		as joined	Tensile strength 800 °C	4.3 – 12.7 MPa	
		as joined	Shear test RT[1]	4.9 - 6.6 MPa	
			Shear test	4.4 – 4.7 MPa	

Glass sealant	Joining partner	Joining conditions	Test type	Result	Reference
Composite glass 87 + 20% YSZ particles (wt.- %)	Crofer22H	as joined	Tensile strength RT[1]	2.9 ± 0.03 MPa	[Gro 2011]
	Sintered bars	as joined	Microhardness RT[1]	E = 73 ± 8 GPa; H = 5.5 ± 1.2 GPa; K_{IC} 0.92 Mpa · $m^{0.5}$	[ZHa 2011]
		Annealed		E = 79 ± 6 GPa; H = 5.1 ± 0.9 GPa; K_{IC} 1.5 MPa $m^{0.5}$	
	Crofer22APU	as joined		E = 80 ± 15 GPa; H = 6 ± 2 GPa; K_{IC} 1.0 MPa $m^{0.5}$	[Mal 2012b]
	Crofer22APU	Stack operated 800°C for 1056 h		E = 70 ± 12 GPa; H = 5 ± 1 GPa; K_{IC} 2 MPa $m^{0.5}$	
	Crofer22APU	Stack operated 800°C for 1559 h		E = 48 ± 10 GPa; H = 4 ± 1 GPa; K_{IC} 1.5 MPa $m^{0.5}$	
	Crofer22APU	Stack operated 800°C for 19,000 h		E = 100 ± 10 GPa; H = 7 ± 1 GPa; K_{IC} 1.6 MPa $m^{0.5}$	
Composite glass 87 + 20% Ag particles (wt.- %)	Crofer22H	as joined	Tensile strength RT[1]	5.2 ± 0.29 MPa	[Gro 2011]
	Sintered bars	as joined	Microhardness RT[1]	E = 75 ± 5 GPa; H = 4.2 ± 0.8 GPa; K_{IC} 1.1 MPa $m^{0.5}$	[ZHa 2011]
		Annealed		E = 74 ± 8 GPa; H = 3.4 ± 1 GPa; K_{IC} 1.55 MPa $m^{0.5}$	
Composite glass 87 + 13% YSZ fibers (wt.-%)	Crofer22H	as joined	Tensile strength RT[1]	3.18 ± 0.03 MPa	[Gro 2011]
	Sintered bars	as joined	Microhardness RT[1]	E = 74 ± 5 GPa; H = 6.21 ± 0.7 GPa; K_{IC} 0.82 Mpa · $m^{0.5}$	[ZHa 2011]
		Annealed		E = 86 ± 5 GPa; H = 6.5 ± 0.8 GPa; K_{IC} 1.3 MPa $m^{0.5}$	

Glass sealant	Joining partner	Joining conditions	Test type	Result	Reference
GC-9 $BaO-B_2O_3-Al_2O_3-SiO_2$	Crofer22H	as joined	Tensile strength RT[1]	16.7 – 23 MPa	[Lin 2012]
		as joined	Tensile strength 800 °C	4.3 – 12.7 MPa	
		as joined	Shear test RT[1]	4.9 - 6.6 MPa	
			Shear test 800 °C	4.4 – 4.7 MPa	

[1] Room Temperature; ² machined, grinded, polished or sandblasted joining surface; E = Elastic modulus; H = Hardness; K_{IC} = Fracture toughness

4.3.1. Testing of shear strength

The first metal-glass sealant-metal joints submitted to shear tests were reported by Schwickert [Sch 2002b], using the glass 58 developed by P. Geasee, based on the BaO-CaO-Al_2O_3-SiO_2 system with additions of ZnO, B_2O_3, and PbO. The shear tests were performed in cooperation with the IWM in Freiburg, Germany. Four similar samples were prepared as a symmetric sandwich, see sketch in Fig. 10, with two 1.4742 steel plates of 6 mm thickness each, and a joining length of 50 mm. The shear strength results were in a range of 8.6-10.5 MPa [Sch 2002b].

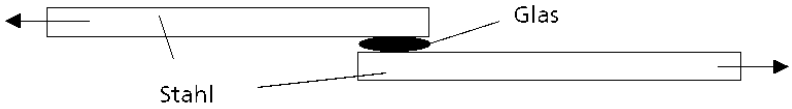

Fig. 10 Simple shear test specimen [Sch 2002b]

Malzbender et al. in 2007 published results of high temperature shear measurements done for one specific glass-ceramic sealant as joined, 850 °C for 10 h, and crystallized during an additional thermal treatment at 800 °C for 30 h. Fig. 11 shows the special symmetric shear specimens developed to characterize the critical shear stress of the glass-ceramic at SOFC operation temperature of 800 °C. These specimens represent the real situation in a SOFC stack; using the glass-ceramic to join a center piece of a NiO-YSZ anode covered by YSZ electrolyte layers on both surfaces between two Crofer22APU interconnect steel blocks. In addition, on the basis of a rheological model, shear modulus and viscosity were determined. The tested glass (SiO_2 34.7 %, CaO 8.6 %, BaO 41.4 %) also contained minor additions of transition metal oxides, such as ZnO, PbO and V_2O_5 to adjust the SOFC relevant physical and chemical properties. The critical shear stress increased from approximately 3 MPa as joined to 4 MPa as crystallized. The higher shear strength and shear modulus show that the additional annealing leads to a sealant with improved mechanical stability. Viscous shear deformation was initially observed at 800 °C. The viscous displacement becomes more difficult with the increase of crystallization, modified by the internal shear resistance contribution, which is influenced by the amount and morphology of the crystalline phases [Mal 2007].

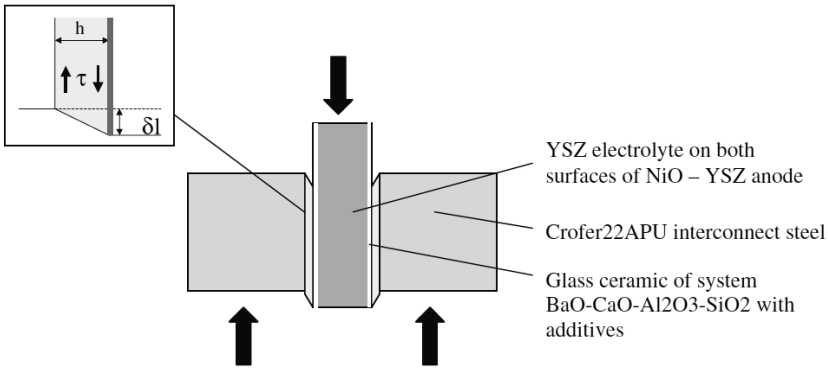

Fig. 11 Special shear specimen developed for the testing of glass sealants [Mal 2007]

Faidel in 2012 described a shear measurement at room temperature to test laser joined samples. In his work, he used a shear test unit of series 4500 from Nordson Dage, commonly used for testing of microelectronic solders. In comparison with other joint mechanical characterizations, the developed specimens allowed easier and faster analysis with limited reproducibility. Two sample designs were considered more in detail, as shown in Fig. 12. The first design was composed of a steel plate with a bead of the glass sealant molten on top, easily prepared by laser joining. The second design was originally devised for furnace joining and used two steel plates, the bottom plate having bigger dimensions of 30 x 30 x 2 mm and the top plate having smaller dimensions of 20 x 20 x 0.5 mm, in between the molten glass sealant forming a sandwich-like sample. Preliminary experiments have shown that the first design was not appropriate because the measurement head often slides up in the glass surface, which is in a half-ball shape, removing part of the glass but not testing the bond of the glass and metal. In an attempt to correct this failure in experiments, a metal bar was used to force transmission in shear. Nevertheless also these measurements had a high deviation of results. With the use of the second design and an adaptation for the laser joining process, sandwich-like samples were tested presenting good results and a reproducibility of ± 9 % deviation. For the joint of glass 87 and Crofer22APU made by laser technique, the shear stress measured was around 12 MPa [Fai 2012].

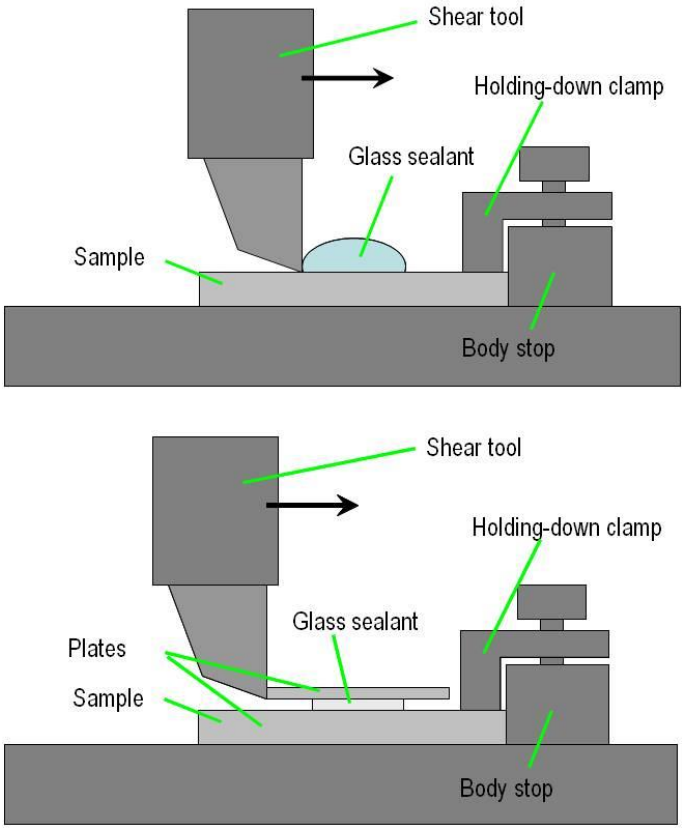

Fig. 12 Work principle of shear test with: a) laser joined test sample; b) furnace joined sample [Fai 2012]

A shear test technique at high temperature was developed by Lin et al. [Lin 2012] using Crofer22H and glass GC-9. Part of the samples was prepared using pre-oxidized metal surface. Specimens were tested as joined and aged in air at 800 °C for 250, 500 or 1000 h after the joining process. The glass GC-9 was applied as double-sided and single-sided shear joint specimens, with a corresponding thickness of 0.44 mm and 0.22 mm. It was found that the double-sided glass deposition increased the strength of the specimens. The pre-oxidation treatment of Crofer22H at 900 °C for 2 h did not improve the shear joint strength in any variant of the conditions. The thermal aging in air at 800 °C for 250, 500 h degraded the shear joint strength at 800 °C by 17 % due to continuous growth of $BaCrO_4$. A longer aging time of 1000 h reduced the strength to 19 %. The interface between the GC-9 glass-ceramic and $BaCrO_4$ chromate layer is generally the weakest layer to resist a shear loading for the joint specimens. For

specimens with 1000 h thermal aging treatment in air, fracture mainly occurs in the GC-9 layer resulting from growth of micro-voids within the glass-ceramic layer.

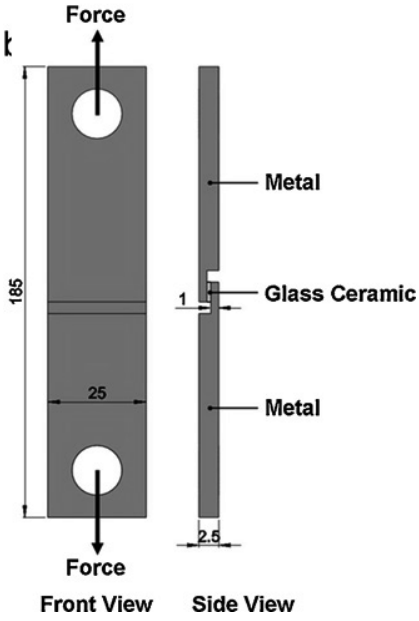

Fig. 13 Joint specimen for shear test, dimensions in mm [Lin 2012]

4.3.2. Micro-mechanical testing

Mal et al. used fracture mechanics tests to characterize the mechanical behaviour of such brittle sealants. The specimens with the sealant sandwiched between steel and/or coated steel were tested in notched bi-material flexure beam geometry. The fracture energy was determined at room temperature as a function of the glass-ceramic variant and the joining parameters. Complimentary fractography provided information about the location of the crack path. Also the influences of glass-ceramic crystallization and metallic oxide scale formation on the fracture resistance were examined [Mal 2009].

In 2011 Zhao et al. analyzed sintered bars of two glass matrices (glass 48 and 87) from the system BaO-CaO-Si_2O. Composites were prepared with glass 87 filled with 20 wt.-% Ag, 20 wt.-% YSZ particles or 13 wt.-% YSZ fibers. The pure glasses and the composites were tested as joined and annealed under SOFC stack operation temperature. By micro indentation testing elastic modulus, hardness and fracture

toughness were determined, as well as self-healing properties of those glass-ceramic sealants. The analysis did not show significant difference in the Young Modulus E among the all the as-joined samples, varying between 72 and 77 GPa with an error of ± 5 GPa [Zha 2011]. The results indicated that the analysis of elastic properties, fracture toughness, and micro-hardness were not different between the sintered bars and the sandwich sample; although the initial motivation of this study was to check the influence of different geometry of mechanical properties [Mal 2012a].

4.3.3. Bending test

An attempt to characterize the sealant materials at SOFC stack operation temperatures was developed by a four-point bending test at 800 °C. The bending test was performed with sintered glass-ceramic bars as well as with steel specimens head-to-head joined with sealant material, which is a geometry that is more compatible with the stack application. These analyses were the basis for obtaining elastic module, fracture stresses, and viscosity values. Sintered bars and head-to-head joints, as shown in Fig. 14, of glass 87 with 20 % YSZ particles were evaluated by this method at room temperature and at 800 °C, while with the glass 48 only sintered bars were investigated in both temperatures.

Malzbender et al. described that the fracture stresses found for the glass 87 with 20 wt.-% YSZ particles in the head-to-head joint at room temperature was equal to 52 ± 1 MPa comparable with the sintered bars result 57 ± 7 MPa. Nevertheless the results at 800 °C were 10 ± 2 MPa for the sintered bars and approximately 1 MPa for head-to-head joint. The authors justify this difference due to significant larger plastic strains during heating. A strong increase in deformation under constant load above a temperature of 700 °C can be associated with viscous flow of the glass ceramic leading eventually to failure as the specimen approaches a temperature of 800 °C. A displacement of approximately 20 µm was observed at 780 °C [Mal 2012b].

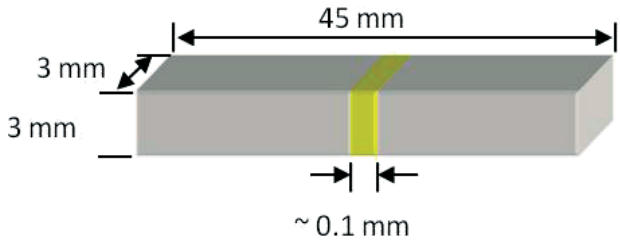

Fig. 14 Head-to-head specimen geometry [Mal 2012b]

4.3.4. Creep test

For amorphous glass materials, creep deformation is unavoidable when the operating temperature reaches the glass transition temperature - T_g. Glass sealant creep behavior has a fundamental importance to the design of SOFC stacks. The creep behavior can cause stresses and deformation of different SOFC stack components.

Researchers from Pacific Northwest National Laboratory (PNNL) in 2011 developed a set-up for short term compression creep tests at relevant load levels and temperatures for comparison to stack operation conditions, in order to evaluate the creep strain with time [Liu 2011]. The samples were sintered cylinders (10 mm length and 5 mm diameter), as show in Fig. 15, of a composition of 56.4 wt.-% BaO, 22.1 wt.-% SiO_2, 5.4 wt.-% Al_2O_3, 8.8 wt.-% CaO, and 7.3 wt.-% B_2O_3. In order to evaluate the as joined sealant, the cylinders were sintered according to the joining thermal treatment. For the analyzed glass the thermal treatment was to heat up till 850 °C for 1 h, followed by 4 h dwell time at 750 °C. Accordingly the specimens were tested under 10, 20 and 30 MPa as compressive load at 700 °C, 750 °C and 800 °C.

The results were used in simulations to investigate the performance of a SOFC stack concluding that bending deformations occurs in various stack components, which caused the change of air and fuel flow paths at the initial stages of operation. The height of flow channels for fuel was reduced, and the height of flow channels for air was enlarged slightly. The maximum equivalent total strain and creep strain remains constant after the initial creep stage, which means no overflow of the glass-ceramic sealing materials will occur with this glass [Liu 2011].

Fig. 15 Sample tested at 800 °C with 43 % strain in comparison with a non-tested sample [Liu 2011]

4.3.5. Testing of tensile strength

Schwickert in 2002 performed the first tensile strength tests to characterize FZJ glasses [Sch 2002b]. The first generation of tensile strength test samples had 20 mm outer diameter and 10 mm inner diameter tapped role. The set-up of measurement was adapted by steel ropes to avoid the creation of tensions and bending stresses during the assembling of the sample in the machine, as showed in Fig. 16. Several glasses were tested for two steel types and three surface end machining conditions. Some of the samples achieved extremely high reproducibility, with Weibull modulus of 20, while usual Weibull modulus values for glass materials would be around 4 to 8. Some results showed a good tensile strength, such as for the glass 73 with HNA steel grinded surface achieved 38 MPa with 10.5 Weibull modulus [Sch 2002b]; nevertheless the samples had glass squeezed out of the joining area, which could have influenced the results.

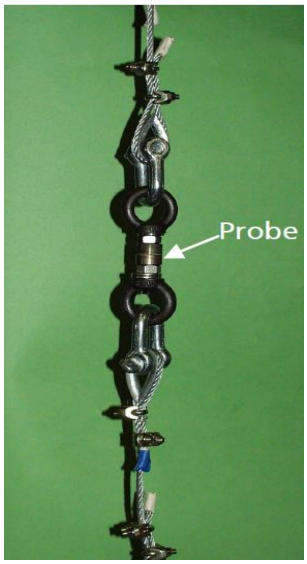

Fig. 16 Joined samples in the tensile strength measurement set-up [Sch 2002b]

Several sample generations for tensile strength tests at room temperature were made in FZJ during the last years. Improvements of the sample set-up increased the reproducibility of results. The set-up was improved by increasing the joining area and by reducing the bending moment of the sample adapter to the testing machine. The latter was achieved by inserting a wire rope of 4 mm in diameter between the fixing units of the sample and the testing machine. Tests were performed with the new butt-joint specimens made of Crofer22H joined with glass matrix 87, as well as with the composites glass matrix 87 with 20 wt.-% YSZ particles, 13 wt.-% YSZ fibers, and 20 wt.-% Ag particles. Even though the reproducibility of results was increased in a set of 10 identical samples, the tensile strength values of the as joined samples were low, being 3.8 ± 0.03 MPa for glass matrix, 2.9 ± 0.03 MPa for samples with YSZ particles, 3.18 ± 0.03 MPa for samples with YSZ fibers, and 5.2 ± 0.29 MPa for samples with Ag particles [Gro 2011].

Many other research groups also evaluated their sealant materials by tensile strength tests. None of them could deliver quantitative strength values [Sme 2008b]; [Lin 2012]; [Cho 2008a]; [Cho 2008b]. Lin et al. observed that the tensile join strength with GC-9 sealant and Crofer22H was much lower than the flexural strength of the bulk glass ceramic and the tensile strength of the Crofer22H [Lin 2012]. Comparing the tensile strength data obtained by the different research groups, as shown in Table 3, it

is noticeable that no significant strength values were found for the different glass compositions.

Table 3 Literature results of joint room temperature tensile strength with glass ceramic sealants

References	**[Gro 2011]**	**[Sme 2008b]**	**[Lin 2012]**	**[Cho 2008a]**
Sealant	Glass 87	SACN	GC-9	YSO75
Glass system	BaO-CaO-SiO_2	SiO_2-Al_2O_3-CaO-Na_2O	BaO-B_2O_3-Al_2O_3-SiO_2	(SrO,CaO)-Y_2O_3-B_2O_3-SiO_2
Joining partner	Crofer22H	Crofer22APU	Crofer22H	Crofer22APU
Sample dimensions	32 outer ∅ x 12 inner ∅ x 6 mm thickness	6 x 6 x 2 mm^3	95 x 25 x 2.5 mm^3	12.5 x 12.5 x 1 mm^3
Tensile strength	3.8 $\pm$ 0.03 MPa	6 MPa	16.7 – 23 MPa	6.3 $\pm$ 0.9 MPa
Fracture through	glass ceramic	glass ceramic	glass ceramic / interface	glass ceramic

The tensile strength experiments performed by Smeacetto et al. (2008), Lin et al. (2012), and Chou et al. (2008) were all carried out at room temperature with different specimens [Sme 2008b]; [Lin 2012]; [Cho 2008a]; [Cho 2008b], as presented in Fig. 17. The improved tensile strength test set-up of FZJ showed very high levels of reproducibility, and was published by Gross et al. [Gro 2011].

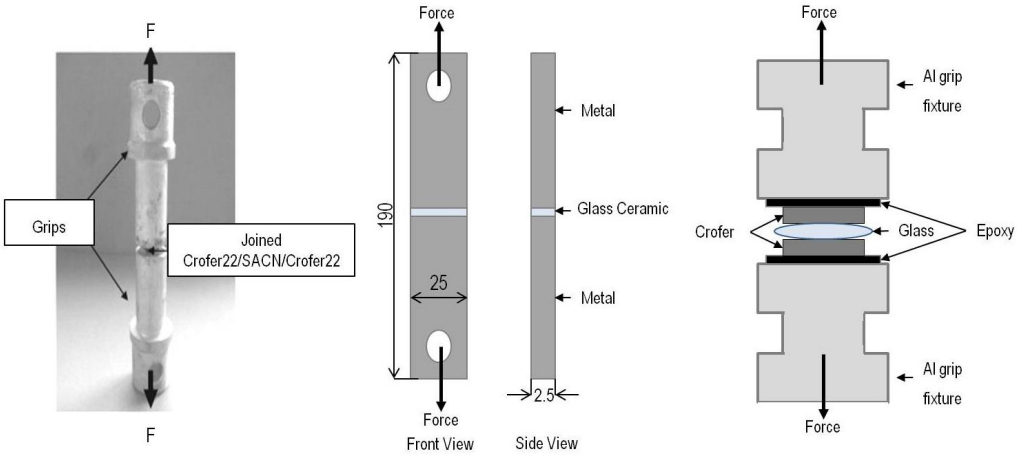

Fig. 17 Tensile strength measurement set-ups used by different groups to evaluate the glass sealants for SOFC [Sme 2008b]; [Lin 2012]; [Cho 2008a]

Lin et al. 2012 developed a tensile strength sample set-up for measuring at operating temperature, 800 °C, using Crofer22H and the glass GC-9. The measurements were done also at room temperature for comparison, as already described. Specimens were prepared with and without pre-oxidized metal surface as well as thermally conditioned as joined and annealed in air at 800 °C for 250, 500 or 1000 h after the joining process, the same procedure as done for shear test samples. The glass GC-9 was applied as double-sided and single-sided shear joint specimens, with correspondent thickness of 0.44 mm and 0.22 mm. It was found that the double-sided glass deposition increased the strength of the specimen. The greater joint strength corresponds to fracture occurring only in the glass-ceramic sealant layer.

It is highly desirable to have qualitative strength data of sealant materials although the current literature tensile strength data [Sme 2008b]; [Lin 2012]; [Cho 2008a]; [Cho 2008b] can only be qualitatively used as a ranking of materials, allowing to compare joints tested under the same conditions.

5. Experimental

In this study the glass “87”, also known as glass composition “H” in literature, based on BaO-CaO-SiO_2 system was chosen as sealant matrix due to its low viscosity and good compatibility with the Crofer22APU surface demonstrated in previous work from Central Institute of Engineering and Technology (ZEA-1) of FZJ. The glass was molten from a batch of pure carbonates and oxides (silica SiO_2, barium carbonate $BaCO_3$, calcium carbonate $CaCO_3$, boron oxide B_2O_3, aluminium oxide Al_2O_3, zinc oxide ZnO, and vanadium pentoxide V_2O_5 in an inductively heated platinum crucible at 1480 °C. The raw materials were distributed by Merck KGaA (Darmstadt, Germany) and had a grade of purity higher than 99%. After a dwell time of 2 h the melt was quenched by pouring into ice water, rinsed with acetone and dried in a heating chamber at 60 °C. For a better homogenization of the glass, the melting procedure was carried out twice. The glass frits were wet-milled in acetone in an agate ball mill to a median particle size of 10–13 µm. The chemical composition was analyzed by inductively coupled plasma optical emission spectroscopy (ICP-OES), results are shown in Table 4. Low angle laser scattering method was used to prove the glass powder particle size distribution.

Table 4 Chemical composition of glass 87 used in this study

	Oxide compositions [wt.-%]			Additions
	BaO	SiO_2	CaO	
Glass 87	48.2	29.8	6.1	Al_2O_3, B_2O_3, V_2O_5, ZnO

The preparation and main part of the glass and glass composite sealants characterization were carried out at FZJ, with exception of hot stage microscopy (HSM) analysis, which were made at GHI, RWTH-Aachen, and torsion tests that were collaboratively carried out at DISMIC of Politecnico di Torino, Italy.

The following analytical tests were carried out for the quality control of the glass powder: the coefficient of thermal expansion was measured by dilatometry, particle size distribution analysis was done by laser scattering measurement, and the chemical composition was checked by ICP-OES.

Glass 87 was used as matrix in a series of composites, which were also characterized by dilatometry, HSM analysis, and SEM equipped with EDS. Furthermore joining experiments were performed to evaluate the interaction of sealant and metallic

interconnector material Crofer22APU. The gas tightness of samples was analyzed by standardized He-leakage test and the electrical resistance was measured by four-point method. Major focus of the work was the testing of joints mechanical strength. Three different methodologies were investigated for the strength measurements, which were: the already used butt-joint tensile strength test adapted in ZEA-1 FZJ; a bond shear test with in-house developed sample setting; and a torsion test carried out at Politecnico di Torino with hour-glass samples geometry.

Another glass composition, so called glass 104, was developed to investigate the influence of vanadium and zinc oxides in the glass 87. All the properties of this glass were investigated accordingly to the same procedures done with glass 87, excepting by mechanical strength tests. The glass 104 composition is shown in Table 5.

Table 5 Chemical composition of glass 104 used in this study

	Oxide compositions [wt.-%]				
	BaO	**SiO_2**	**CaO**	**B_2O_3**	**Al_2O_3**
Glass 104	50.6	31.3	6.4	7.9	3.8

5.1. Chemical analysis

Chemical analysis is part of the quality control of each glass batch, which is molten in the laboratories of ZEA-1. The composition of the glass powder was investigated by spectroscopic methods on the dissolved glasses (ICP-OES). This method is a type of emission spectroscopy, which uses inductively coupled plasma to produce excited atoms and ions, emitting electromagnetic radiation at wavelengths characteristic of a particular element. The intensity of this emission is a quantitative of the concentration of the element in the sample. The ICP-OES analysis for this work was carried out by the central institute for analytics (ZEA-3) at FZJ.

The ICP-OES sample preparation was done by melting 50 mg of the glass samples in 1 g of NaOH for about 30 min at 550 °C in a closed gold crucible. The melt was dissolved in water, 50 mL 3% HCl was added and completed with deionizer water until 100 mL volume.

The measurements relative error was determined by the ZEA-3. The relative error is ± 3 % for the elements with concentrations bigger than 1 %, and ± 20 % for the elements with determined concentrations lower than 0.1 % Furthermore 37 elements were searched in a qualitative way to check for possible contaminations.

5.2. Measurement of viscous behaviour by hot stage microscopy (HSM)

High-temperature optical microscopy is an essential characterization and monitoring technique with wide applications in different areas of materials science. The equipment used in this work was EM 201, Hesse-Instruments (Osterode am Harz, Germany). Heating microscope is normally used to analyze the shadow area and height of a test object and its altering shape and dimensions over a defined temperature range. Through software the image captured is analyzed and a plot can be generated correlating different parameters, for example area or sintering versus temperature.

The Hot Stage Microscopy (HSM) is an effective technique to determine ash fusibility, sintering point, softening point, melting point and wetting behaviour of the melting phase on a substrate. Furthermore, HSM can also show the results as viscosity curves of the powdery pure glasses, following the methodology established by Scholze [Sch 1962] and Pascual et al. [Pas 2001]; [Lar 2004]; [Pas 2005]. Conventional viscosity measurement techniques do not allow the evaluation of viscous behaviour of glass-ceramic composites in its joining conditions; therefore this methodology is highly useful for the observation of viscosity changes with different filler additions to a glass matrix.

The viscosity of sealing materials plays a major role for the successful joining and the rigidity during operation. At joining temperature, sealants should not have too high viscosity because it causes a too thick seal and could avoid the contacting of cells. On the contrary, if the viscosity is too low, bead drops can be formed and leakage may occur due to non-ideal stress. The appropriate viscosity of sealants for joining process, for glass 87 at 850 °C, should be ≤ 10^6 dPa·s [Ley 1996] as well as at the operating temperature of SOFC, around 800 °C. The viscosity should also be more than 10^6 dPa·s [Con 2011] as otherwise the sealing materials are not rigid anymore, they will flow out of the joint gap which causes leakage as well.

On the basis of the relation between the temperatures measured by HSM and their corresponding viscosities, Scholze [Sch 1962] and Pascual [Pas 2001]; [Lar 2004]; [Pas 2005] defined the characteristic points of the viscosities according to DIN 51730:1984-05 [DIN 1984] and DIN 51730:1998-04 [DIN 1998], shown in Fig. 18.

a) First shrinkage point or sintering point is defined as the first temperature at which the pressed sample starts to shrink.
b) Maximum shrinkage point or densification point is the first temperature at which maximum shrinkage of the sample takes place before it starts to soften.
c) Softening point or deformation point is the first temperature at which the first signs of softening are observed. This is generally shown by the appearance or rounding the small protrusions at the edges of the sample. The sample shape factor has changed by 1.5 % with respect to the first image and the tracked corner angle has increased by 10 %. Spherical point is the temperature at which the sample becomes sphere. The height/width ratio of the sample must be at least one time between 0.9 and 1 (not less than 0.85). In addition, both corner angles must be greater than or equal 150° and the shape factor must be at least 0.8.
d) Half ball point or hemisphere point is the first temperature at which the section of the sample observed form a semicircle. The shape factor is at least 0.985 and the height of the test piece is half of its base width.
e) Flow point (DIN 51730:1984-05) is the first temperature at which test piece is melted to one-third of its original height.
f) Flow point (DIN 51730:1998-04) is the first temperature at which test piece is melted to one-third of its height at hemisphere temperature.

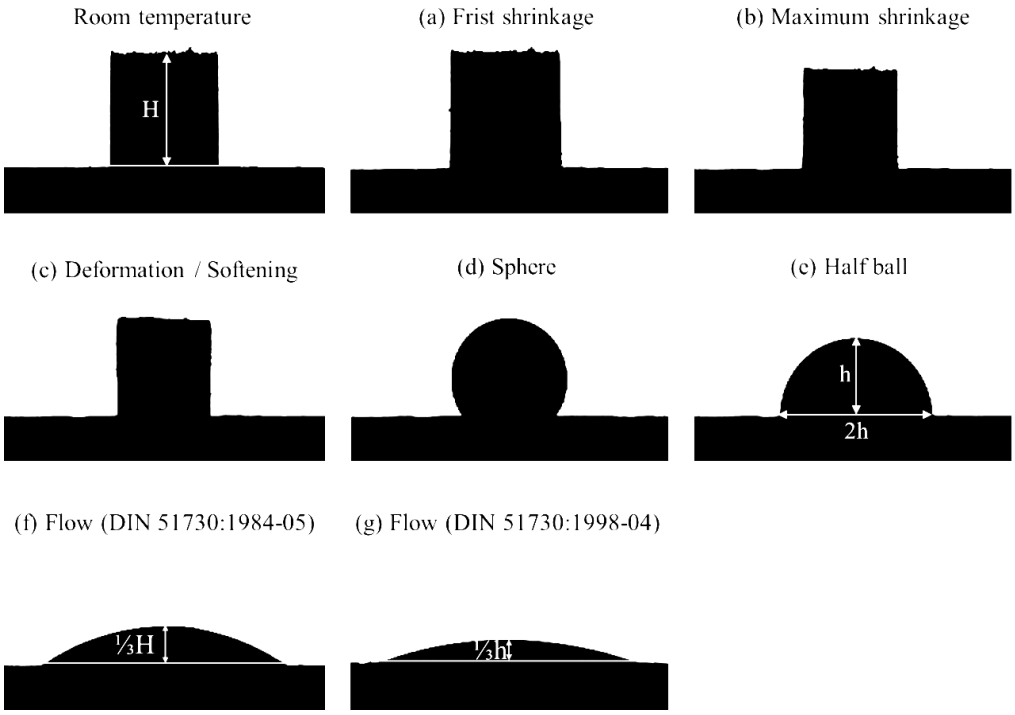

Fig. 18 Geometric shape corresponding to each fixed viscosity point [Pas 2001]; [Pas 2005]; [DIN 1984]; [DIN 1998]

As illustrated in Table 6, the fixed viscosity points determined based on two norms i.e. DIN 51730:1984-05 and DIN 51730:1998-04 which define the flow point in different meaning [Sch 1962]; [PAb 1997]; [Pas 2005]. In this study the softening temperature is defined to be the beginning of the joining temperature range. At this temperature the sealant is in estimated viscosity level of approximately $10^{6.3}$ dPa·s. The half ball temperature is the upper limit of the joining temperature range, which corresponds to a viscosity level of $10^{4.1}$ dPa·s. Above this temperature the glass sealant has too low viscosity and the sealant would flow, being squeezed out from the gap between the interconnector plates.

Table 6 Comparison of fixed viscosity points attained by HSM

	Corresponding viscosity log η / dPa·s		
Characteristic fixed points	**[Sch 1962]**	**[PAb 1997]**	**[Pas 2005]**
First shrinkage	10.0 ± 0.3	10	9.1 ± 0.1
Maximum shrinkage	8.2 ± 0.5	-	7.8 ± 0.1
Deformation / Softening	6.1 ± 0.2	6.8 ± 0.8	6.3 ± 0.1
Sphere	-	-	5.4 ± 0.1
Half ball	4.6 ± 0.1	4.5 ± 0.3	4.1 ± 0.1
Flow	4.1 ± 0.1	3.1 ± 0.3	3.4 ± 0.1

The effect of the filler materials on viscous behaviour of the glass-ceramic sealant (glass 87) could be observed by the HSM images and compared with fixed points defined by Scholze [Sch 1962] and Pascual [Pas 2001]; [Lar 2004]; [Pas 2005]. Using these points should be possible to plotted graphs with the linearized Vogel-Fulcher-Tammann (VFT) equation. The VFT equation is widely used for presenting viscosity of glasses. The viscosity level (*log* η) of a glass melt is presented in Eq. (2) with empirical fit constants. If three pairs of viscosity values (L_1,L_2, L_3) and temperatures (T_1, T_2, T_3) are known, the calculation of viscosities as a function of temperatures is possible. The constants T_0, A and B can be evaluated by three independent viscosity measurements i.e. (L_1, T_1), (L_2, T_2), (L_3, T_3) in a straight-forward way. This is conventionally performed at certain fixed points [Voe 1921]; [Ful 1925]; [Tam 1925].

$$\log \eta = A + \frac{B}{T - T_0} \qquad \text{Eq. (2)}$$

5.3. Dilatometry

In this work, dilatometric measurements were performed in a Linseis vertical two samples pushrods dilatometer model L75V (Germany) in order to obtain the coefficient of thermal expansion (CTE). Sintered bars were pressed in metal matrix with the dimensions of 40 x 5 x 5 mm and sintered on folded platinum foils, as shown in Fig. 19, which makes possible to remove the bars without damaging them. During the sintering process at 850 °C for 10 h with a heating and cooling rate of 2 $K \cdot min^{-1}$, the glass bars get soft and deform losing the bar shape. It is necessary to recover the geometrical shape needed for dilatometry measurements. The sintered samples are shaped by cut and polishing. The final samples have approximately rod shape with dimensions of 25 mm length and 6 mm diameter. Some of the samples were measured after annealing at 800 °C for 500 h to evaluate the CTE after crystallization.

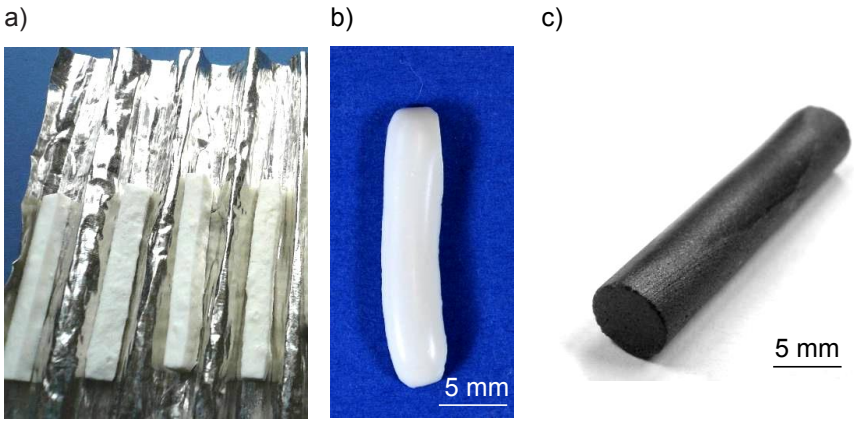

Fig. 19 Preparation of the samples for dilatometry measurement: a) pressed samples sintered in waved platinum foil; b) after sintering the glass bar is deformed; c) to obtain a precise measurement the sintered bars need to be reshaped by cutting and polishing to obtain 25 mm length, 6 mm diameter and parallel extremities

The measurements were performed with a heating rate of 3 $K \cdot min^{-1}$ and the furnace was turned off when the sample achieved the softening point. This heating rate was chosen for better reproducing the conditions in the stack ramp up phase.

Additionally due to the length of the glass sealant it is easier to observe the first sintering point, softening point, and T_g that can happens in a narrow temperature range, by using a low heating rate. The results were corrected with a zero measurement data to eliminate the influence of the device in the analysis, which means that all the samples measured in this device can be compared. Nevertheless there are still possible sources of errors during dilatometric measurements of glass, i.e. the glass samples cannot be heated up twice in most of the cases due to crystallization and geometrical changes of the sample. The dilatometer pushrods and/or the sample can change their positions slightly during the first heating and this can have an influence on the results. For most glasses the expansibility increases sharply within the transition range. If the CTE is reported up to a temperature only slightly below T_g(dil), the CTE value might be too high for comparison with other investigators.

5.4. Joining tests

In order to analyze the gas-tightness, sandwiched samples prepared with two steel plates of 50 mm × 50 mm size and thickness of 2.0 mm were joined with the glass-ceramic sealants, as shown in Fig. 20. One of the steel squares had a drill hole of 10 mm diameter in the center, which allows checking the gas tightness by He-leakage detection. These metallic sheets used in the sandwich samples and all the other experiments in this work was high chromium containing ferritic steel produced by Thyssen Krupp VDM and distributed under the name Crofer22APU [Cro 2010]. The surface of the alloy sheets was used as delivered or subsequently ground, polished, annealed in vacuum furnace and ultrasonically cleaned with ethanol and acetone to remove organic substances.

Cross-sections of the sandwich samples were analyzed by optical and scanning electron microscopy (Cambridge Stereoscan 360) with EDS (Oxford) at an operating voltage of 20 kV. In addition, this sample type was also used for high temperature electrical resistance measured by four-point method. Four platinum wires were spot welded in two corners of the upper plate and two corners of the lower plate.

The typical joining parameters of glass 87 and its composites was defined by previous work at ZEA-1, FZJ, and was maintained in this work at 850 °C, dwell time of

10 h, and heating and cooling rate of 2 K·min^{-1}. Some samples of each composite were annealed at 800 °C for 500 h after the joining process with the same heating and cooling rate from the first thermal treatment. The thermal treatments were carried out in electric resistive furnaces by Carbolite.

a) b)

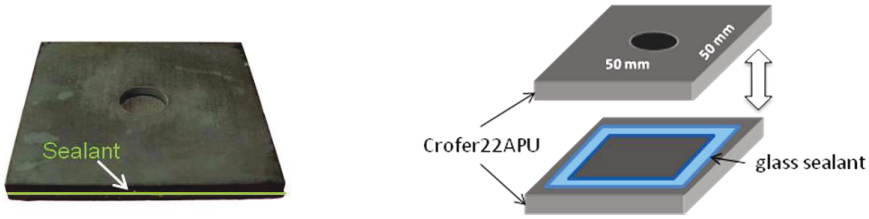

Fig. 20 a) Sandwich sample formed of two Crofer22APU plates of 50 x 50 mm^2 dimension joined by glass-ceramic sealant. b) Schematic view of a sandwich sample open with the applied sealant

5.5. Gas tightness test

The gas tightness of the samples was checked by helium leakage detection (UL200, Inficon) at a difference in pressure of 1000 mbar. The sandwich sample is placed with the hole side to a vacuum pump; after evacuation of the inner part of the sample, helium gas is released through a gas pistol around the outer side of the sample. A mass spectrometer in the helium detector device recognizes and counts the He molecules entering the sealed sample, further it calculates automatically the leakage rate using the Eq. (3).

$$q_L = \frac{\Delta(p \cdot V)}{\Delta t} \qquad \text{Eq. (3)}$$

where q_L is the leakage rate; p is the pressure or pressure variation in [mbar]; V is the volume or volume variation in [l] and Δt is a time period in [s]. Due to the unities from the parameters used in the leakage rate calculation, the leakage rate is expressed by mbar·l·s^{-1} [Pay 2000].

5.6. Four-point electrical resistance measurement

High temperature electrical resistance was measured by four-point method, using a fixed voltage of 5 V and heating up to maximum temperature of 800 °C in the 50 x 50 mm^2 sandwiched samples with spot welded platinum wires, as shown in Fig. 21. The device used in his work was in-house assembled and it's composed by an electric resistive furnace, four platinum wires that connect the sample to a transformer that will provide electrical powder to the sample and measure the output resistance.

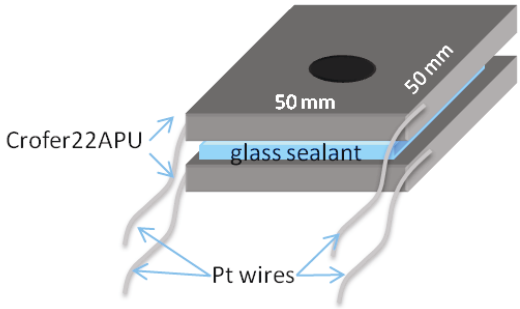

Fig. 21 Schematic drawing of sandwich sample prepared for the four-point electrical resistance measurement with spot welded platinum wires

Some samples were submitted to four-point electrical resistivity test on the pure sealant in cylinder shape as sintered and annealed. The measurements were done at the IEK-1, FZJ in an in-house developed device, from 600 °C to 850 °C, and the sample prepared for the measurement is shown in Fig. 22. For these four-point measurements the current was fixed, and the voltage was according to the ohmic resistance of the sample. Voltage values varied from 0.001 V to 12 V. The fixed currents were $\pm 1x10^{-6}$, $\pm 1x10^{-5}$, $\pm 5x10^{-5}$, $\pm 1x10^{-4}$ A for each testing point. At low temperatures these values cannot be reached because of the high ohmic resistance, instead it could only be given $1x10^{-9}$ or $1x10^{-8}$ A.

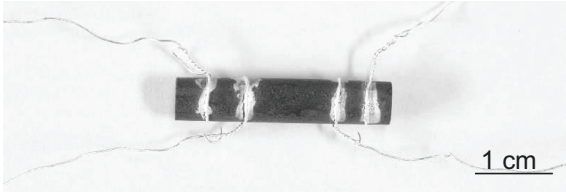

Fig. 22 Sintered bar sample prepared with silver paste and platinum wires for the four-point electrical resistance measurement

In order to evaluate the insulating function of the glass sealant the resistance of the glass needs to be compared with the internal cell resistance, according to maximum power transfer theorem.

To be able to calculate the current losses through the sealant it is necessary to assume that an SOFC is operated with a typical voltage of 0.7 V and current density of the cell is 1 A/cm². For the calculations in this work was considered that the Forschungszentrum Jülich SOFC stack design called F10, which is formed by cells with 10 cm by 10 cm area producing a current of 100 A. In the diagram of Fig. 23, power is transferred from the cell, with voltage U_{cell} here determined as 1.1 V and a fixed cell resistance of 0.4 Ωcm², to a total external load that consists in a real external load with resistance R_{load} and a parallel glass sealant resistance R_{glass}, resulting in a current of 100 A. By Ohm's law, the total internal resistance R is the cell voltage divided by the current, as shown in Eq. (4). The glass resistance is the measured value by the four - point method and calculated load resistance parameter, as shown in Eq. (5). Developing Ohm's law, as shown in Eq. (6), (7) and (8) is possible to find an equation where the current that pass through the glass sealant is expressed as function of the current that pass through the external load, Eq. (9). As lower the current that pass through the sealant the less current losses are happening in the circuit, which means the better is the glass sealant insulation.

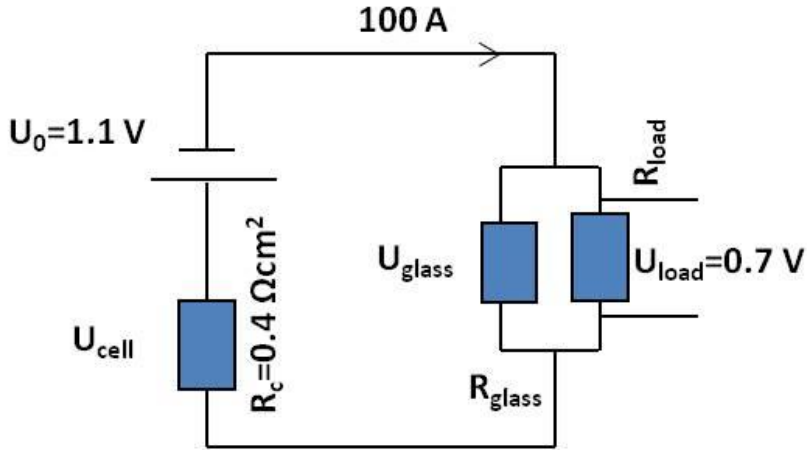

Fig. 23 Diagram of an electrical circuit of one solid oxide cell

$$R = \frac{U}{I} = \frac{0.7\ V}{100\ A} = 0.007\ \Omega \qquad \text{Eq. (4)}$$

$$\frac{1}{R} = \frac{1}{R_{glass}} + \frac{1}{R_{load}} \quad \rightarrow \quad R_{load} = \frac{1}{\frac{1}{R} - \frac{1}{R_{glass}}} \qquad \text{Eq. (5)}$$

$$0.7\ V = R_{glass} \cdot I_{glass} \qquad \text{Eq. (6)}$$

$$0.7\ V = R_{load} \cdot I_{load} \qquad \text{Eq. (7)}$$

$$R_{glass} \cdot I_{glass} = R_{load} \cdot I_{load} \qquad \text{Eq. (8)}$$

$$I_{glass} = I_{load} \cdot \frac{R_{load}}{R_{glass}} \qquad \text{Eq. (9)}$$

For example considering the F10 design with a joining gap of 0.03 cm and joining area of 84 cm², and a glass resistance R_{glass} measured of 128.5 Ω, the current that pass through the glass sealant is $5 \cdot 10^{-5}$ times the current that pass through the real load, as shown at Eq. (10) and (11). This value means that a current lost by the sealant is on the range of 0.0001 %, that can be negligible.

$$R_{load} = \frac{1}{\frac{1}{0.007} - \frac{1}{128.5}} = 0.007\ \Omega \qquad \text{Eq. (10)}$$

$$I_{glass} = I_{load} \cdot \frac{0.007}{128.5} = 5 \cdot 10^{-5} \cdot I_{load} \qquad \text{Eq. (11)}$$

5.7. Glass paste and application methods

Two application methods of glass sealant on steel substrate were used in this work: extrusion by robot dispenser and screen printing, as shown in Fig. 24. The dispenser method is used since the beginning of SOFC stack assembling activities in ZEA-1 and in this work was used for the preliminary experiments. The high speed and consequently lower costs of the printing process obtained by screen printing motivated

the further development of this technique for the SOFC stack sealant application, which is the reason of current optimization process and utilization of this method in this work.

a) b)

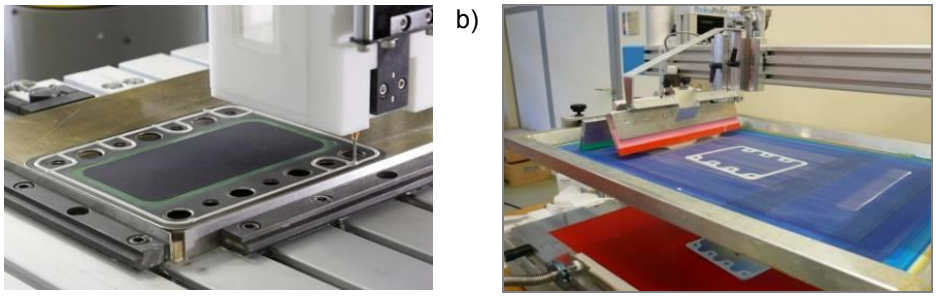

Fig. 24 Glass sealant application methods: a) robot dispenser; b) screen printing

Significant differences can be found on the paste preparation for each of the application methods to achieve certain paste viscosity for obtaining a specific layer thickness. Variations in the amount of organic binder solution and addition of additives to change viscosity and sintering properties can produce a final sealant with low porosity or cracks. The recipe of binder solution for the robot dispenser used at ZEA-1 of the FZJ is ethyl cellulose dissolved in terpineol, while the binder solution, called BM12, as component of the pastes for screen printing used in this work was composed of a solvent mixture of butyl glycol acetate, texanol, and α-terpineol and ethyl cellulose. The organic system of the screen printing paste was based on a multicomponent mixture of polymers with different melting characteristics to spread the decomposition over a wider range of temperature [Her 1991].

In order to achieve thinner or thicker printed layers by screen printing, one of the most important parameters is the screen. Particularly thinner layers were obtained with screen that had 12 wires per cm in this work, with wire diameter of 250 µm, and 30 µm undercoating (emulsion over mesh, EOM), whereas the screen used for thicker green layer, had 10 wires per cm, wire diameter of 300 µm, and 100 µm undercoating (EOM).

The composite pastes were prepared by adding the glass powder to the binder solution, homogenizing it by hand mixing and slowly adding the filler powder. The final homogenization was done by applying an ultrasound finger for 1 minute. Filler particles agglomeration could be avoided with this method. Rheological test were carried out to evaluate the paste printability. The optimal viscosity for the screen printing pastes was found at 100 seconds of around 30-40 Pa·s depending on the paste.

5.7.1. Rheological testing

5.7.1.1. Test at controlled shear rate (CSR mode)

With this measuring method, the rotational speed is preset at the rheometer, and the shear rate is calculated based on the gap and the rotational speed (or circumferential speed of the shearing area). The flow resistance moment (or the shear force) of the braking, tough material under investigation is measured. This torque is converted into the rheological parameter of shear stress using the shear area A of the measuring system. The dynamic viscosity is calculated from the shear stress and shear rate [Mal 2008]; [Lin 2008].

5.7.1.2. Plate-plate measuring systems

The plate-plate measuring system consists of two parallel plates. It is characterized by the plate radius and the variable distance between the places, as shown in Fig. 25. The material under investigation is disposed between the two plates. DIN 53018 specifies that the plate distance shall be much smaller than the radius of the measuring plate. Plate-plate measuring devices are used if the material under investigation contains large filler particles. The gap should be determined such that it is at least five times as large as the largest particles contained in the material. The shear rate is not constant across the entire plate radius, like in the cone-plate system, but there is a relatively large shear rate range. The shear rate in the center of the upper measuring plate is zero. The specified shear rate is always that related to the outer radius of the measuring plate, that is the maximum shear gradient. At a constant angular speed or rotational speed, if the plate distance is increased the shear rate in the measuring gap will fall [Mal 2008]; [Lin 2008].

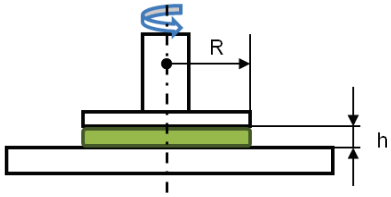

Fig. 25 Schematic draw of plate-plate viscosity measuring system. R is the radius of the measuring plate and h is the gap between the upper and lower measuring plate

5.8. Glass-ceramic sealant reinforcement

The state of the art development of glass-ceramic composite sealants at the Forschungszentrum Jülich is based on three composites of glass 87 with reinforcement of 20 wt.-% YSZ particles, 13 wt.-% YSZ fibers, and 20 wt.-% silver powder. Further characterization of these composites was done in this work, such as dilatometry of annealed samples, high temperature electrical resistance and mechanical tests. Furthermore these three composites were tested in a multilayer configuration, as already described.

Inspired by the good achievements of first reinforced sealants, new composites were proposed using the same glass matrix, glass 87, with the addition of alternative metallic and ceramic particles. The metallic particles were chosen according to ductility, considering cost limits, therefore the chosen fillers were copper, nickel and nickel-chromium alloy (NiCr 80-20). The ceramic particles tested were chemically and physically, CTE, compatible with the glass matrix not reacting or dissolving in the glass phase. These fillers were $Ce_{1-x}Gd_xO_{2-x/2}$ (CGO), being x equal to 10 mol% and 20 mol% Gd and montmorillonite for being a mineral with plasticity. The filler materials properties are shown in Table 7, the price of a kg of the metal fillers were found in the daily quotation [Ben 1979]; [Mor 2010]; [Sig 2012]; [Nan 2012]; [Mat 2012]. In order to evaluate the influence of the filler material in the sealant a complete set of characterization have been done for the composites as well for the pure glass matrix, such as dilatometry analysis, joining tests, microstructure analysis, and mechanical tests.

Copper metal powder, produced by former Norddeutsche Affinerie AG currently Aurubis AG, was used in 5 and 25 wt.-% in glass matrix 87. In parallel, composites were prepared containing nickel, produced by Riedel-de Haen AG. Initially five compositions containing nickel were tested: 1, 5, 25, 50 and 75 wt.-% Ni. The use of nickel chromium alloy as filler material for glass sealant was previously reported as improving the CTE and maintaining the electrical resistance at high temperatures sufficiently high [Con 2005]. Therefore the addition of NiCr (80-20) particles, produced by HCST Ampersint, was tested with 10 and 20 wt.-% in glass matrix 87 as well.

For the ceramic reinforcement of glass 87, 20 wt.-% of a powder of commercial montmorillonite produced by Sigma Aldrich was used. Gadolinium-doped ceria ceramic powders have a relatively high CTE of above 12 x 10^{-6} K^{-1} at 800 °C, as shown in

Fig. 26 [Hay 2000], having similar properties concerning stability at high temperature as the YSZ. These materials are already used as part of the components in the SOFC as electrolyte functional layer, substituting YSZ, which makes it a good candidate as filler for the sealant. Two types of CGO were tested, both synthesized in FZJ, one with 10 mol % Gd dopant (CGO10) and the other 20 mol% Gd dopant (CGO20), in order to evaluate possible differences in between them, for example in the crystallization of the glass or in the mechanical strength.

Table 7 Comparison of the filler materials properties [Ben 1979]; [Mor 2010]; [Sig 2012]; [Nan 2012]; [Mat 2012]; [Thy 2013]; [Wsj 2013]; [Tax 2013]; [Fue 2013]

Basic materials properties	**Ag**	**Cu**	**Ni**	**NiCr (80-20)**	**CGO10**	**CGO20**	**YSZ**	**Mont-morillonite**
Crystalline structure	FCC	FCC	FCC	__	FCC	FCC	Fluorite	Monoclinic prismatic
CTE (µm/m·K at 20 °C)	19.0	16.5	13.3	13	12	12	10	__
Density (g/cm³ at 20 °C)	10.5	8.9	8.9	8.3	7.2	7.2	6.1	2-3
Cost (€ per kg)	741.44	6.2	13.7	12.3	1100	1100	230	100
Young's modulus (GPa)	72	140	207	214	200-240	190-230	220-260	__
Tensile strength (MPa)	150-360	220-320	380-620	730	__	__	__	__
Yield strength (MPa)	55	50-270	100-480	350	__	__	__	__

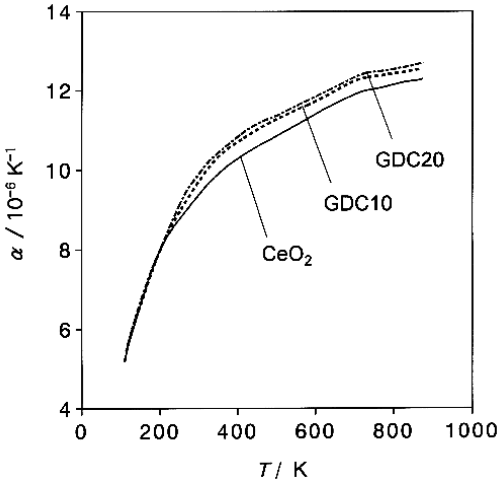

Fig. 26 Thermal expansion coefficient of CeO_2, GDC10 (CGO with 10 mol% Gd) and GDC20 (CGO with 20 mol% Gd) [Hay 2000]

5.9. Multilayer concept

The multilayer concept, as shown in Fig. 27, is an attempt to combine sealant layers with distinct reinforcement mechanisms, specially improved by the metallic filler additions, and electrical insulation properties, layers without metallic fillers. Each specific layer of the multilayer concept is formed by a composite type. Glass 87 was reinforced with following fillers: YSZ particles stabilized with 13 mol% Y_2O_3 by United Abrasives Inc. (North Windham, USA), YSZ fibers stabilized with 10 mol% Y_2O_3 produced by Zircar Zirconia Inc. (Florida, USA), and silver particles supplied by Alfa Aesar GmbH & Co.KG (Karlsruhe, Germany). These composites were already studied in previous research [Gro 2006]; [Gro 2010]; [Gro 2011]; [ZHa 2011]. Therefore they were used in defined possible combinations of layers, as shown in Table 8, and were always prepared two samples.

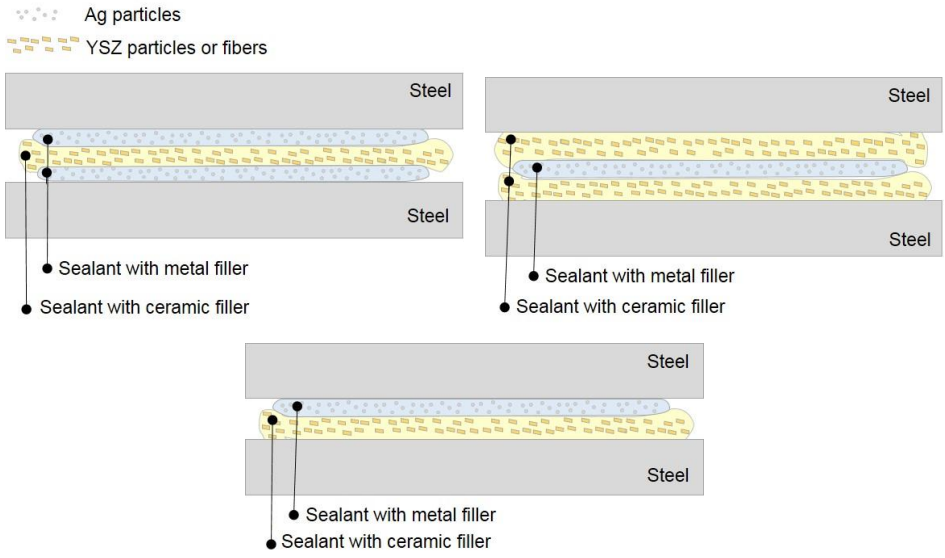

Fig. 27 Multilayer sealant designs

Table 8 The multilayer possibilities

Sample type	Layer 1	Layer 2	Layer 3
Double layer	YSZ fiber	Ag	----
	YSZ particle	Ag	----
Triple layer	YSZ fiber	Ag	YSZ fiber
	Ag	YSZ fiber	Ag
	YSZ particle	Ag	YSZ particle
	Ag	YSZ particle	Ag
	Glass Matrix	Ag	Glass Matrix
	Ag	Glass Matrix	Ag

Multilayer glass-ceramic sealants were formed by screen printing technique. In order to prepare different layer thickness and wider or thinner geometries two screens were used for the two types of composites, which was necessary for the insulation concept. The screen used with the composite containing metal particles was 5 mm wide and the other 8 mm wide for the composite containing ceramic particles or fibers.

5.10. Strength measurements

Three approaches have been investigated in this work to improve the evaluation of toughness of the glass sealants. The methods used were adaptation of tensile strength, shear test and torsion test.

5.10.1. Tensile strength

A test method was developed in ZEA-1 to test tensile strength of the glass-ceramic joints at room temperature with a high sensitivity of the method and good reproducibility of the results [Gro 2011]. Adaptors were constructed with carabiners, as a second adaptor's generation, allowing the axial adjustment of the circular butt joint

sample to prevent bending moments and failure of the brittle samples before the measurement, as shown in Fig. 28.

In order to investigate the tensile strength properties, circular butt joints of two Crofer22APU plates of an outer diameter of 36 mm were joined with the composite sealants. The steel circles were ground using BN grit (125 µm), and both of them had an internal thread of 8 mm in the centre. For the application of the glass, the powder was blended with an organic media solution, binder solution BM12, forming a screen printing paste. The paste was applied by screen printing to the steal surface. Before printing the glass, the steel samples were cleaned with ethanol in an ultrasonic bath for 10 min and subsequently rinsed with acetone. The glass paste was applied with a ring contour of 32 mm external diameter and 12 mm internal diameter to one of the metallic circles. In order to maintain a minimal joining gap, small zirconia chips of a thickness of 0.14 mm were put on the uncoated outer part of the steel plate.

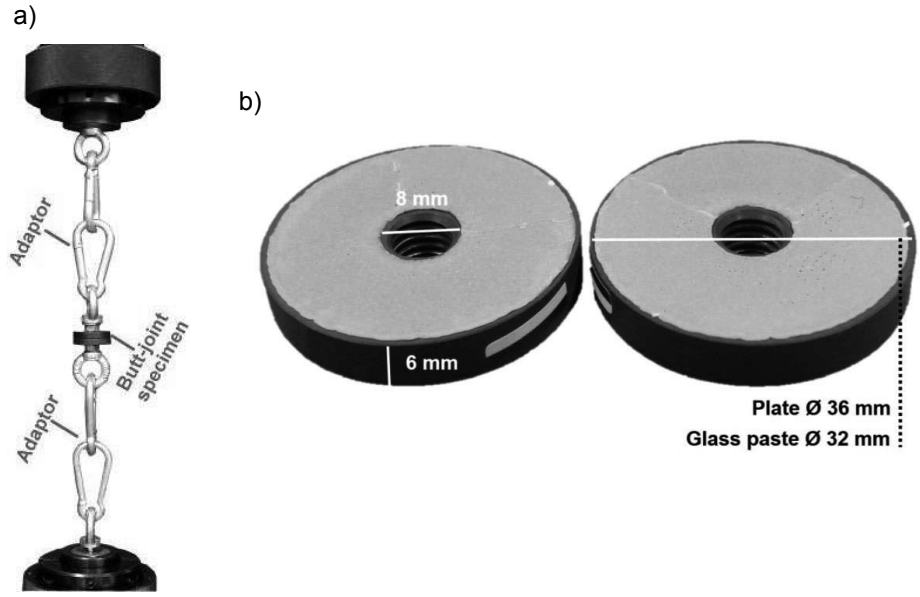

Fig. 28 Tensile strength test: a) measurement set-up with adaptors and specimen assembled in universal machine; b) tested butt-joint open sample

The joining of the sample was carried out by placing a dead load of 1000 g on top of the second steel plate and heating up to 850 °C with a dwell time of 10 h in a

resistance heated chamber furnace in air. The samples were cooled to room temperature at a rate of 2 K min^{-1}. Some samples were additionally annealed at 800 °C for 500 h. For the tensile strength measurement, ten samples of each materials combination were positioned by the adapters to a universal testing machine with a maximum test range up to 500 kN and were disrupted with a load sensor of 10 kN and a traverse of 2000 µm. One of each sample combination was epoxy-mounted and sectioned for SEM analysis of the interfaces.

5.10.2. In-house shear test set-up development

In the present study, the joints strength was investigated at room temperature by bond tester Dage 4500, Nordson DAGE (Aylesbury, UK). The schematic draw of this shear test work principle is exposed in Fig. 29. The wedge moves in parallel direction to the substrates and the joint to push the upper substrate till it breaks off. The tear at the sealant occurs due to shear stress. The bond tester machine measures the total force taken into the upper steel plate. After testing, the joint areas were measured in order to calculate the specific joining area. As described in the Eq. (12) and the joint strength will be calculated from the input force divided by the sealant coated area.

a)

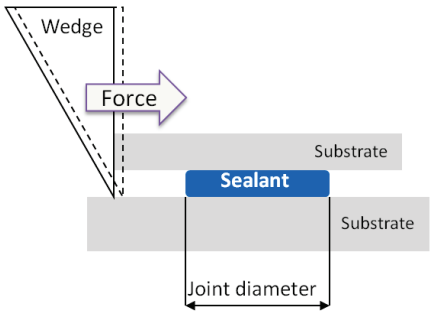

b)

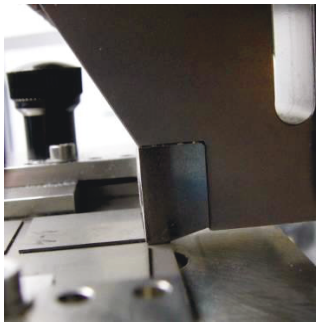

Fig. 29 Principle of shear test: a) Schematic draw from joint shear test; b) Shear test machine in the start of a measurement, wedge touching the sample to be measured

$$shear\ strength = \frac{F}{A} \qquad \text{Eq. (12)}$$

The sample was prepared by squeezing the sealant paste, same as used in the sandwich samples, through a template onto Crofer22APU plates. After drying in a heating chamber at 60 °C for at least 2 h the plate was assembled in a joining device and covered by a larger Crofer22APU plate and put a load of 800 g on top. The joining of the samples follow the same heat treatment as already described for the joining test samples. In order to obtain accurate results, 16 samples of each type of materials were tested.

5.10.3. Torsion test developed by Politecnico di Torino

The DISMIC (Dep. of Material Science and Chem. Engineering) of Politecnico di Torino (Italy) in cooperative work with Oak Ridge National Laboratory (USA) and Kyoto University (Japan) had developed a modified torsion test as an alternative to asymmetrical four-point bending test to measure pure shear strength of the joints, as shown in Fig. 30. A miniature hourglass shaped sample and torsion test equipment were designed and built at Politecnico di Torino and in the other partners' facilities. The method was tested with steel miniature samples bonded with epoxy and silicon carbide components joined by glass-ceramic demonstrating that it was possible to obtain pure shear strength values in both cases [Fer 2012a]; [Fer 2012b].

a) b)

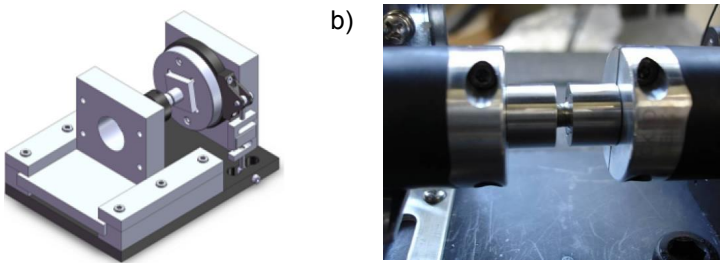

Fig. 30 Torsion machine set up: a) general view; b) details on the sample holder [Fer 2012a]

Miniaturized hourglass shaped joint samples had joining surface of 5 mm diameter. This size of hourglass sample had to be used due to the dedicated equipment designed and built at Politecnico di Torino for torsion tests. Originally this equipment was fabricated for purpose of neutron irradiation studies. In addition, studies showed that the best compromise for specimens' type is the hourglass-shaped samples, having a reduced circular joined area and an easy-to-clamp cross section [Fer 2012a]; [Fer 2012b]. In this study the hour-glass shaped samples were manufactured from chromium ferritic steel, Crofer22APU, and joined with glass-ceramic composite pastes at ZEA-1, FZJ, and the torsion tests were collaboratively carried out by DISMIC.

The sealant pastes were prepared using 20 wt.-% of organic binder system based on terpineol, ethylcellulose and additives (the same binder system used for screen printing), and glass matrix 87 powder with additions of filler materials. Using a template, the layer of composite paste was applied on Crofer22APU hourglass shaped parts surface. To achieve a joining gap of 0.2 mm, corresponding to the joining gap existing in real application, it was necessary to print one paste layer on each half- sample and to control the weight of each single piece. Furthermore the samples parts were dried in heating chamber for 2 hours and disposed in a samples holder, as shown in Fig. 31. The samples holder had the function of holding the samples in position during the joining, as well as allows a dead load application, corresponding to the joining procedure of a SOFC stack. According to previous studies on this glass matrix [Gro 2006] [Gro 2011], the joining was performed at 850 °C for 10 hours with heating and cooling rate of 2 $K \cdot min^{-1}$. On top of the samples holder was applied a dead load of 1600 g. The green layer and the joint thickness were controlled by measurements using a micrometer.

a) b)

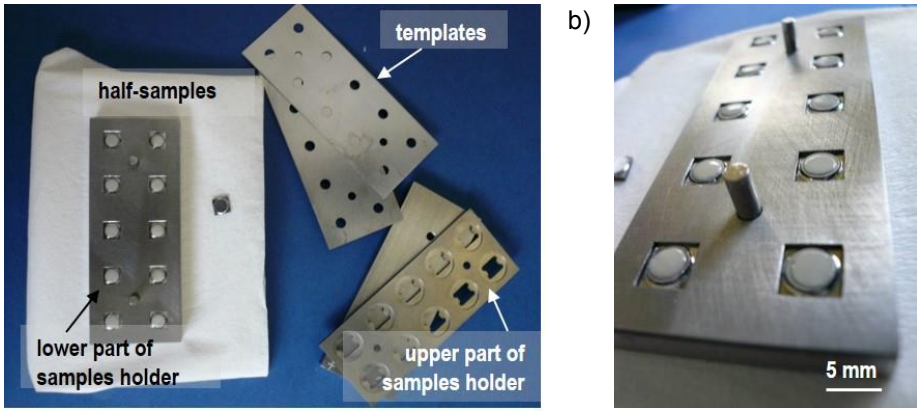

Fig. 31 Samples holder and printed miniature hourglass shaped samples. a) templates, samples holder and joining pieces; b) lower part of the samples holder with printed half-samples

6. Results and discussion

6.1. Alternative filler reinforcement evaluation

6.1.1. Feasibility investigation

The preparation of composites was systematically analyzed by testing the interaction of both components. Pellets with a diameter of 3 mm, as shown in Fig. 32, were pressed with a hand press and sintered at 850 °C for 10 h with a heating and cooling rate of 2 °C·min^{-1}. In addition to the fillers already tested (Ag and YSZ particles and fibers), three ductile metallic particles, Cu, Ni, and NiCr (80-20), and three ceramic particles, montmorillonite and gadolinium-doped ceria (CGO) with 10 mol% Gd and 20 mol% Gd, were evaluated as reinforcements for the glass matrix 87. These materials were chosen either by their plasticity, i.e. ductile particles and montmorillonite, or due to their high CTE and compatibility with the other components of the SOFC stack, i.e. CGO particles.

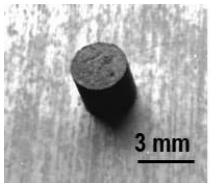

Fig. 32 First feasibility investigation analyzing the interface between sintered pressed pellets of the composites and Crofer22APU substrates

6.1.1.1. Copper

The particle size distribution of the copper particles were measured as D_{10} = 11.2 µm, D_{50} = 21.5 µm, and D_{90} = 39.8 µm. The Cu particles were dissolved in the glass matrix, where they reacted and formed crystalline phases other than those observed in the pure glass (see Fig. 33a). A barium-rich phase was formed at the interface of the composite containing 5 wt.-% Cu with Crofer22APU, as shown in Fig. 33b. The increase in the filler amount to 25 wt.-% Cu provoked more changes in the microstructure of the glass-ceramic composite with the appearance of new phases containing Cu, as shown in Fig. 34 and by EDS results in Table 9. As this filler material

did not fulfill the expectations and reacted strongly with the glass, no further experiments were performed with Cu particles.

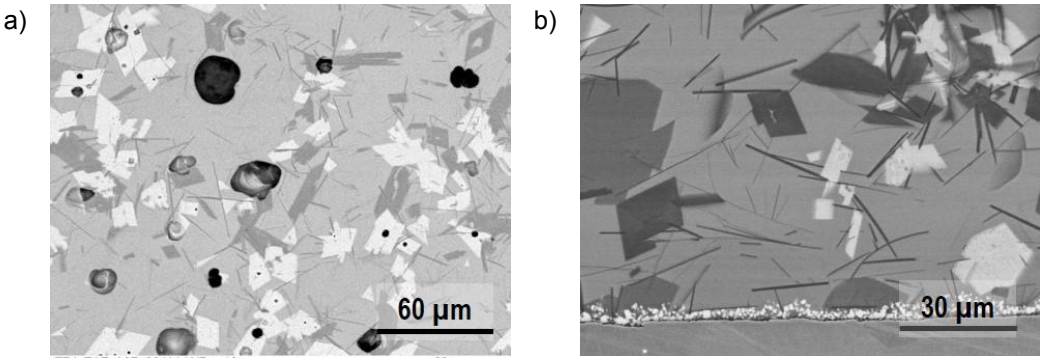

Fig. 33 SEM image of: a) pure glass 87; and b) glass 87 with 5 wt.-% Cu

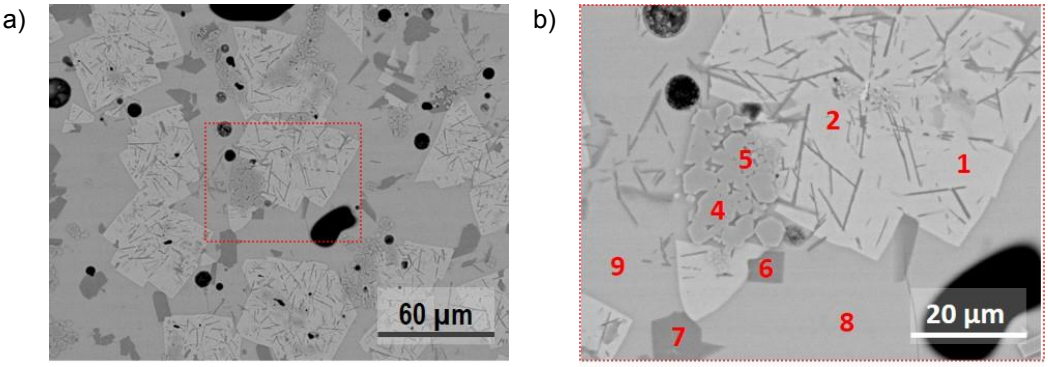

Fig. 34 Glass 87 with 25 wt.-% Cu filler a) microstructure overview; and b) detailed microstructure showing different crystalline phases, marked points analysed by EDS

Table 9 EDS point analysis of composite with 25 wt.-% Cu particles shown in Fig. 35. Results in atom%

Point	O	Al	Si	Ca	Cu	Zn	Ba	Observation
1	71.3		10.9		11.7		6.1	Light color phase (Ba-Cu-Si)
2	70.6		11.1		12.0		6.3	
3	70.6		11.3		11.8		6.3	
4	62.9				37.1			Agglomerate (Cu)
5	63.4		0.3	0.2	35.4	0.2	0.5	
6	74.0	8.7	10.6		0.6	0.5	5.6	Dark gray phase (Ba-Si)
7	74.1	8.7	10.6	0.2	0.4	0.4	5.6	
8	74.0	0.9	7.2	5.0	3.8	2.1	7.0	Remain glassy phase (Ba-Si-Ca-Cu-Zn-Al)
9	74.2	0.7	7.2	5.0	3.5	2.2	7.2	

6.1.1.2. Nickel

Nickel particles were initially tested in five concentrations. The composites contained 1 wt.-%, 5 wt.-%, 25 wt.-%, 50 wt.-%, and 75 wt.-% Ni in glass 87 matrix. The particles had a measured particle size distribution of D_{10} = 5.7 µm, D_{50} = 11.7 µm, and D_{90} = 35.7 µm. As a ductile particle, the nickel was expected to increase the toughness of the composite. Furthermore, its high CTE of 13.4 x 10^{-6}/K at room temperature meant that it was expected to contribute to the CTE optimization of the glass sealant depending on the amount of filler added.

An increased amount of Ni particles in the composite provoked more oxidation reactions and enhanced the composite porosity, as shown in Fig. 35. More nickel particles also influenced the crystallization of the glass matrix. The composite containing 1 wt.-% Ni was very similar to the sample with 5 % Ni: no significant oxidation of the nickel grains was observed. The progressive growth of the oxidation layer in the nickel particles follows the increasing amount of particles, as shown in Fig. 36, which was analyzed by EDS line scans. By EDS line scan, it was possible to measure the oxidized layer thickness. For the sample with 50 wt.-% Ni, the particles were already entirely oxidized. The same effect was observed for the sample with 75 wt.-% Ni. The oxidation layer around the Ni particle was minimal until the addition of 25 wt.-% Ni and there was no reaction between the glass matrix and the fillers. Therefore, in concordance with the results, further joining tests, dilatometer analysis, and strength tests were conducted with 10 wt.-% and 20 wt.-% Ni particles only.

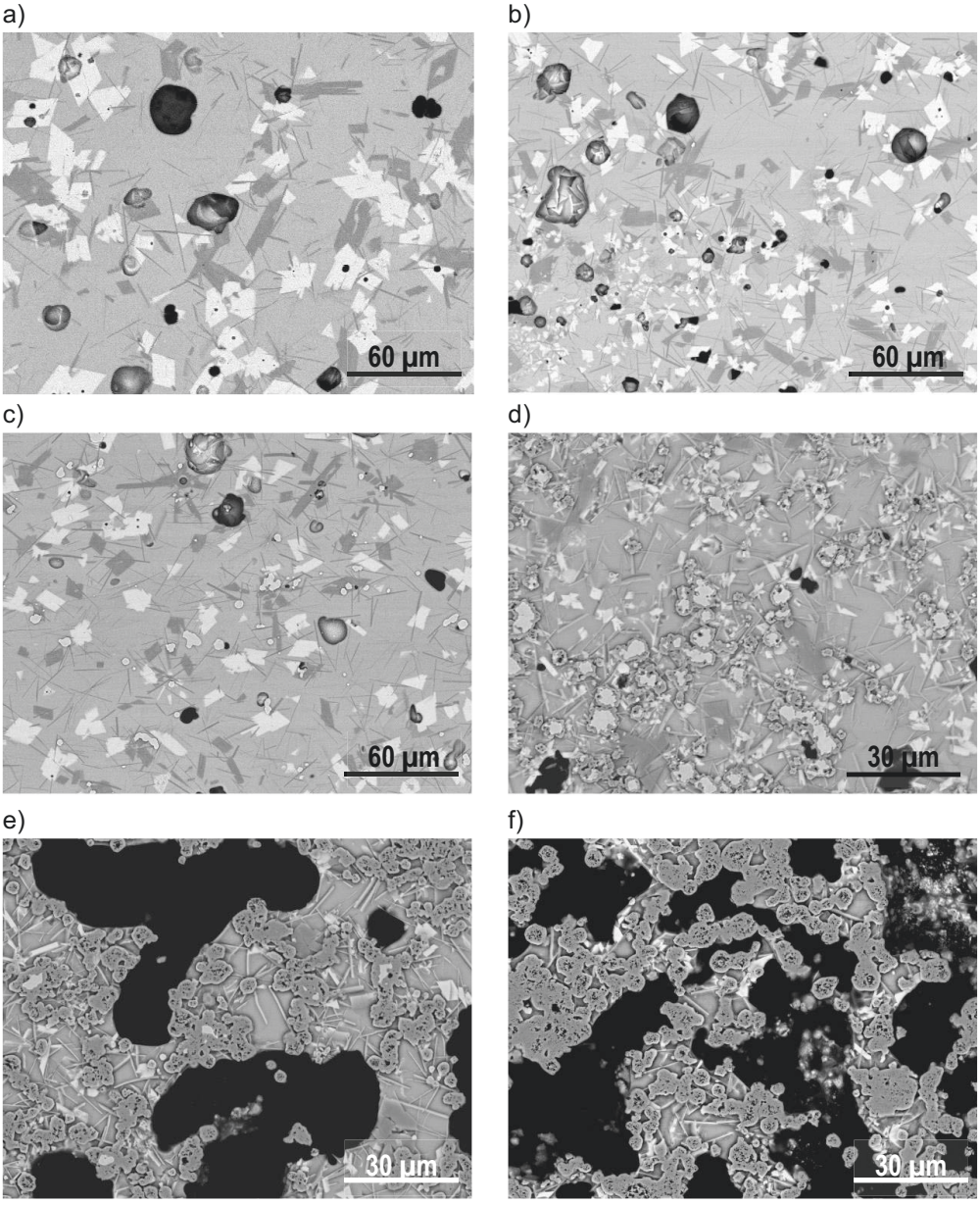

Fig. 35 Microstructure of glass 87-Ni composites as joined. Filler in wt.-% from a to f: 0, 1, 5, 25, 50 and 75

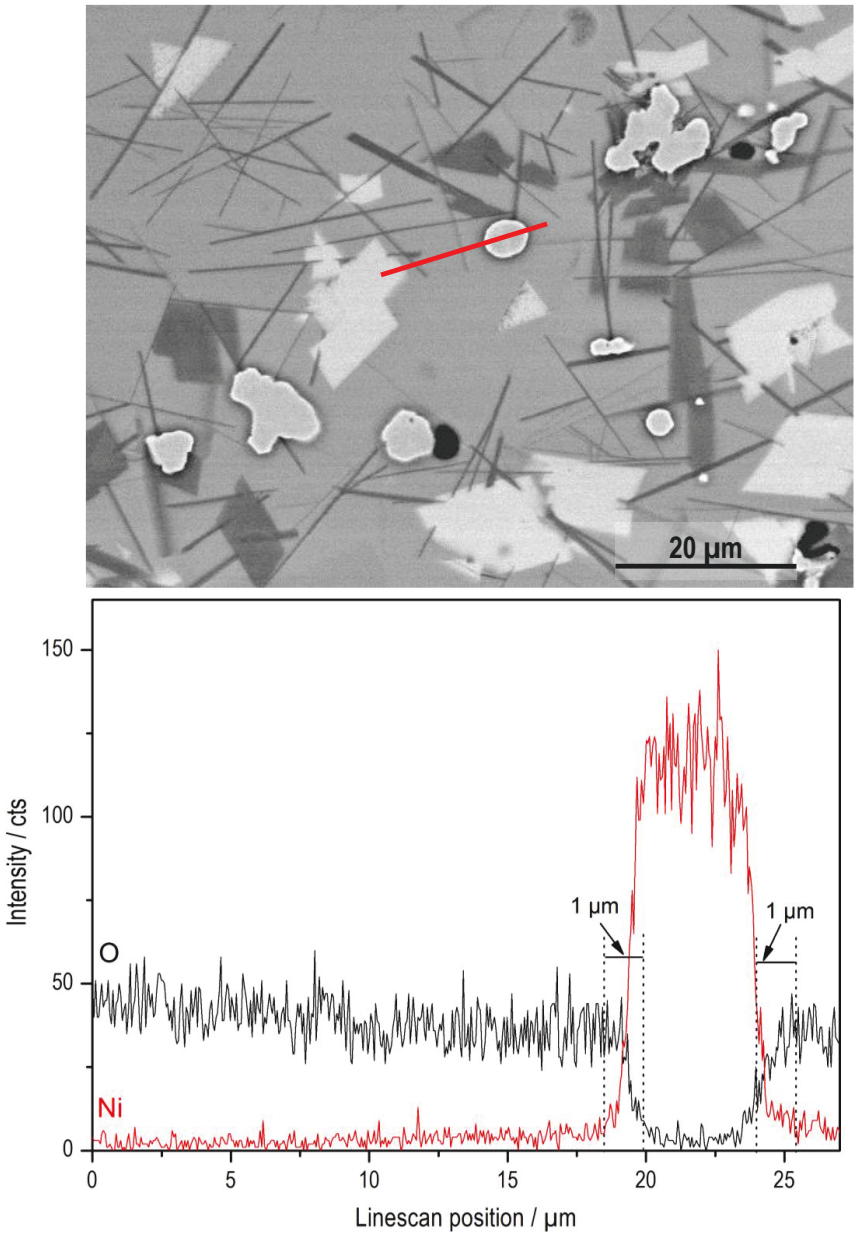

Fig. 36 a) Thickness of oxide layer formed around the nickel particles in the 5 wt.-% Ni composite; measured by EDS line scan

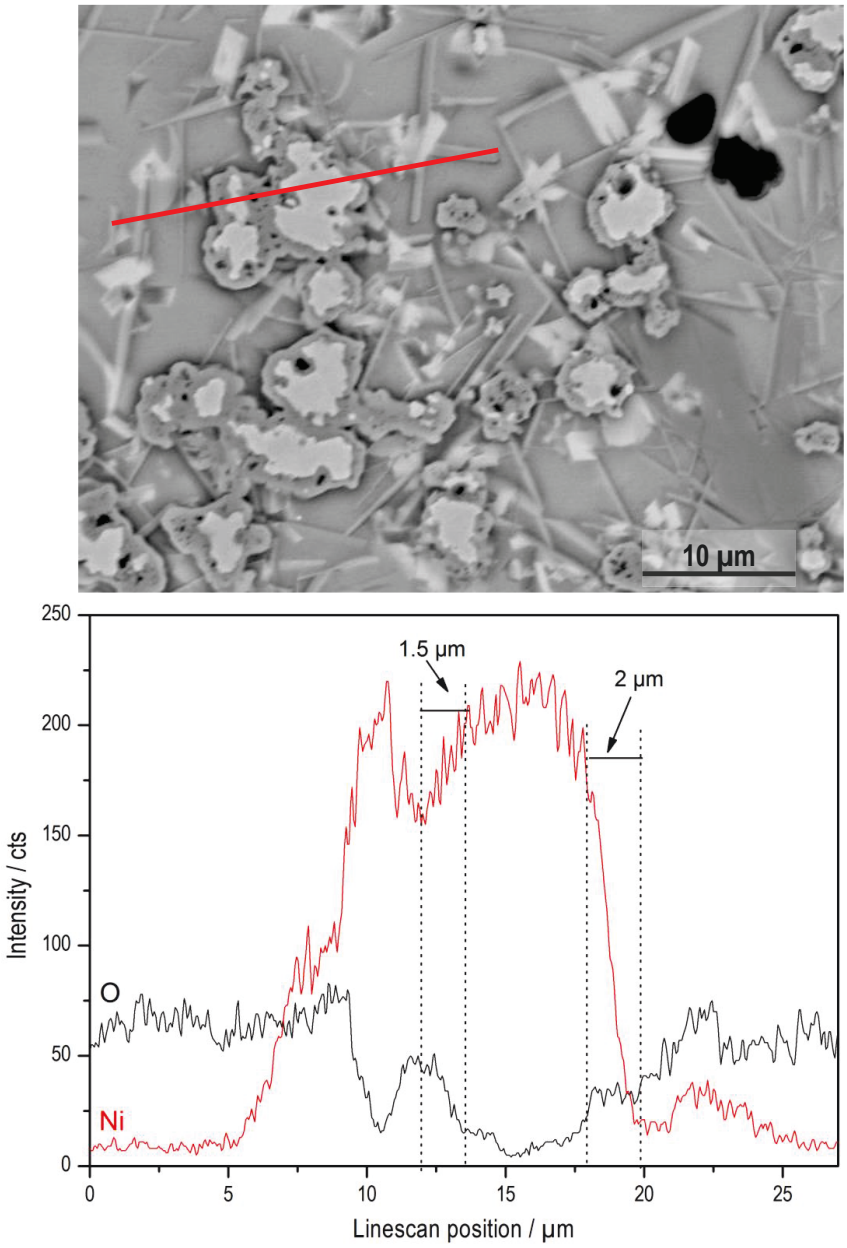

Fig. 36 b) Thickness of oxide layer formed around the nickel particles in the 25 wt.-% Ni composite; measured by EDS line scan

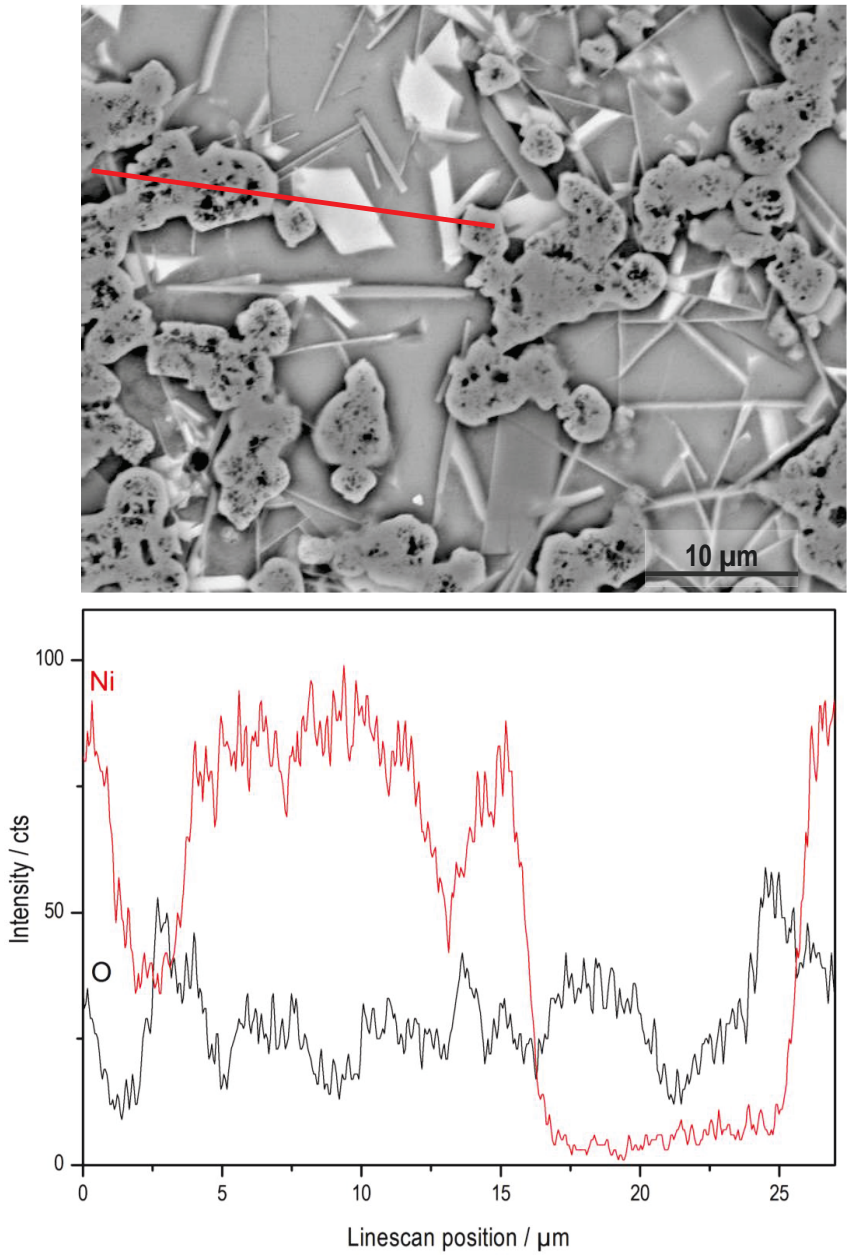

Fig. 36 c) Thickness of oxide layer formed around the nickel particles in the 50 wt.-% Ni composite; measured by EDS line scan

6.1.1.3. Nickel Chromium - NiCr (80-20)

The use of a nickel chromium alloy as a filler material for glass sealant was previously found to improve the CTE and maintain the electrical insulation at high temperatures, making it sufficient for the sealant [Con 2005]. The composites formed with particles from the alloy NiCr (80-20), produced by HCST Ampersint, were tested in combination with glass matrix 87 and additions of 10 wt.-% and 20 wt.-%. Good dispersions of the filler were achieved in the pellets, and no strong oxidation was observed for the standard joining procedure. In the bulk material, no advanced oxidation of the particles was found, and the matrix was highly crystallized, as shown in Fig. 37a. However, the closest particles to the interface with the air degraded and reacted with the barium-calcium silicate glass, forming undesirable barium chromate (the lighter gray phase shown in Fig 37b). As barium chromate also formed after thermal treatment in the joining process, it was decided to pursue further investigations with a reduced amount of NiCr particles of about 10 wt.-%.

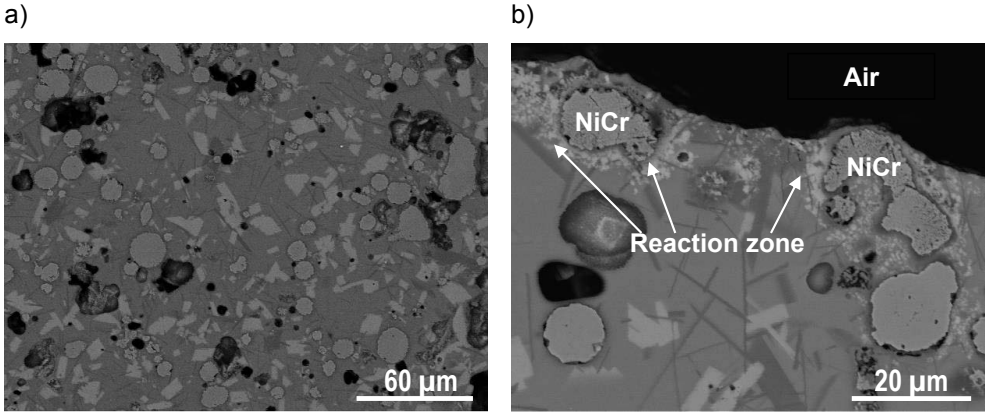

Fig. 37 SEM image of glass 87 with 20 wt.-% NiCr added to glass 87 matrix: a) bulk sealant in the center of the sample cross section; b) outer part of the sealant, interface with air, with the formation of barium chromate (light gray)

6.1.1.4. Montmorillonite

The montmorillonite, which is an aluminosilicate in plate-like structures, provoked increased crystallization. The samples containing 20 wt.-% filler were completely crystallized after the joining procedure, and diffusion of Na and K occurred from the particles to the glass matrix (see Fig. 38). These alkali elements were found in the crystalline phases by EDS analysis combined with SEM. Because of the alkali diffusion, undesirable elements in SOFC sealants, and fast crystallization, this filler was considered an inadequate choice for this application.

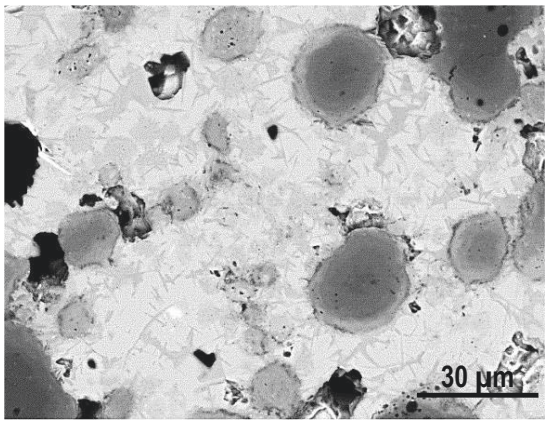

Fig. 38 SEM image of highly crystallized composite sample thermally treated at 850 °C for 10 h, composed of glass 87 with 20 wt.-% Montmorillonite

6.1.1.5. Gadolinium-doped ceria – CGO

Both types of CGO presented similar microstructures after joining, with good distribution of filler all over the glass matrix and no strong influence on the crystallization of the glass matrix. Moreover, no interaction was found between the CGO particles and the glass matrix after the joining process (shown in Fig. 39), which makes these particles good candidates for further tests.

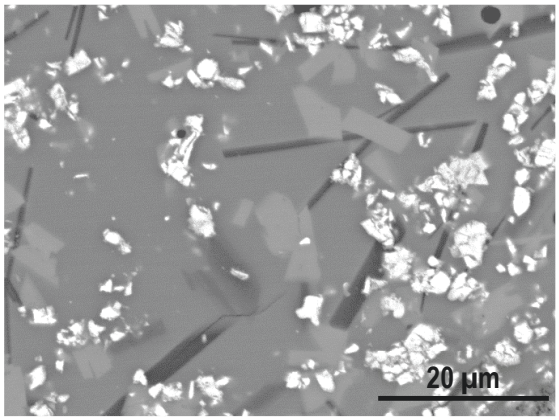

Fig. 39 Good dispersion of 20 wt.-% CGO particles in glass matrix 87. No interface or reaction zone formed between the filler and glass

6.1.1.6. Coefficient of thermal expansion – CTE

The coefficients of thermal expansion (CTEs) of all composites were measured by dilatometry using bars previously sintered at 850 °C for 10 h with heating and cooling rates of 2 °C·min^{-1} as well as bars that were annealed at 800 °C for 500 h after sintering. The results shown in Table 10 indicate that the composites, except the composite containing YSZ fibers, maintained CTEs that were higher than those of the pure glass 87 in the sintered and annealed states. This can be explained by the fact that the CTEs of the single fillers are considerably higher than the CTE of the pure glass 87, while YSZ typically has a CTE around 10 x 10^{-6} K^{-1}. As the volume percentage of fillers was significantly low due to the low density of the glass compared to the density of the fillers, the increase in CTEs for each composite was not expressively high. After the annealing process, the composites had lower CTEs because of changes in the crystalline structure that occurred during thermal treatment. At this stage, all samples were completely crystallized. The addition of 20 wt.-% Ni resulted in the highest CTE values after annealing (approximately 10 x 10^{-6} K^{-1}), which is compatible with the joining requirements. It is also noticeable that glass 87 with 13 wt.-% YSZ fibers was the only glass that maintained the same technical alpha in both stages. In other words, this material suffered less thermal stress due to low CTE changes during stack operation.

Table 10 Measured technical alpha and softening point of the composites as-sintered and technical alpha of annealed samples

Composite	Softening point (°C) (as sintered)	Technical alpha [10^{-6} K^{-1}] (200–600°C)	
		sintered	annealed
Glass 87 pure	605	9.6	8.1
Glass 87 + 10 wt.-% Ni	600	10.6	8.9
Glass 87 + 20 wt.-% Ni	610	10.8	9.8
Glass 87 + 10 wt.-% NiCr	615	10.6	9.2
Glass 87 + 20 wt.-% NiCr	635	10.6	not measured
Glass 87 + 20 wt.-% Ag	570	11.5	8.8
Glass 87 + 13 wt.-% YSZ fibers	630	9.3	9.3
Glass 87 + 10 wt.-% CGO1	600	10.2	8.8
Glass 87 + 20 wt.-% CGO1	605	10.2	9.3
Glass 87 + 10 wt.-% CGO2	600	10.2	8.7
Glass 87 + 20 wt.-% CGO2	605	10.2	9.5

6.1.1.7. Hot Stage Microscopy – HSM

The composites were also examined using HSM to investigate future joining profile optimizations and to analyze the influence of each filler addition on the viscous behavior of the glass matrix. An attempt was made to plot a viscosity curve using the three points obtained by HSM in the form of a VFT linearization. The only approved correlation between viscosity levels and fixed HSM points were the three viscosity points 6.3 for T_{DF}, 4.1 for T_{HB}, and 3.4 for T_F. This correlation is approved for conventional glasses. Nevertheless, it was not possible to obtain the melting temperature T_F. It was assumed that a crystallization process occurs in most of the cases. Therefore, viscosity levels are estimations and are not suitable for use in the VTF plot.

However, it is possible to compare the temperatures of the fixed points obtained by HSM with the corresponding estimated viscosity levels determined in the literature

[Sch 1962]; [PAb 1997]; [Pas 2005]. The HSM analyses showed that the joining temperatures for all composites were approximately in the same range of 750–900 °C. This comparison is shown in Table 11. The pure glass 87 had a lower viscosity, meaning that this sealant already passed its half-ball temperature at the defined joining temperature of 850 °C and could flow more than the composites.

Table 11 Characteristic fixed-point temperature for the pure glass matrix and the composites, correlated with the estimated viscosity level at those points

Sample	Fixed viscosity (log η)					
	9.1	7.8	6.3	5.4	4.1	3.4
	Thermal parameter [± 10 °C]					
	T_{FS}	T_{MS}	T_{DF}	T_S	T_{HB}	T_F
Pure glass 87	610	725	730	795	844	-----
Glass 87 plus filler in wt.-%						
20 YSZ	650	731	745	820	900	-----
13 YSZ Fibers	615	730	740	840	900	-----
20 CGO20	650	750	765	828	890	-----
20 Ag	610	700	710	791	880	-----
10 NiCr	635	740	745	835	900	-----
10 Ni	645	725	730	790	864	-----
20 Ni	625	716	719	825	880	-----

The shadow images of the pure glass and composites at the typical joining temperature of a SOFC stack, 850 °C, are shown in Fig. 40. It is visually possible to discern that all filler additions provoked an increase in the viscosity of the sealant. The addition of 10 wt.-% Ni particles provoked the smallest change in the half-ball temperature, as well as the silhouette at 850 °C. This means that this composite will settle better during the joining process.

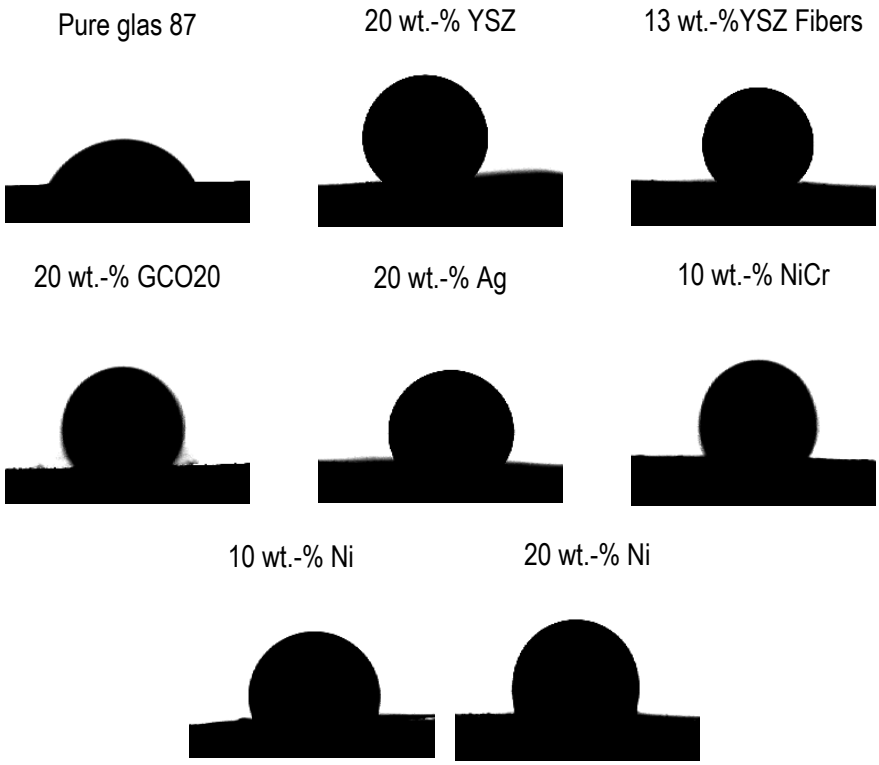

Fig. 40 Shadow images at 850 °C of pure gass 87 and glass matrix 87 with the corresponding filler additions in Crofer22APU substrate

The HSM results of each material could be compared with each other by shrinking the initial area, as shown in Fig. 41. It is possible to observe the sintering behavior of the different composites. The graphs show that the ceramic-filled composites sinter after the pure glass, while the metallic fillers sinter at lower temperatures than the pure glass. The exception is the NiCr-containing composite. This filler material reacted with the glass matrix, forming different crystalline phases, which could be the reason for sintering at higher temperatures than with the pure glass.

a)

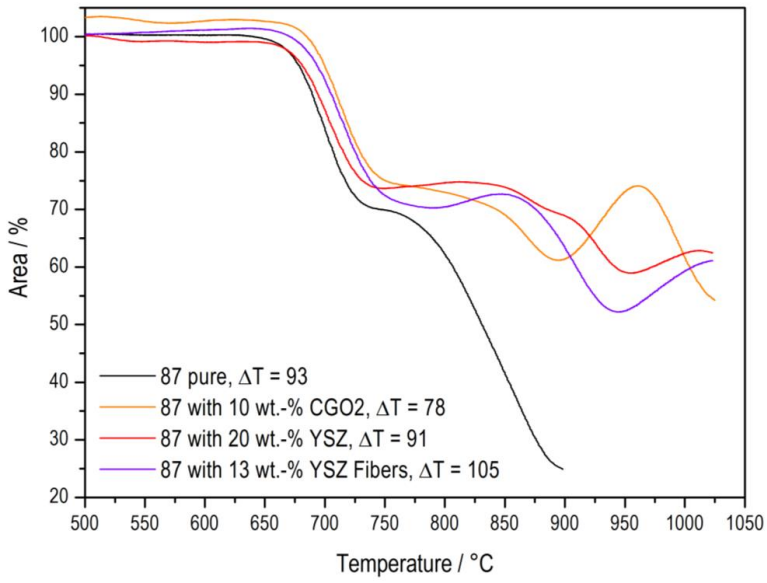

b)

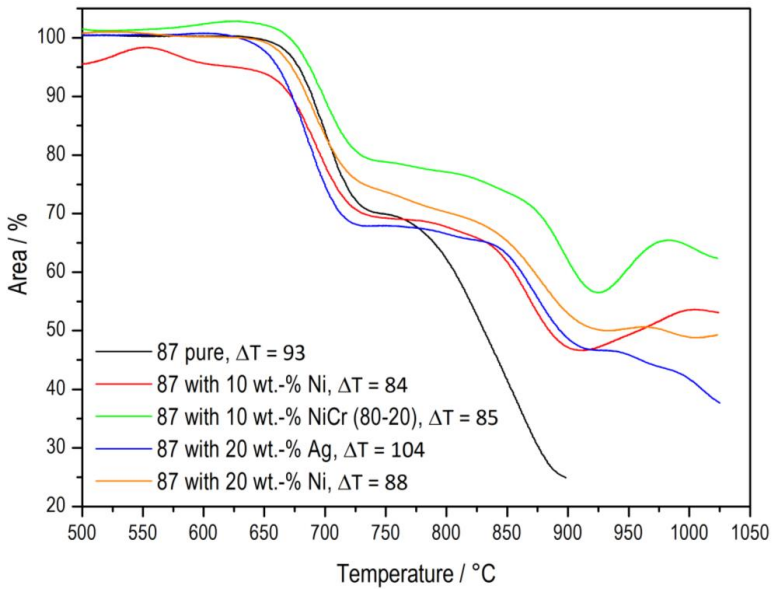

Fig. 41 Hot-stage microscopy results of area transformation and sintering ΔT of each composite: a) pure glass 87 and composites of glass 87 with ceramic fillers; b) pure glass 87 and composites of glass 87 with metallic fillers

6.2. Joining test

Based on the results from the previous feasibility tests, some composites had already been excluded before the joining tests. The composites that were submitted for joining tests were glass 87 with 10 wt.-% and 20 wt.-% of Ni, NiCr, and CGO. Sandwich samples were prepared by screen printing the composite paste in Crofer22APU plates. These plates were joined at 850 °C for 10 h. Some of the joined plates were annealed at 800 °C for 500 h. After joining and annealing, all samples were gas-tight at 10^{-9} mbar·l·s^{-1}. Microstructural investigation by optical and electronic microscopy showed no significant reaction zone in the filler-matrix or sealant-steel interfaces. The microstructures were similar to the images shown before.

6.3. Electrical resistance measurements of composites

The electrical resistivity was tested for screen-printed sandwich samples. At room temperature, all samples were electrically insulating with values higher than 2 GΩ. However, the four-point measurements at high temperatures have shown other results. The specific electrical resistance (ASR) of the glass sealant area at operating temperature (around 800 °C) must be higher than 1 kΩ·cm². The higher the ASR value, the less current that is lost due to current passing through the sealant. In other words, sealants that are more electrically resistant produce more efficient stacks. The measurements on the sandwich samples showed that the ceramic-filled samples were sufficiently resistant, while the joint with the pure glass matrix had very low resistance values at 800 °C. Similarly unsatisfactory results were achieved with the samples containing metallic particles.

In order to evaluate possible influences of the organic media used in the paste, some samples of the pure matrix were prepared with a dispenser using a different media recipe containing only ethyl cellulose and terpineol. The results of these samples were above 1 kΩ·cm². A sample with 20 wt.-% Ni was also prepared using the dispenser and results above the limit were also obtained. When the tests were repeated, it was observed that sometimes the sample had sufficient resistance while at

other times it did not, as shown in Table 12. These findings lead to a hypothesis that the sandwich sample four-point electrical resistance method has a systematic error and the results do not correspond to reality as they are influenced by other factors yet to be identified.

Therefore, another sample type was used in the four-point electrical resistivity test. Identical samples to those used for dilatometry were used for the four-point measurement, namely as-sintered and annealed bars. The measurements were performed between 600 °C and 850°C at IEK-1 in a device developed in-house. The samples analyzed were pure glass 87 and glass 87 with the addition of 20 wt.-% Ni. The results are shown in Fig. 42. The resistances of the glass sealants compared to the internal SOFC cell resistance show that in all four cases, the influence of the sealant is negligible and the current losses are minimal. It is noticeable that the addition of 20 wt.-% Ni particles had no influence on the electrical conductivity in comparison with the annealed (aged) glass 87 and maintained the same range as-sintered and after annealing. This can be explained by the different crystallization behavior of the samples with and without Ni. Without nickel particles, the glass matrix tends to crystallize slower. Both samples achieved microstructure stabilization after the annealing process.

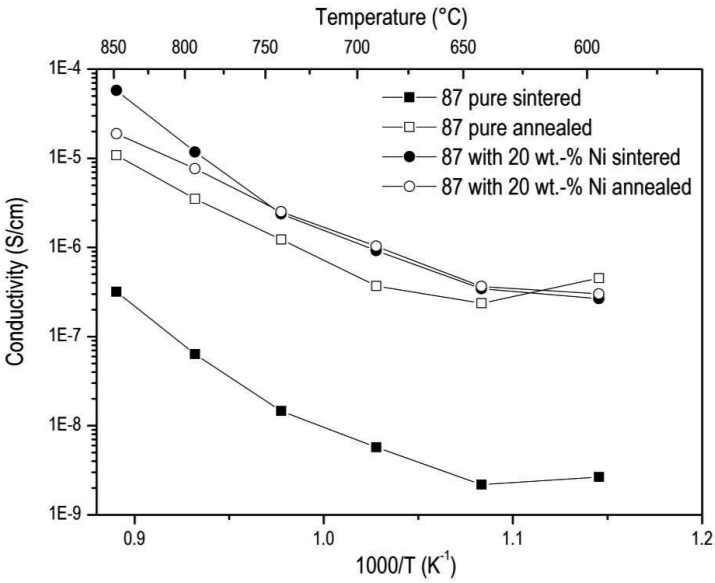

Fig. 42 Four-point electrical resistance measured in bar-shaped samples. Similar conductivity behavior was found for the samples containing nickel and the annealed pure glass matrix

Table 12 Four-point electrical resistance measurements results for as-joined and annealed samples

Sample	Calculated R_{glass} for 100 cm² cells stack (Ω)	Current losses through the sealant (%)
Sandwich samples screen printing		
Glass 87 as joined	0.13	E-02
Glass 87 aged	0.05	E-01
20 % Ni as joined	128	E-05
20 % Ni aged	0.69	E-02
Reproduction sandwich samples		
dispenser 87	277	E-05
screen print 87	41	E-04
dispenser 87 aged	95	E-05
screen print 87 aged	74	E-05
Sintered bars		
Glass 87 sintered	152777	E-08
Glass 87 aged	11337	E-07
20 % Ni sintered	934	E-06
20 % Ni aged	7936	E-07

6.4. Strength evaluation

Mechanical properties are the key features for the development of a SOFC sealant. Several approaches have been investigated to improve the fracture resistance of the glass sealants. Reinforcement increases the toughness of the brittle matrix, for example by dispersing ductile phases, dissipating energy by bridging and/or deflection of the propagating crack by the fillers dispersed in the glass matrix. Many new glass and glass-ceramic composites can be investigated for use as SOFC sealants. Nevertheless, quantitatively evaluating the mechanical strength of a joined sandwich of steel-glass and sealant-steel remains problematic. Together with the need for reliable joining, a widely accepted standard for testing the mechanical strength of joined ceramics and

composites is still unavailable, and measuring the shear or tensile strength of the same joining material with different test methods leads to different results.

Many studies have reported on the mechanical properties of brazes and glass solders for different applications. In spite of this, most of the studies were performed on bulk material or analyzed tensile strength in the absence of constraint effects which are present in real joint configurations [Rhe 2003]; [ZHa 2011]; [Liu 2011]; [Mal 2012]; [Lin 2012]; [Cho 2010]; [Gro 2011]; [Sme 2008a]. A relatively wide variety of specimen configurations have been devised to test the strength of brazed and soldered joints, and even more specifically glass sealants for SOFCs, featuring varying degrees of tensile or shear loading and varying degrees and types of stress concentration along the joint. There are specific advantages and disadvantages to each of the existing specimen and test designs, and the choice made in each study was motivated by a compromise between the ease of brazing and lack of ambiguity in mechanical test data. A common method is to test brazed joints under shear loading, which is a frequently representative loading state for real brazed joints [Kim 2005]. Due to the thermal mismatch of the ceramic and metallic materials in the SOFC stack, the seals predominantly experience shear stresses and therefore, similar to the brazed joint, they should also be tested under shear loading.

6.4.1. Tensile strength

Although the tensile strength results presented in this study and in the literature [Sme 2008b]; [Lin 2012]; [Cho 2008a]; [Cho 2008b] can only be used qualitatively as a ranking, they allow us to compare joints tested under the same conditions. It is highly desirable to have qualitative strength data for sealant materials. The low strength values found for the circular butt joint in the tensile test in our study indicates that forces other than tension were present during the measurements. Hence, it can be hypothesized that the maximum tension arose in the most inner area of the circular butt joint because of the centric force due to the thread pitch. As the reproducibility of the results was very high, the adaptor effect of the force application can be considered as negligible. The thickness of 6 mm of the metal counter parts had the highest influence on the values, as the bending of the considerably thin metal parts created additional lateral forces.

In order to investigate the influence of the thicknesses of the metal counter parts on the tensile strength results, new tests were carried out with Crofer22APU cylinders of two different heights and with two joining geometries of different areas using a reference sealant material, referred to here as glass K. The new geometries were prepared using Crofer22APU cylinders with a thickness of 22 mm. The results showed an increase in the measured strength of glass K for 22 mm thick cylinders compared to the 6 mm thick cylinders, as shown in Fig. 43 and Table 13. Computational investigation showed that the tensile force is transmitted by the studs, especially on the inner rim of the glass sealant layer. Therefore, the higher the cylinders, the better the load is distributed on the glass sealant. Through calculations, it was possible to determine that the glass sealant middle layer in every case had a maximal tensile strength of approximately 95 MPa ± 10 MPa at fracture. A small difference in tensile strength was found when the thermal residual stresses were considered in the calculations, as shown in Table 13. Optimization of the joint tensile specimens was suggested by Pabst [Pab 2013]. Pabst suggested that the stress distribution would be more uniform if the thread was positioned in a different way.

Fig. 43 Butt-joint samples with increased metal thickness led to better significant strength results due to decreased bending during the test

Table 13 Comparison of the maximum and average tensile strengths for the different sample geometries at breaking force calculated by simulation

Height of Crofer cylinder (mm)	Outer-/ Inner-∅ of the glass sealant layer (mm)	Measured force F_{max} (N)	Measured average tensile strength $F_{max}/A_{sealant}$ (MPa)	Calculated maximal tensile strength at failure (MPa)	
				without thermal stresses	with thermal stresses
6	32 / 24	1788	5	85	82
22	32 / 24	9715	28	95	91
6	24 / 12	1997	6	85	82
22	24 / 12	11255	33	103	99

6.4.2. In-house developed shear test

An in-house set-up was developed for shear tests of joined samples. Several attempts failed to obtain satisfactory results concerning reproducibility. Nevertheless, the sample set-up was easy to prepare, using less machining effort and material compared to the tensile strength test, and it could also be used to rank the sealants.

Two set-ups obtained the best results. Both are shown in Fig. 44. The first sample concept was to prepare four shear bond samples in one 50 x 50 mm² substrate Crofer22APU plate. The glass sealant paste was printed using a template with equidistant four circles. The Crofer22APU top plates, with dimensions of 10 x 10 mm², were also fixed in equidistant positions during the joining process using a sample holder. The joining process used was the same as that used for the preparation of the gas-tightness sample and the same used for stack joining. The samples were tested one after the other in the bond tester Dage 4500. The main problem during sample testing was the possibility that the first plate tested would hit the subsequent top plate and pre-damage the bond of that sample. Damage to the bond generates a much lower strength value, making the test inconsistent and irreproducible. This effect is shown in Fig. 45, where there was one sample in every substrate plate with a much lower result.

In an attempt to eliminate the impact of sample A on sample B, C, or D (Fig 44a), the sample concept was modified. Smaller Crofer22APU substrate plates were

prepared, 20 x 20 mm², for use with the same type of top plate. The sealant was applied and the plates were joined in the same way as the previous sample concept. However, the results were still not reproducible enough. The development of the shear test of joints using the bond tester Dage 4500 was stopped after several changes in sample design and measurements, as this method was not robust. Collaboration was therefore established with Politecnico di Torino to develop a method of measuring the pure shear strength of the joints. A torsion test was developed at this institution for the samples joined at FZJ.

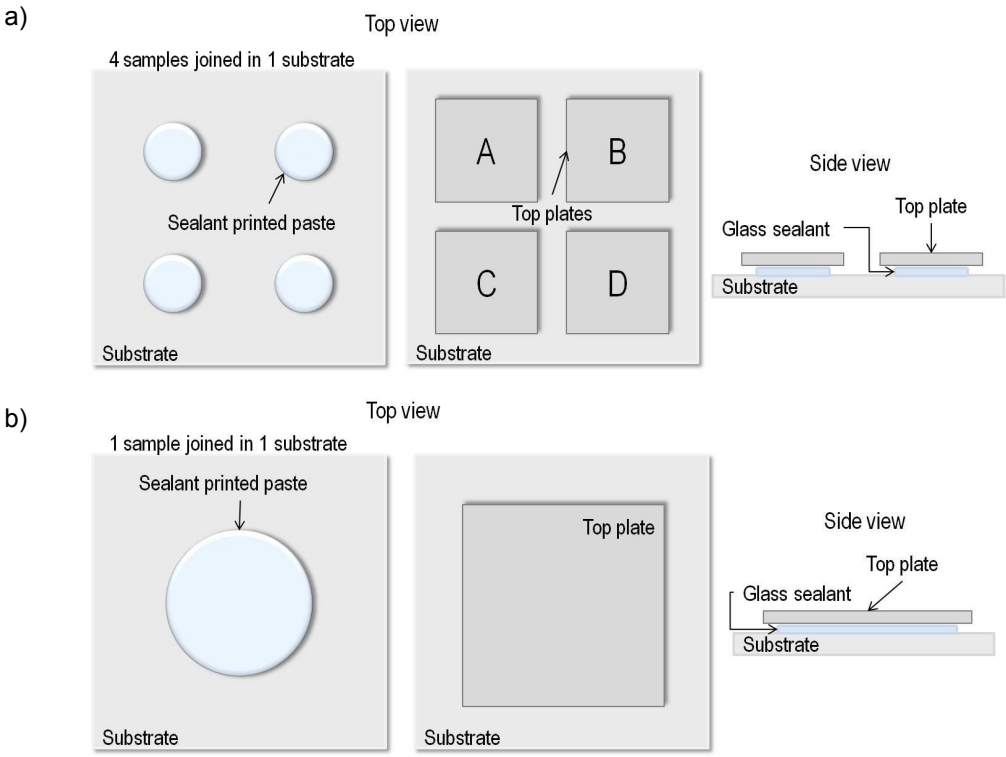

Fig. 44 Shear test of joined samples: a) four samples joined in the same 50 x 50 mm² plate; b) single sample set-up

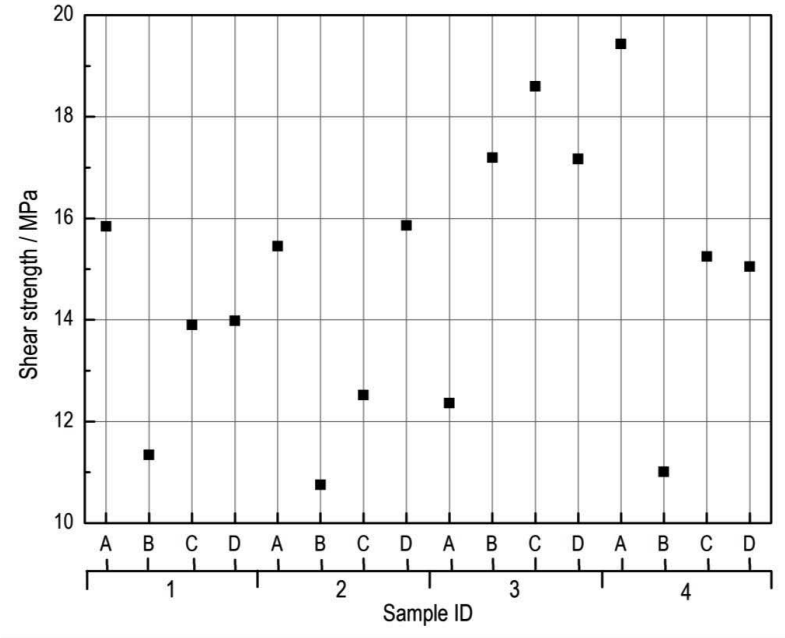

Fig. 45 Shear strength results attained with the first sample concept (Fig. 44a). The variation in shear strength could be the result of pre-damage caused by sample A to sample B, C, or D

6.4.3. Torsion test

The Politecnico di Torino (Italy) in collaboration with Oak Ridge National Laboratory (USA) and Kyoto University (Japan) developed a modified torsion test as an alternative to an asymmetrical four-point bending test to measure the pure shear strength of the joints. A miniature hourglass-shaped sample and torsion test equipment were designed and built at Politecnico di Torino and in their partners' facilities. The method was tested with small steel samples bonded with epoxy and silicon carbide components joined by glass-ceramics. It was shown that pure shear strength values could be obtained in both cases [Fer 2012a]; [Fer 2012b].

We used miniaturized hourglass-shaped joined samples with a joining surface of 5 mm diameter. Hourglass samples of this size were necessary in order to be used with the dedicated equipment for torsion tests designed and built at Politecnico di Torino,

Italy. Originally, this equipment was fabricated for neutron irradiation studies. In addition, studies showed that the best compromise for specimens are hourglass-shaped samples as they have a reduced circular joined area and an easy-to-clamp square section [Fer 2012a]; [Fer 2012b]. For this study, the hourglass samples were prepared using Crofer22APU steel parts and glass-ceramic composite pastes at Forschungszentrum Jülich.

The sealant paste was prepared using 20 wt.-% of the same organic binder system used for screen printing. It was based on terpineol, ethyl cellulose, and additives (the same binder system used for screen printing), and glass matrix 87 powder with additions of filler materials. The green layer of composite paste was applied on the surface of the Crofer22APU hourglass-shaped parts using a template. To achieve a joining gap of 0.2 mm, corresponding to the requirements of the real application, it was necessary to print one paste layer on each joining partner and to control the weight of each single piece. The joining device held the joining sample in position during the joining process and allowed load application corresponding to the joining procedure of a SOFC stack. In accordance with previous studies on this glass matrix [Gro 2006] [Gro 2011], joining was performed at 850 °C for 10 h with a heating and cooling rate of 2 $K \cdot min^{-1}$. A dead load of 1600 g was applied on top of the joining device. The green layer and joint thickness were controlled by measurements using a micrometer.

Contrary to the results found in tensile tests in the literature, the torsion test achieved more significant results that are compatible with expected glass strength. The results of the torsion test showed that the pure glass matrix had the lowest strength values with an average of 42 MPa. Following the pure glass 87, the composite with 20 wt.-% YSZ particles and increased porosity had an average of only 43 MPa. The third-lowest results were with the composite containing 20 wt.-% CGO1 with an average of 46 MPa, which is close to that of the pure glass and composite with YSZ particles. The best results were found for composites with the addition of metallic particles. Shear strength average values for composites with 10 wt.-% NiCr, 20 wt.-% Ni, and 20 wt.-% Ag were 83 MPa, 94 MPa, and 105 MPa, respectively. The average strength values obtained, as well as the lowest and highest values for the joined sample sets subjected to thermal treatment at 850 °C for 10 h are shown in Fig. 46.

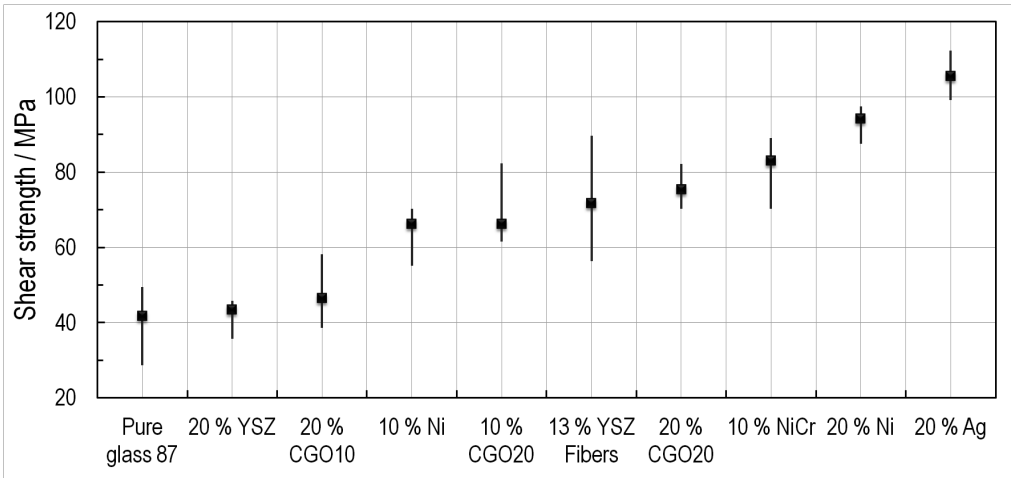

Fig. 46 Shear strength low-high-close chart of as-joined composite-to-steel torsion test. Composites made of glass 87 and filler additives in wt.-%

Moreover, the same test was repeated with hourglass samples annealed after joining treatment. Annealing was performed at 800 °C for 500 h in air. Due to an increase in crystallization, the shear strength values generally increased. Nevertheless, the pure glass 87 still had the lowest shear strength value with an average of 58 MPa. The shear strength values of the variants with filler materials differed compared to each other. This phenomenon can be explained by possible interaction of the fillers with the glass matrix and by the different crystallization provoked by different fillers during the long time at 800 °C. The glass filled with silver had the best results after joining with 105 MPa, dropping to the fourth-worst place after the annealing process with only 84 MPa. Finally, the best composite after the long-term experiment was the glass matrix with 20 wt.-% Ni with an average of 99 MPa, as shown in Fig. 47.

.

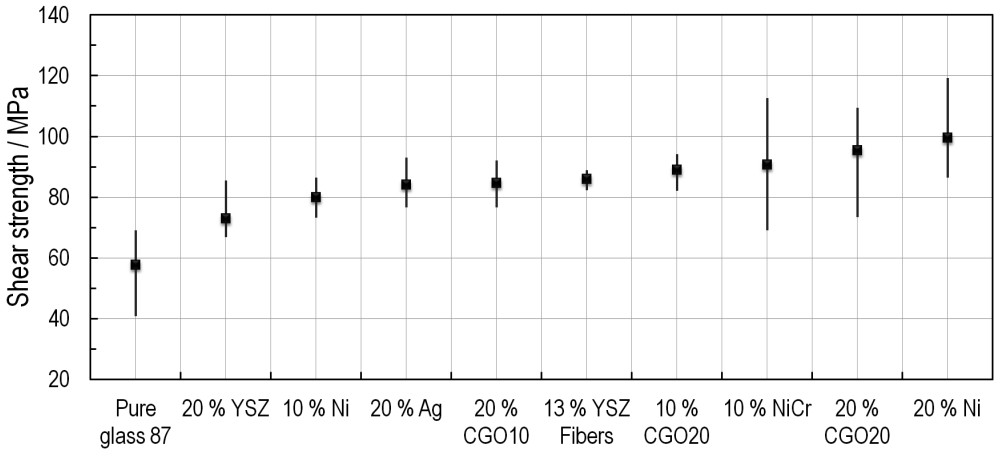

Fig. 47 Shear strength low-high-close chart of annealed composite-to-steel torsion test. Composites made of glass 87 and filler additives in wt.-%

6.5. Multilayer sealant design

The multilayer concept was developed in an attempt to improve sealant toughness by combining two or three different reinforced sealant layers. Each specific layer in the multilayer concept was formed by a composite type. In this concept, three fillers were used: Ag, YSZ particles and YSZ fibers. These fillers were chosen due to their properties as fillers demonstrated in previous studies [Gro 2006]; [Gro 2010]; [Gro 2011]; [ZHa 2011]. The Ag-filled composite had the best mechanical properties of the three types of materials. However, its electrical insulation did not meet the requirements for a SOFC sealant. Sufficient electrical resistance was one of the properties encountered in the composites filled with ceramic particles or fibers. Therefore, printing a multilayer sealant with layers containing Ag and YSZ particles or fibers should result in a tough sealant with good electrical resistance.

6.5.1. Joining tests

In order to compare the composites sealants to each other, the same characterization methods that were used on the single-layer samples were also used on the multilayer samples. Sandwich samples prepared by screen printing were joined and tested for gas-tightness and the microstructure was analyzed on cross sections. The results were then compared with the single composite layers previously tested. All samples obtained maximum measurable gas-tightness higher than 10^{-9} mbar·l·s^{-1}.

Microstructure investigations showed that the crystallization of the glass composites was influenced by the presence of silver particles, which mostly enhanced the crystallization. The other two ceramic fillers apparently did not strongly influence crystallization kinetics, as shown in Fig. 48, Fig. 49, and Fig. 50. No percolation of metallic particles or intermixture of one of the composite layers was encountered in the analyzed samples. Nevertheless, the addition of YSZ particles clearly increased the size and amount of porous, as shown in Fig. 48b and Fig. 49b. Hence, it was hypothesized that porosity is caused by the production or milling process of the YSZ particles. This hypothesis is also sustained by the considerable decrease in porosity with the use of YSZ fibers.

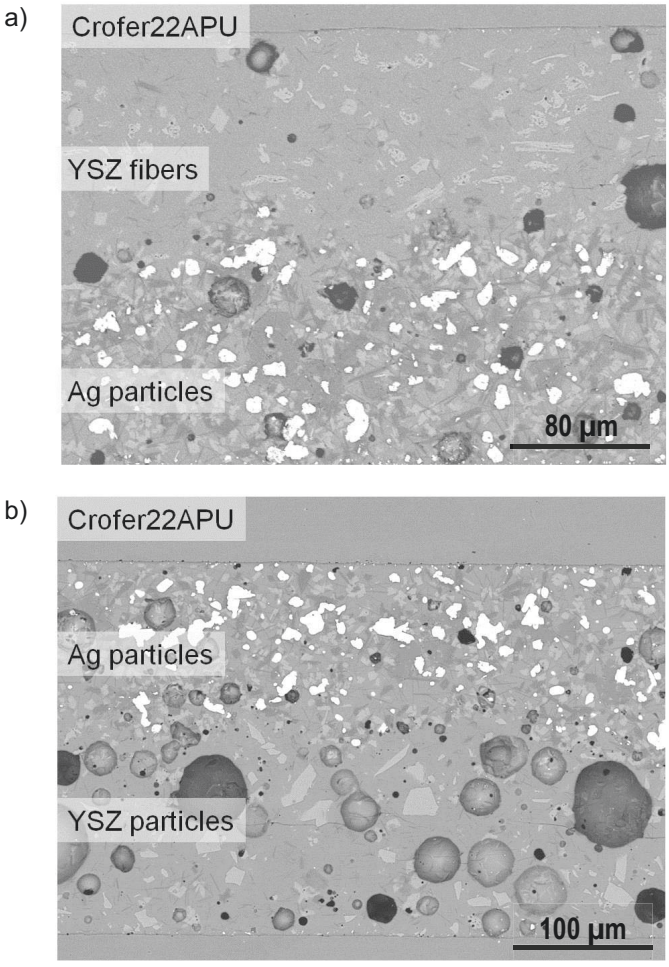

Fig. 48 Double-layered sandwich samples as joined: a) upper layer filled with YSZ fibers (low porosity) and lower layer with Ag particles; b) upper layer filled with Ag particles and lower layer with YSZ particles (high porosity)

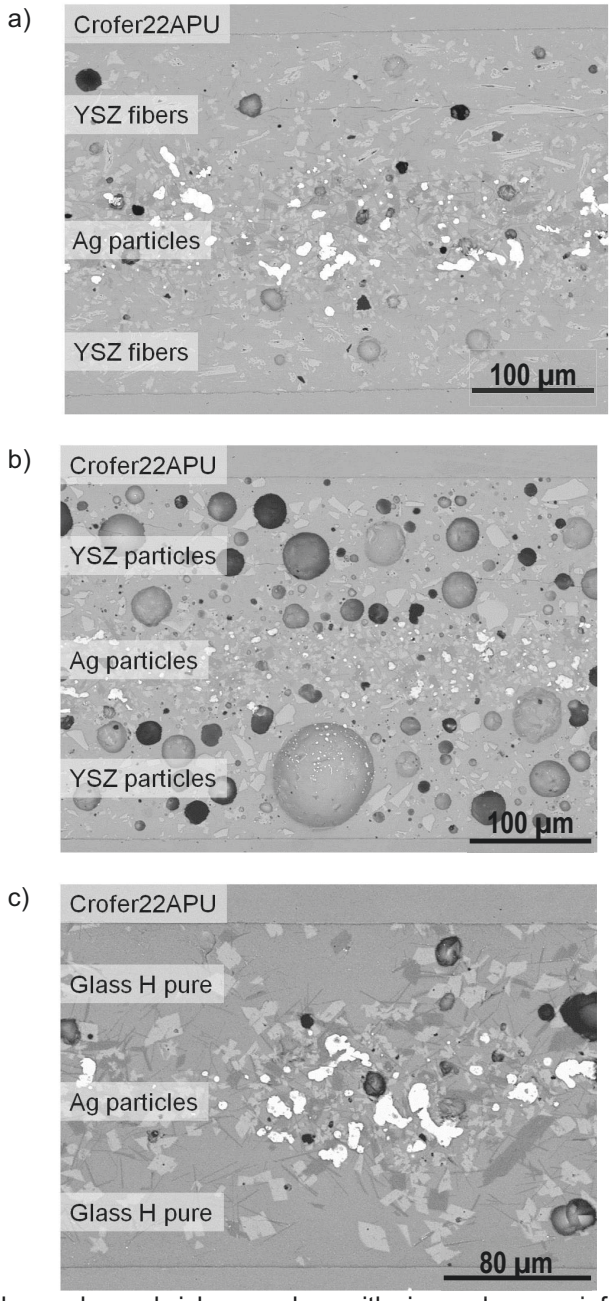

Fig. 49 Triple-layered sandwich samples with inner layer reinforced with silver particles, and outer layers filled with: a) YSZ fibers; b) YSZ particles (high porosity); c) pure glass

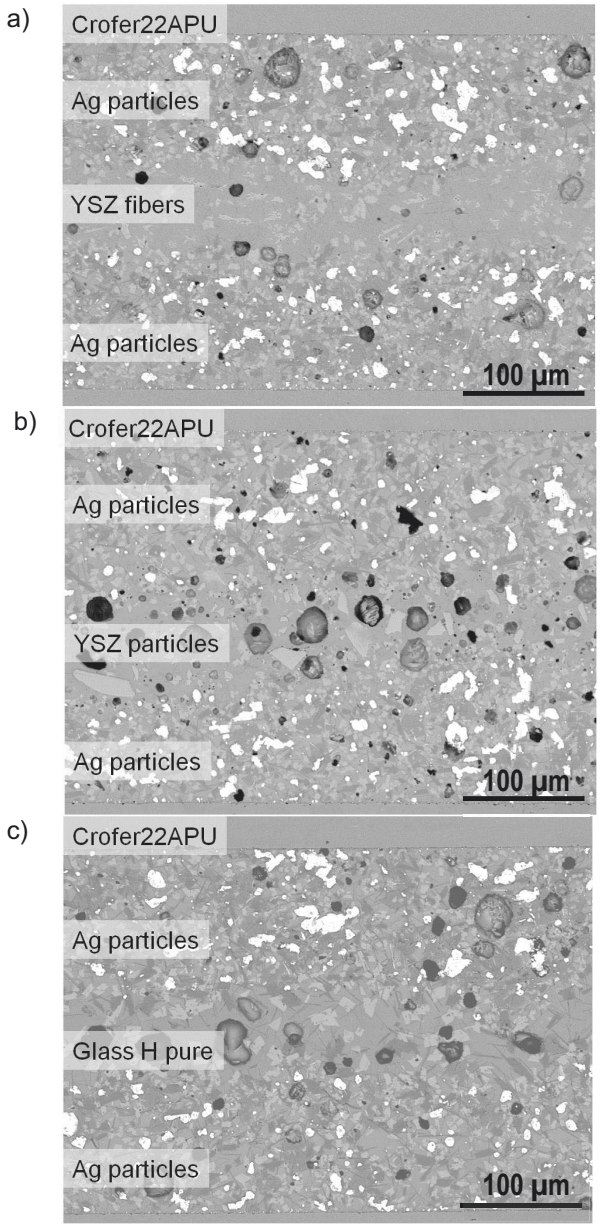

Fig. 50 Triple-layered sandwich samples with outer layers reinforced with silver particles, and inner layer filled with: a) YSZ fibers; b) YSZ particles; c) pure glass

The presence of nanoscaled silver particles was visible in high-magnification SEM images during the investigation of the cross sections of multilayered samples. The nature of these particles was confirmed by EDS line scans in layers that originally contained no Ag particles as filler. Moreover, the silver particles were found in diverse parts of these layers in nearly every multilayer sample. High amounts of silver nanoparticles were encountered closer to the interface with metal, as shown in Fig. 51. The possibility that these particles were introduced by contamination was discarded because the Ag-containing layers were printed with an exclusive screen for that process. It was assumed that these small particles were formed by silver migration into the glass matrix, and that this phenomenon occurred due to redox reactions in the glass matrix involving polyvalent ions like zinc or vanadium. It was impossible to verify this mechanism analytically because of the small amount of V in the glass. However, it can be assumed that the Ag nanoparticles and the migration phenomenon of silver through the whole width of the joining gap causes electrical conductivity.

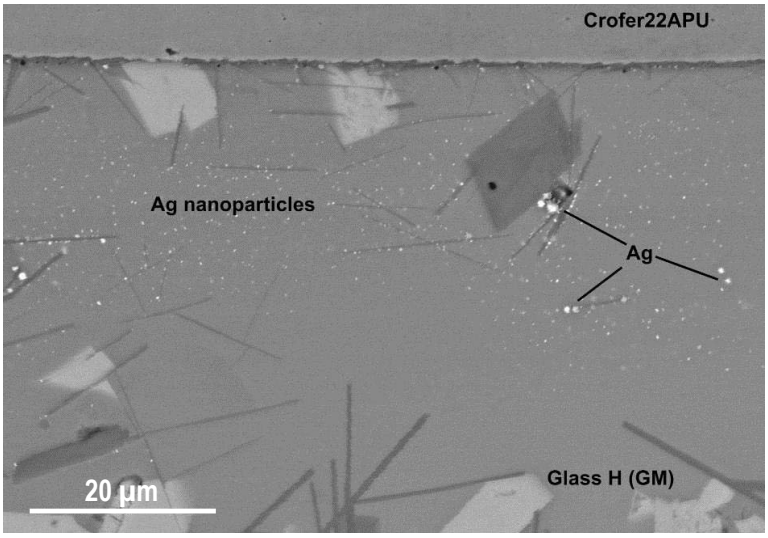

Fig. 51 Nanoparticles of silver were encountered in a layer of pure glass in the multilayer design of pure glass/glass with 20 wt.-% Ag/pure glass. The Ag particles migrated from the silver-containing inner layer to the other layers

A diffusion test was elaborated to confirm that silver particles were formed during the joining process and not by contamination. In order to simulate the diffusion process,

a glass pellet containing 13 wt.-% YSZ fibers was pressed and placed on top of a 99.9 wt.-% Ag foil. It was thermally treated with a heating rate of 2 $K \cdot min^{-1}$ up to 850 °C with no dwell time and the furnace was immediately cooled. The cross section, as shown in Fig. 52, was analyzed by SEM with EDS. Silver particles randomly dispersed in the glass pellet were detected by EDS line scan, as shown in Fig. 53.

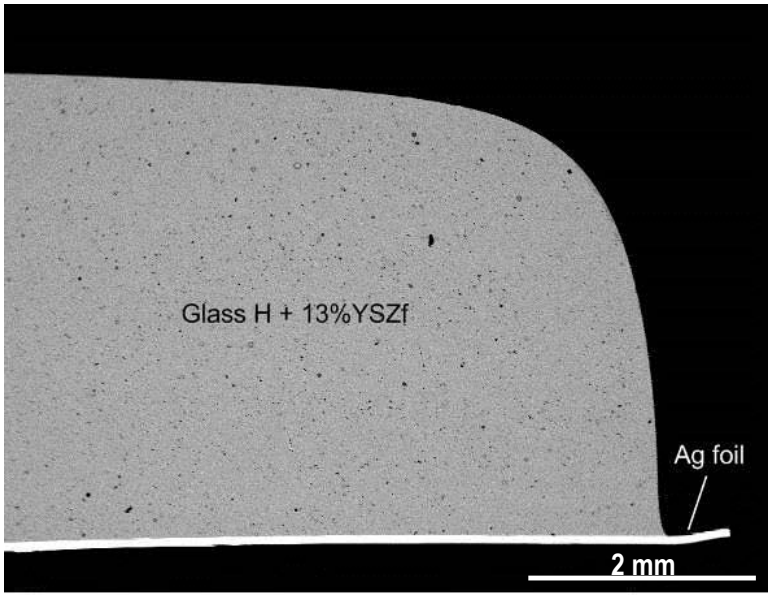

Fig. 52 Cross section of the glass 87 (H) with 13 wt.-% YSZ fibers sintered in silver foil

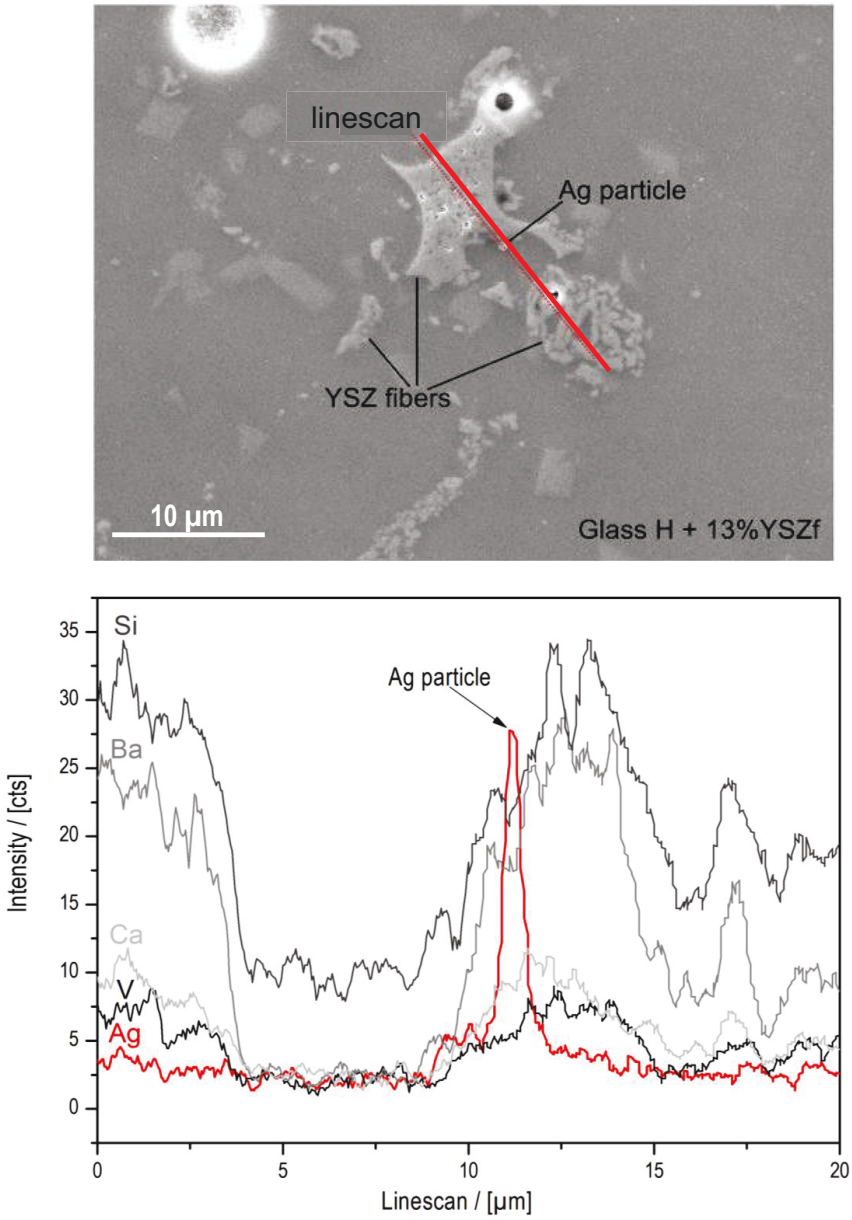

Fig. 53 EDS line scan showing the presence of a silver particle in the middle of the glass ceramic pellet of Fig. 51

Despite the short thermal treatment, silver ions diffused into the glass ceramic pellet. Hence, it can be hypothesized that the silver from the foil reacts with the glass, is oxidized depending on the oxygen partial pressure, and diffuses through the glass,

followed by a reduction reaction forming silver particles. Considering that a polyvalent ion is needed to interact in these redox reactions, the only possible candidate for the glass 87 composition was vanadium. Regarding the Ellingham plot (see Fig. 54 [Con 2010]), it is possible that the vanadium is the responsible reactant for the silver reduction, forming the small dispersed nanoparticles. This reaction mechanism is shown in Eq. (13), Eq. (14), Eq. (15), and Eq. (16). Due to the small concentration of vanadium oxide in the glass composition, it was impossible to prove an enrichment of this element around the metallic silver particles.

$$V_2O_5 + e^- \rightarrow 2\ VO_2 + ½\ O_2 \qquad \text{Eq. (13)}$$

$$V_2O_5 + 2\ e^- \rightarrow V_2O_3 + O_2 \qquad \text{Eq. (14)}$$

$$2\ Ag_{(s)} + ½\ O_{2(g)} \rightarrow Ag_2O_{(\text{in glass})} + 2\ e^- \qquad \text{Eq. (15)}$$

$$2 \cdot Ag_2O_{(\text{in glass})} + V_2O_3 + 4\ e^- \rightarrow 4\ Ag_{(s)} + V_2O_5 \qquad \text{Eq. (16)}$$

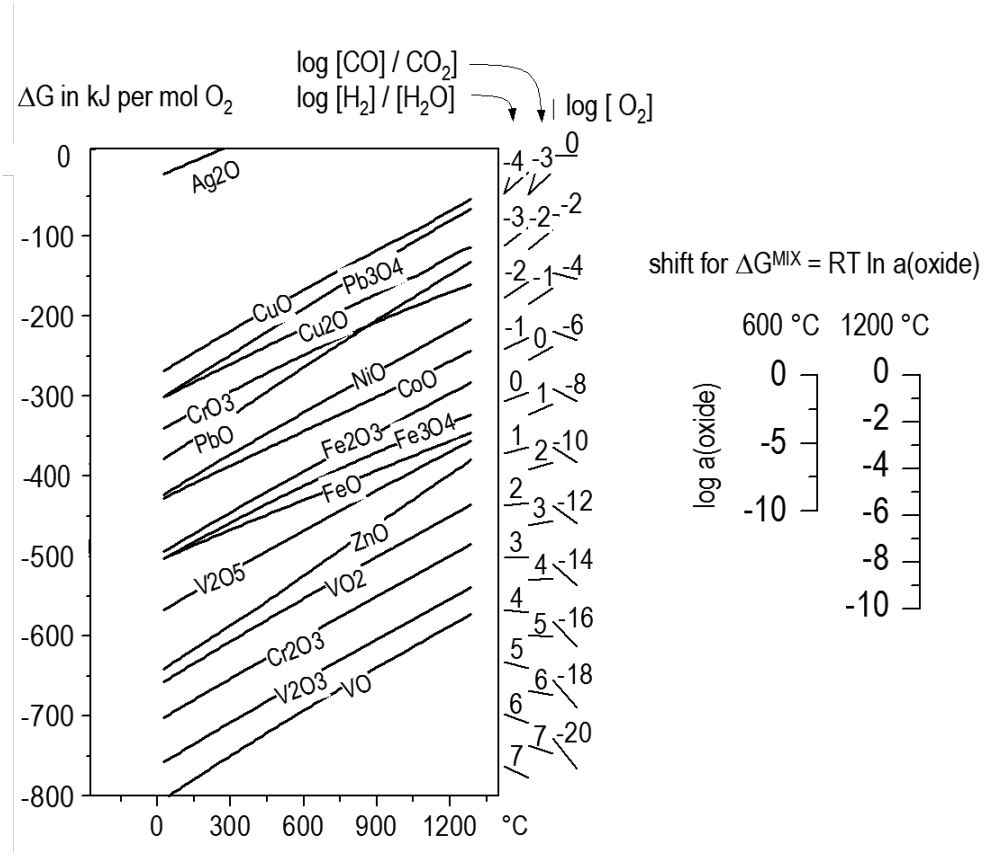

Fig. 54 Ellingham diagram for the oxides stability [Con 2010]

6.5.2. Electrical resistance measurement

The electrical resistance of the multilayer sandwich samples was tested by the four-point method. The samples were measured in three states: as-joined at 850 °C with a dwell time of 10 h; annealed after joining at 800 °C for 500 h; and thermally cycled with 30 cycles. Each thermal cycle corresponded to heating up to 1100°C at a rate of 100 K/min with 10 min dwell time, cooling down to 800°C at a rate of 20 K/min for 40 min, and finally cooling down to 100°C at a rate of 100 K/min with 13 h dwell time.

Current losses through the sealant were calculated based on the assumption that these sealants were used in a F10 stack design, the parameters of which have already been described. The relevant equations are shown in chapter 5.6. The measurement results and the calculated current losses through the sealants are shown in Table 14.

Table 14 Results of four-point electrical resistance measurements of the multilayer sandwich samples as-joined, annealed, and thermally cycled. Calculated current losses through the sealant based on 100 cm² cells in the Jülich stack design (F10)

Multilayer samples	Thickness (cm)	Resistance from measurement (Ω)			Current losses through the sealant (%)		
		As-joined	Annealed	Thermal cycled (30 cycles)	As-joined	Annealed	Thermal cycled (30 cycles)
YSZ fiber + Ag + YSZ fiber	0.026	16083	40900	9730	E-06	E-06	E-06
YSZ + Ag + YSZ	0.032	23245	8300	15770	E-06	E-06	E-06
YSZ fiber + Ag	0.025	5474	45870	16500	E-06	E-06	E-06
YSZ + Ag	0.023	9643	9156	229.6	E-06	E-06	0.0001
Matrix + Ag + Matrix	0.029	0.604	**short circuit**	0.335	0.01	**short circuit**	0.1
Ag + Matrix + Ag	0.020	713	44.8	412.3	E-05	0.001	0.0001
Ag + YSZ fiber + Ag	0.029	3.5	**short circuit**	0.9	0.01	**short circuit**	0.01
Ag + YSZ particle + Ag	0.029	0.372	**short circuit**	0.41	0.1	**short circuit**	0.1

Sufficient electrical resistance was measured in the multilayer variant with two layers reinforced with ceramic and the intermediate layer reinforced with Ag particles. The samples that presented less electrical resistance were those with three layers of which two were filled with Ag or two had pure glass layers. The insulation of the samples with outer layers filled with Ag or the pure glass matrix decreased with the additional thermal treatments. On the other hand, the current losses for the sealant between two or three layers with ceramic-filled outer layers were stable and very low. These findings implicate that the intermediate layer reinforced with ceramic and the pure glass 87 layers do not function as insulating functional barriers as expected. No cause was found for the short circuits. The samples with insufficient insulation were not used for further strength investigation.

As already discussed for the single-layer composites, it is possible that the four-point measurement on sandwich samples has systematic errors that have not yet been identified. Several aspects, for example, the spot welding of the metal plates could provoke a short circuit at high temperatures. It is recommended that the conductivity of composite bars be evaluated to confirm these results. As sample preparations for such experiments were not easily accessible, this analysis was not done during this work.

6.5.3. Tensile strength

Butt-joint samples of steel-sealant-steel were prepared for tensile strength test. The results are shown in Fig. 55. They cannot be used as quantitative values, but they allow us to qualitatively rank the sealants in comparison to each other. They revealed that the multilayer design improved mechanical strength in comparison to the single layers of ceramic-filled glass-ceramic composites.

According to the results, the three-layer design with YSZ fibers on the outside and silver particles in-between achieved an acceptable compromise between strength and electrical insulation. The three-layer sealant with two layers of YSZ-particle-filled composite and one middle layer containing silver showed only a poor improvement in strength compared to the single- or two-layer design reinforced with the same fillers. In contrast, the single-layer silver-reinforced sealant offered no electrical insulation, while the outer layers reinforced with ceramic fibers improved the electrical resistance with a slight decrease in strength.

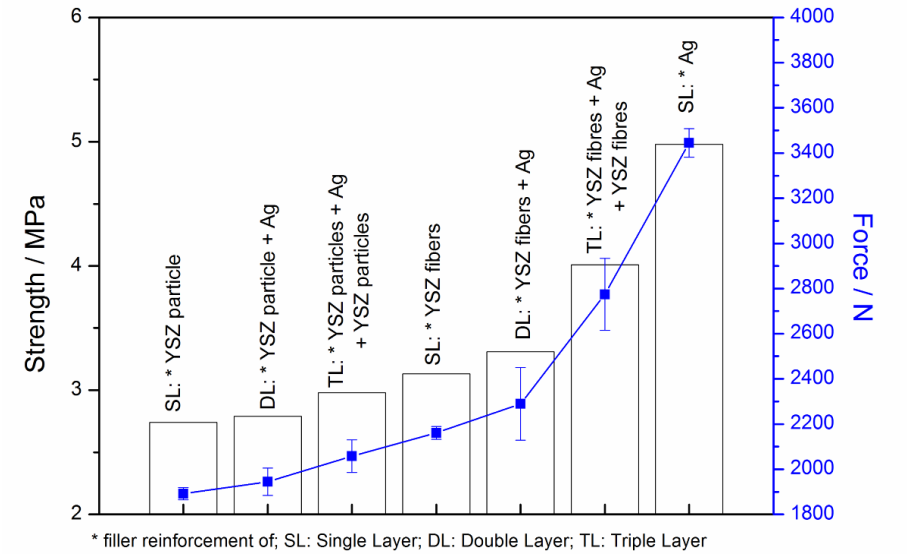

Fig. 55 Strength comparison of single-layer and multilayer composites

6.5.4. Glass 104

To test the influence of vanadium on the silver migration, the same type of experiments with pellets and silver foils were carried out using glass 104, which has a similar composition to glass 87 but contains no V and Zn. All of the properties of this glass were investigated using the same procedures used for glass 87. The sinterability and viscous behavior of this glass was compared to that of glass 87 and of the composite containing YSZ fibers by HSM analysis. The results are shown in Fig. 56. The removal of vanadium and zinc from glass 87, forming glass 104, significantly changed the viscous behavior of the glass. The pure glass 104 had a slightly different sinterability than the glass 87 with reinforcement, and the softening of the sample also occurred later than for the pure glass 87. This phenomenon could be caused by crystallization. The shift in temperature ΔT during the sintering of each composite is shown in the legends of Fig. 56. Dilatometry results of sintered bars are shown in Table 15. The sintering program used was the same as that used for glass 87.

Table 15 Technical alpha of the glass 104 and composites

Composite	Technical alpha (10^{-6} K^{-1}) (20–600°C)	
	sintered	annealed
Glass 104 pure	9.9	9.2
Glass 104 + 13 wt.-% YSZ fibers	9.9	9.3
Glass 104 + 20 wt.-% Ag	10.5	9.5

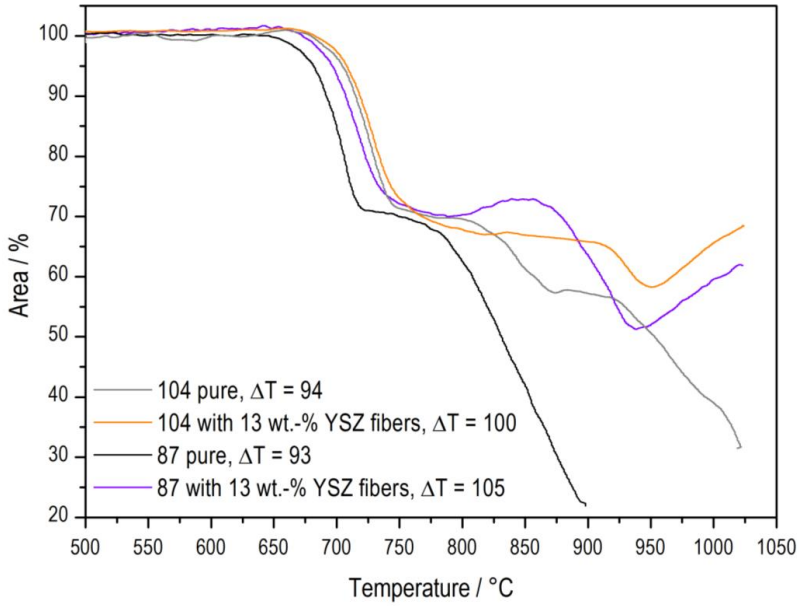

Fig. 56 Hot stage microscopy of glass 87 and glass 104, pure and with YSZ fibers, showing the change in area corresponding to an increase in temperature and the ΔT during sintering of each composition

Joining tests were performed with dispensed glass pastes in the form of sandwiched samples. Three variants were tested comparing the pure glass 87 and its composites, which were pure glass 104, glass 104 with 20 wt.-% Ag, and glass 104 with 13 wt.-% YSZ fibers. All samples were gas-tight with the maximum measurable helium leakage rate < 10^{-9} mbar·l/s and all showed electrical resistance > 2 GΩ at room temperature. The results for the four-point electrical resistance test at 800 °C showed

that the glass with silver particles behaved in the same way as the comparable composite of glass 87 and yielded a short circuit. The other two samples exhibited good electrical insulation, with around 10^{-6} current losses through the sealant.

The microstructures of glass 104 and composite joints are shown in Fig. 57. They are very different to the microstructures of glass 87 and its corresponding composites. The pure glass matrix had already totally crystallized after the joining treatment at 850 °C for 10 h with a heating rate of 2 $K \cdot min^{-1}$. The composite with YSZ fibers showed less crystallization at this point of thermal treatment. The composite with silver addition presented less crystallization than the pure glass but nevertheless more crystallization than the composite containing fibers. Similar behavior was also observed for the glass 87 composites. The crack through the joint in Fig. 56 c was caused by the metallographic preparation of the sample. The reaction zones at the interface between the interconnect and the glass were of insignificant dimensions for all samples.

Furthermore, diffusion tests similar to the test on glass 87 in silver foils were performed with pure glass 104 and glass 104 with YSZ fibers. The same joining program was used as for glass 87: 850 °C for 10 h with 2 $K \cdot min^{-1}$ as the heating rate. Microstructure investigations on cross sections and EDS analysis failed to identify any migration of silver into the glass sealant, as shown in Figure 58. This supports the hypothesis that the vanadium and zinc could be involved in a series of reactions for the oxidation/reduction and transport of silver in the glass.

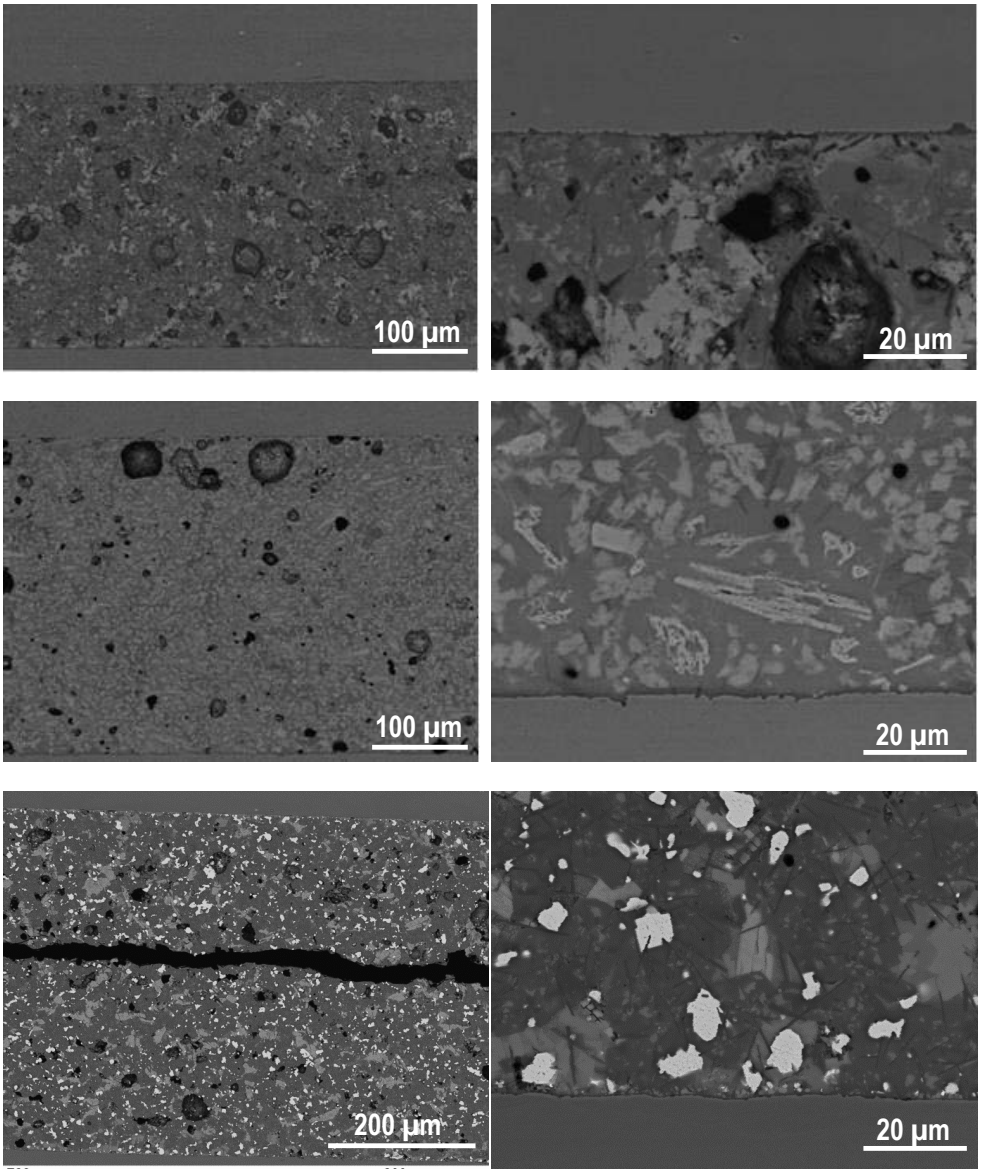

Fig. 57 Joint microstructures of sandwich samples composed of Crofer22APU and sealant based on matrix glass 104 and filler from a to c: 0 wt.-% YSZ, 13 wt.-% YSZ fibers, and 20 wt.-% Ag

a) b)

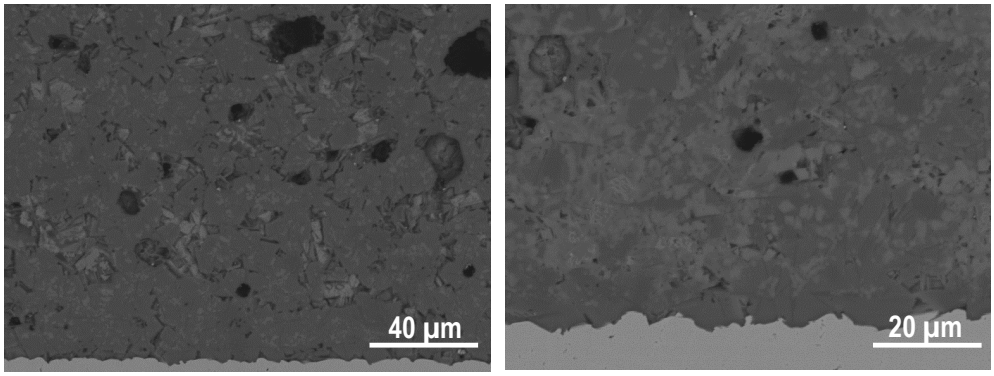

Fig. 58 Diffusion test with glass sealant pellet on pure silver foil sintered at 850 °C for 10 h: a) pure glass 104, b) glass 104 with 13 wt.-% YSZ fibers

7. Summary

The aim of this work was to develop and evaluate options for improving the mechanical strength of glass-ceramic composite sealants based on a composition of the system BaO-CaO-SiO2, and to propose a new and reliable method of mechanical strength characterization for joint samples.

Two approaches were suggested to obtain tougher sealants. The first approach was to add filler materials to the glass matrix 87. Several possible filler materials were chosen and pre-tested in terms of compatibility with the glass matrix. Finally, three new alternative fillers were comprehensively tested in different proportions in this glass matrix. These materials were Ni particles, NiCr (80-20) particles, and gadolinium-doped ceria particles.

The second approach of producing a stronger sealant was to prepare laminated structures with two or three layers containing different composites. The main goal of this multilayer design was to combine mechanical strengths from certain composites with sufficient electrical insulation from other composite types.

Additionally, three methods of mechanical characterization were investigated in this work. The tensile strength test using the geometry of circular butt-joint samples achieved reproducible results with extremely low tensile strength values. These values were useful for ranking the samples in comparison to each other. The finite element method showed that the sample geometry had to be changed to a more uniform stress distribution for quantitative measurements. Moreover, the thermal mismatch of the ceramic and metallic materials in the SOFC stack led to shear stress in the sealant experiences. They should therefore be tested under shear loading. The development of a shear test set-up for joint samples failed to achieve reproducible results for the tested samples. The strength values were still lower than expected from theory and thus no further optimization attempts were carried out. A joining jig was developed for torsion tests using hourglass-shaped samples of Crofer22APU pieces joined by the composite sealants. This last method was shown to be very reliable and it produced strength values that were close to those expected for glass-ceramics. The torsion test results were used to identify the toughest composite at room temperature in a quantitative evaluation.

Overall, this work confirmed that the reinforcement of glass-ceramic sealants was successful with several fillers. It also showed that is possible to obtain a multilayer design with improved properties by screen printing, and that quantitative shear module data from the joint samples can be obtained in torsion tests. Among the several filler materials tested, the best results concerning CTE and shear strength were obtained for the glass matrix 87 reinforced with 20 wt.-% Ni. This lower-cost material was nearly twice as tough as the pure matrix and surpassed the best results previously obtained with the more expensive Ag filler additions. An additional prospect is the insulating behavior of the Ni-filled composite, which does not provoke any electrical current losses in the system. With these properties, it is possible to meet the requirements of a sealing material for SOFC stacks.

8. Appendices

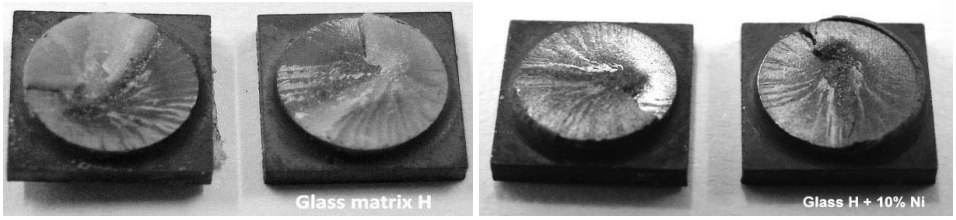

Fig. 59 Fracture of hour-glass samples after the torsion test measearument. All the composite sealants showed similar fracture patterns.

Table 16 Four-point electrical resistance measurements results for as joined and annealed samples

Sample	Thickness (cm)	Area (cm^2)	Measured glass resistance (Ω)	F10 corresponding glass resistance (Ω)	F10 Load resistance (Ω)	Current losses through the sealant (%)
Sandwich samples screen printing						
Glass 87 as joined	0.018	14	1.3	0.13	0.0074	6E-02
20%CGO1 as joined	0.024	14	963.4	128.45	0.0070	5E-05
10%CGO2 as joined	0.021	14	76.6	8.94	0.0070	8E-04
20%CGO2 as joined	0.023	14	704.7	90.05	0.0070	8E-05
10%Ni as joined	0.019	14	8.9	0.94	0.0071	7E-03
20%Ni as joined	0.027	14	853.7	128.06	0.0070	5E-05
10%NiCr as joined	0.019	14	5.8	0.61	0.0071	1E-02
Glass 87 aged	0.016	14	0.6	0.05	0.0081	1E-01
20%CGO1 aged	0.023	14	600.2	76.69	0.0070	9E-05
10%CGO2 aged	0.018	14	623.4	62.34	0.0070	1E-04
20%CGO2 aged	0.021	14	449.6	52.45	0.0070	1E-04
10%Ni aged	0.018	14	2.5	0.25	0.0072	3E-02
20%Ni aged	0.026	14	4.8	0.69	0.0071	1E-02
10%NiCr aged	0.02	14	7.7	0.86	0.0071	8E-03
Reproduction sandwich samples						
dispenser 87	0.0135	14	3700.3	277.52	0.0070	2E-05
screen print	0.01	14	748.8	41.60	0.0070	2E-04
dispenser 87 aged	0.135	14	1274.7	956.02	0.0070	7E-06
screen print aged	0.16	14	828.8	736.74	0.0070	9E-06
Sintered bars						
Glass 87 sintered	0.7	0.165	3.3E+06	152777.78	0.007	4E-08
Glass 87 aged	1	0.2	1.4E+05	11337.87	0.0070	6E-07
20 % Ni sintered	1.06	0.2	1.1E+04	934.74	0.0070	7E-06
20 % Ni aged	1	0.2	1.0E+05	7936.51	0.0070	9E-07

9. References

[Ash 1992] M.F. Ashby, Materials Selection in Mechanical Design (2nd edition) Pergamon Press, Oxford, 1992.

[ASM 2000] ASM International, ASM Specialty Handbook: Nickel, Cobalt and their alloys. Can be found at: www.asminternational.org/content/ASM/StoreFiles/ACFA9D7.pdf, 2000.

[Bah 1972] D. Bahat, Several metastable alkaline earth feldspar modifications, Journal of Materials Science **7** (1972) 198-201.

[Ban 1991] N.P. Bansal, M.J. Hyatt and C.H. Drummond III, Chaper 23. Crystallization and Properties of Sr-Ba Aluminosilicate Glass-Ceramic Matrices. *Ceram. Eng. Sci. Proc.* **12** (7–8) (1991) 1222-1234.

[Ban 1997] G. Banuprakash, V. Katyal, V.S.R. Murthy, G.S. Murty, Mechanical behavior of borosilicate glass-copper composites. Composites Part A 28A (1997) 861-867.

[Bea 2005] C.C. Beatty, Compliant glass-silver seals for SOFC applications. SOFC-IX, Proceedings - Electrochem. Soc., 2005.

[Ben 1979] D. Benjamin, Properties and selection: nonferrous alloys and pure metals. 9. ed. Metals-Park, OH, American Society for Metals, 1979.

[Ber 2004] E. Bernardo, G. Scarinci, A. Maddalena, D. Hreglich, Development and mechanical properties of metal-particulate glass matrix composites from recycled glasses. Composites Part A 35 (2004) 17-22.

[Bis 1980] D.R. Biswas, Strength and fracture toughness of indented glass-nickel compacts. Journal of Material Science 15 (1980) 1696-1700.

[Blu 2005] L. Blum, H.P. Buchkremer, S.M. Gross, L.G.J. de Haart, J. W. Quadakkers, U. Reisgen, R. Steinberger-Wilckens, R. W. Steinbrech, F. Tietz. Overview of the development of solid oxide fuel cells at

Forschungszentrum Juelich. SOFC-IX, Electrochemistry Society (2005) 39-47.

[Blu 2010] L. Blum, S.M. Gross, J. Malzbender, U. Pabst, M. Peksen, R. Peters, I. C. Vinke, Investigation of SOFC sealing behavior under stack relevant conditions at Forschungszentrum Jülich. Proceedings of 9th European Solid Oxide Fuel Cell Forum, Lucerne, 2010.

[Blu 2011] L. Blum, S. M. Groß, J. Malzbender, U. Pabst, M. Peksen, R. Peters, I. C. Vinke, Investigation of solid oxide fuel cell sealing behavior under stack relevant conditions at Forschungszentrum Jülich. Journal of Power Sources 196 (2011) 7175-7181.

[Blu 2012] L. Blum, B. de Haart, J. Malzbender, N. H. Menzler, J. Remmel, R. Steinberger-Wilckens, Recent Results in JÜLICH SOFC Technology Development. 10th European SOFC Forum, Lucerne 2012.

[Buc 2010] H. P. Buchkremer and R. Conradt, Durable sealing concepts with glass sealants or compression seals, Handbook of Fuel Cells – Fundamentals, Technology and Applications, Ed. by W. Vielstich, H. A. Gasteiger, A. Lamm and H. Yokokawa, 2010 John Wiley & Sons, Ltd. ISBN: 978-0-470-97400-1.

[Cha 2000] S.-Y. Chang, S.-J. Lin, M.C. Flemings, Thermal expansion behavior of silver matrix composites. Metallugical and materials transactions A 31 (1) (2000) 291-298.

[Cho 2002] Y.-S. Chou, J.W. Stevenson, L.A. Chick, Ultra-low leak rate of hybrid compressive mica seals for solid oxide fuel cells. Journal Power Sources 112 (2002) 130–136.

[Cho 2003a] Y.-S. Chou, J.W. Stevenson, Phlogopite mica-based compressive seals for solid oxide fuel cells: effect of mica thickness. Journal Power Sources 124 (2003) 473–478.

[Cho 2003b] Y.-S. Chou, J.W. Stevenson, Mid-term stability of novel mica-based compressive seals for solid oxide fuel cells. Journal Power Sources 115 (2003) 274–278.

[Cho 2003c] Y.-S. Chou, J.W. Stevenson, L.A. Chick, Novel silver/mica multilayer compressive seals for solid-oxide fuel cells: The effect of thermal cycling and material degradation on leak behavior. Journal of Materials Research 18 (2003) 2243–2250.

[Cho 2004] Y.-S. Chou, J.W. Stevenson, Novel infiltrated Phlogopite mica compressive seals for solid oxide fuel cells. Journal Power Sources 135 (2004) 72–78.

[Cho 2005] Y.-S. Chou, J.W. Stevenson, P. Singh, Thermal cycle stability of a novel glass–mica composite seal for solid oxide fuel cells: Effect of glass volume fraction and stresses. Journal Power Sources 152 (2005)168–174.

[Cho 2006] Y.-S. Chou, J.W. Stevenson, Compressive mica seals for solid oxide fuel cells. Journal of Materials Engineering and Performance 15 (4) (2006) 414-421.

[Cho 2007] Y.-S. Chou, J.W. Stevenson, R.N. Gow, Novel alkaline earth silicate sealing glass for SOFC Part II. Sealing and interfacial microstructure. Journal of Power Sources 170 (2007) 395-400.

[Cho 2007] Y.-S. Chou, J.W. Stevenson, R.N. Gow, Novel alkaline earth silicate sealaing glass for SOFC Part I. The effect of nickel oxide on the thermal and mechanical properties. Journal of Power Sources 168 (2007) 426-433.

[Cho 2008a] Y.-S. Chou, J.W. Stevenson, P. Singh, Effect of pre-oxidation and environmental aging on the seal strength of a novel high-temperature solid oxide fuel cell (SOFC) sealing glass with metallic interconnect. J. Power Sources 184 (2008) 238-244.

[Cho 2008b] Y.-S. Chou, J.W. Stevenson, P. Singh, Effect of aluminizing of Cr-containing ferritic alloys on the seal strength of a novel high-temperature solid oxide fuel cell sealing glass. J. Power Sources185 (2008) 1001-1008.

[Cho 2010] Y.-S. Chou. J.W. Stevenson, J.-P. Choi, Alkali effect on the electrical stability of a solid oxide fuel cell sealing glass. Journal of the electrochemical society, 157 (3) (2010) B348-B353.

[Cho 2012] Y.-S. Chou, E.C. Thomsen, J.-P- Choi, J.W. Stevenson, Compliant alkali silicate sealing glass for solid oxide fuel cell applications: The effect of protective YSZ coating on electrical stability in due environment. Journal of Power Sources 202 (2012) 149-156.

[Con 2005] R. Conradt, Glaskeramische Werkstoffe für Fügeschichten. DGM Seminar, Jülich, 2005.

[Con 2010] R. Conradt, Material Science Glass – Thermomechanical Properties and Fracture Mechanics. Lecture scripts, October 2010.

[Con 2011] R. Conradt, Glass-ceramic materials for joining layers for example the Jülich concept for high-temperature fuel cell - „Glaskeramische Werkstoffe für Fügeschichten dargestellt am Beispiel des Jülicher Konzepts für die Hochtemperatur-Brennstoffzelle“, Symposium “Glasig-kristalline Funktionswerkstoffe”, BAM, Berlin, 12.-13.05.2005, http://www.ghi.rwth-aachen.de/www/pages/glas/konferenzen/Paper%20SOFC%202004%20FZJ.pdf_ 2011.

[Cor 2008] E.L. Corral, B.D. Gauntt, R.E. Loehman, Properties of particle-filled glass composites used for sealing solid oxide fuel cells. Advances in Solid Oxide Fuel Cells III: Ceramic Engineering and Science Proceeding. 28 (4) (2008) 315-323.

[Cro 2010] *Crofer 22 APU*. Material Data Sheet No. 4146 January 2010 Edition, *ThyssenKrupp VDM*, 58778 *Werdohl*, *Germany*.

[DIN 1984] DIN 51730 1984-05: Prüfung fester Brennstoffe-Bestimmung des Asche-Schmelzverhaltens: Beuth Verlag, Berlin (1984).

[DIN 1998] DIN 51730:1998-04: Prüfung fester Brennstoffe-Bestimmung des Asche-Schmelzverhaltens: Beuth Verlag, Berlin (1998).

[Dlo 1997] Dlouhy, M. Reinisch, A. R. Boccaccini and J. F. Knott, Fracture characteristics of borosilicate glasses reinforced by metallic particles. Fatigue Fract. Eg. Mater. Struct. 20 (1997) 1235-1253.

[Don 1993] I.W. Donald, Preparation, properties and chemistry of glass- and glass-ceramic-to-metal seals and coatings. Journal of Materials Science 28 (1993) 2841-2886.

[Don 2000] I.W. Donald, P.M. Mallinson, B.L. Netcalfe, L.A. Gerrard and J.A. Fernie, Recent developments in the preparation, characterization and applications of glass- and glass-ceramic-to-metal seals and coatings. J. Mater. Sci. 46 (2011) 1975-2000.

[Don 2008] I.W. Donald, B.L. Netcalfe and L.A. Gerrard. Interfacial reactions in glass-ceramic-to-metal seals. J. Am. Ceram. Soc. 91 (3) (2008) 715-720.

[Dur 2000] Durschang B. R.: "Verwendung von alkalifreien Glaskeramiken als Fügenmaterial für den Hochtemperatureinsatz", DE 198 57 057 C1, (2000).

[Eag 1994] T.W. Eagar; W.A. Baeslack, R. Kapoor “Joining of Advanced Materials”, Encyclopedia of Advanced Materials, D. Bloor, M. Flemings, R. Brook, E. Mahajan, eds., Pergamon Press, Oxford, 1207, 1994.

[Fai 2012] D. Faidel, Laserstrahllöten mit glas-keramischen Zusatzwerkstoffen. PhD thesis, RWTH Aachen, Shaker Verlag 2012.

[Fer 1994] M. Ferraris, C. Badini, M. Montorsi, P. Appendino, H. W. Scholz, Joining of SiC_f/SiC compostes for thermonuclear fusion reactors. Journal of Nuclear Materials 212-215 (1994) 1613-1616.

[FEr 2005] J. W. Fergus, Sealants for solid oxide fuel cells. J. Power Sources 147 (1-2) (2005) 46-57.

[Fer 2008] M. Ferraris, M. Salvo, V. Casalegno, A. Ciampichetti, F. Smeacetto, M. Zucchetti, Joining of machined SiC/Sic composites for thermonuclear fusion reactors. Journal of Nuclear Materials 375 (2008) 410-415.

[Fer 2012a] M. Ferraris, M. Salvo, V. Casalegno, M. Avalle, A. Ventrella, *Torsion tests on AV119 epoxy - joined SiC.* International journal of applied ceramic technology, 4 (9) (2012) 795-807.

[Fer 2012b] M. Ferraris, M. Salvo, S. Rizzo, V. Casalegno, S. Han, A. Ventrella, T. Hinoki, Y. Katoh, *Torsional Shear Strength of Silicon CarbideComponents Pressurelessly Joined by a Glass-Ceramic.* International journal of applied ceramic technology, 4 (9) (2012) 786-794.

[Fue 2013] Fuel Cells Materials, CGO prices. [Online] 2013 Available: http://www.fuelcellmaterials.com/site/powders-and-pastes

[Ful 1925] G. S. Fulcher, Analysis of recent measurements of the viscosity of glasses, J. Am. Ceram. Soc. **8**, 1925, 339–355.

[Gea 2001] P. Geasee, T. Schwickert, U. Diekmann, R. Conradt, in: J.G. Heinrich, F. Aldinger (Eds.), Ceramic Materials and Components for Engines, Wiley-VCH Verlag GmbH, Weinheim, Germany, 2001, pp. 57–62.

[Gea 2003] P. Geasee, Development of crystallizing glass sealants for high temperature planar solid oxide fuel cells. Dissertation, RWTH Aachen University, 2003.

[Gro 2005] S.M. Gross, T. Koppitz, J. Remmel, U. Reisgen, V. Verlotski, R. Conradt, Glass-Ceramic Composite as a new sealing material for SOFCs. Electrochemical Society Proceedings 7 (2005) 1924-1934.

[Gro 2006] S.M. Gross, T. Koppitz, J. Remmel, J. B. Bouche and U. Reisgen, Joining properties of a composite glass-ceramic sealant, Fuel Cells Bulletin, Sep. 2006, 12 -15.

[Gro 2007] S.M. Gross and U. Reisgen, Glass soldering - a demanding joining technique not only for the high-temperature fuel cell - „Glaslöten – eine anspruchsvolle Fügetechnik nicht nur für die Hochtemperatur-Brennstoffzelle“, Schweißen und Schneiden, 2, 2007, 70–77.

[Gro 2010] S.M. Gross, D. Federmann, J. Remmel, M. Pap, Ceramic Fiber Reinforcement of glass-ceramic sealants, 10th ESG Conference Magdeburg, Germany, 2010.

[Gro 2011] S.M. Gross, D. Federmann, J. Remmel, and M. Pap, Reinforced Composite Sealants for SOFC applications, J. of Power Sources, 196, 2011, 7338– 7342.

[Haa 2005] V.A.C. Haanappel, V. Shemet, S.M. Gross, Th. Koppitz, N.H. Menzler, M. Zahid, W.J. Quadakkers, Behaviour of various glass–ceramic sealants with ferritic steels under simulated SOFC stack conditions. Journal of Power Sources 150 (2005) 86–100.

[Has 1970] D.P.H. Hasselman, R.M. Fulrath, Proposed fracture theory of a dispersion-strengthened glass matrix. Journal of the American ceramic society 49 (2) (1970) 68-72.

[Hat 2010] J. Hatcher, M. J. Pascual, D. Poulidi, I. S. Metcalfe, Development and testing of an intermediate temperature glass sealant for use in mixed ionic and electronic conducting membrane reactor. Solid State Ionics 181 (15–16) (2010) 767–774.

[Hay 2000] H. Hayashi, M. Kanoh, C. J. Quan, H. Inaba, S. Wang, M. Dokiya, H. Tagawa, Thermal expansion of Gd-doped ceria and reduced ceria. Solid State Ionics 132 (3–4) (2000) 227–233.

[Her 1991] L. Hermansson, Organics removal. Engineered Materials Handbook Volume 4 – Ceramics and Glasses. 1991, 134-140.

[Hla 1996] V. Hlavacek, J.A. Puszynski, Chemical Engineering Aspects of Advanced Ceramic Materials. Ind. Eng. Chem. Res. 35 (1996) 349-377.

[Hus 2003] S. Hussain, I. Barbariol, S. Roitti, O. Sbaizero, Electrical conductivity of an insulator matrix (alumina) and conductor particle (molybdenum) composites. Journal of the European Ceramic Society 23 (2) (2003) 315-321.

[Hut 1989] J. W. Hutchinson, Mechanism of toughening ceramics. Theoretical and applied Mechanics (1989) 139-144.

[Ima 2005] Y. Imanaka, Multilayered Low Temperature Cofired Ceramics (LTCC) Technology. Springer, 2005.

[Kim 2005] J.Y. Kim, J.S. Hardy, K.S. Weil, Silver-copper oxide based reactive air braze for joining yttria-stabilized zirconia. Journal of Materials Research 20 (3) (2005) 636-643.

[Krs 1981] V.V. Krstic, P.S. Nicholson, R.G. Hoagland, Toughening of glasses by metallic particles. Journal of American Ceramic society 64 (9) (1981) 499-504.

[Lah 2000] N. Lahl, K. Singh, L. Singheiser, K. Hilpert, D. Bahadur, Crystallisation kinetics in ao-Al_2O_3-SiO_2-B_2O_3 Glasses (a = Ba, Ca, Mg). Journal of materials science 35 (2000) 3089-3096.

[Lar 2004] C. Lara, M. J. Pascual**,** M. O. Prado and A. Durán: Sintering of glasses in the system RO–Al_2O_3–BaO–SiO_2 (R=Ca, Mg, Zn) studied by hot-stage microscopy. Solid State Ionics 170 (3-4) (2004) 201-208.

[Le 2006] S. Le, K. Sun, N. Zhang, M. An, D. Zhou, J. Zhang, D. Li, Novel compressive seals for solid oxide fuel cells. Journal of Power Sources 161 (2006) 901-906.

[Le 2007] S Le, K Sun, N Zhang, Y Shao, M An, Q Fu, X. Zhu, Comparison of infiltrated ceramic fiber paper and mica base compressive seals for planar solid oxide fuel cells. Journal of Power Sources 168 (2007) 447-452.

[Les 2007] P. A. Lessing, A review of sealing technologies applicable to solid oxide electrolysis cells. Journal of Material Science 42 (2007) 3465-3476.

[Ley 1996] L. Ley, M. Krumpelt, R. Kumar, JH Meiser, I. Bloom, Glass-Ceramic Sealants for Solid Oxide Fuel Cells: Part I. Physical Properties. Journal of Materials Research 11 (6) (1996) 1489-1493.

[Lin 2008] H.-W. Lin, C.-P. Chang, W.-H. Hwu, M.-D. Ger, The rheological behaviors of screen-printing pastes. Journal of Materials Processing Technology 197 (1–3) (2008), 284-291.

[Lin 2012] C.-K. Lin, J-Y. Chen, J.-W. Tian, L.-K. Chiang, and S.-H. Wu. Joint strength of a solid oxide fuel cell glass-ceramic sealant with metallic interconnect. Journal of Power Sources 205 (2012) 307-317.

[Lip 1994] P. Lipetzky, and S. Schmauder, Crack-particle interaction in two-phase composites Part I: Particle shape effects. International Journal of Fracture 65 (1994) 345-358.

[Lip 1995] P. Lipetzky, and Z. Knesl, Crack-particle interaction in a two-phase composite Part II: crack deflection. International Journal of Fracture 73 (1995) 81-92.

[Liu 2011] W.N. Liu, X. Sun, B. Koeppel, E. Stephens, M.A. Khaleel, Creep behavior of glass/ceramic sealant and its effect on long-term performance of solid oxide fuel cells. Int. J. Appl. Ceram. Technol., 8 (1) (2011) 49-59.

[Mah 2008] M.K. Mahapatra, K. Lu, Effects of nickel on network structure and thermal properties of a new solid oxide cell seal glass. Journal of Power Sources 185 (2008) 993-1000.

[Mah 2010] M.K. Mahapatra, K. Lu, Thermochemical compatibility of a seal glass with different solid oxide cell components. International Journal of Applied Ceramic Technology 7 (1) (2010) 10-21.

[Mah 2010a] M.K. Mahapatra and K. Lu, Seal glass for solid oxide fuel cells. Journal Power Sources 195 (21) (2010) 7129-7139.

[Mah 2010b] M.K. Mahapatra and K. Lu, Glass-based seals for solid oxide fuel and electrolyzer cells- A Review. Materials Science and Engineering R 67 (2010) 65-85.

[Mal 2007a] J. Malzbender, R.W. Steinbrech, Advanced measurement techniques to characterize thermo-mechanical aspects of solid oxide fuel cells. Journal of Power Sources 173 (2007) 60-67.

[Mal 2007b] J. Malzbender, J. Mönch, R.W. Steinbrech, T. Koppitz, S.M. Gross, J. Remmel, Symmetric shear test of glass-ceramic sealants at SOFC operation. Journal of Materials Science 42 (2007) 6297-6301.

[Mal 2008] S. Mallik, M. Schmidt, R. Bauer and N.N. Ekere, Influence of Solder Paste Components on Rheological Behaviour. 2nd Electronics Systemintegration Technology Conference, Greenwich, UK, 2008.

[Mal 2009] J. Malzbender, R.W. Steinbrech, E. Wessel, Brittle fracture studies of solid oxide fuel cells. Key engineering materials 409 (2009) 81-93.

[Mal 2012a] J. Malzbender, Y. Zhao, Micromechanical testing of glass-ceramic sealants for solid oxide fuel cells. Journal of Materials Science 47 (2012) 4342-4347.

[Mal 2012b] J. Malzbender, Y. Zhao, Flexural strength and viscosity of glass ceramic sealants for solid oxide fuel cell stacks. Fuel Cells 12 (1) (2012) 47-53.

[Mat 2012] Matbase, Material properties database [Online] 2012 Available: http://www.matbase.com/

[Mes 1995] R. W. Messler, Jr. The challenges for joining to keep pace with advancing materials and designs. Materials & Design 16 (5) (1995) 261-269.

[Moo 1987] R.H. Moore, S.C. Kunz, Metal Particle-Toughened Borosilicate Sealing Glass. Ceramic Engineering and Science Proceedings 8 (7-8) (1987) 839-847.

[Mor 2007] A. B. Morgan, Polymer-clay nanocomposites: design and application of multi-functional materials. Material Matters, 2 (1) (2007) 20-26.

[Mor 2010] M. Morales, J.J. Roa, X. G. Capdevilla, M. Segarra, S. Pinol, Mechanical properties at the nanometer scale of GDC and YSZ used as electrolytes for solid oxide fuel cells. Acta Materialia 58 (2010) 2504-2509

[Nan 2012] Nanodynamics, GDC price in November 2012 [Online] Available: http://www.yourcompanyshop.com/nano/catalog/default.aspx?lid=236&ProductTypeIdent=204

[Ner 1899] W. Nernst, Electrolytic conduction through the solid body at very high temperatures - „Über die Elektrolytische Leitung fester Köper bei sehr hohen Temperaturen“: Z. Elektrochem., 6, 1899, 41-43.

[Nie 2007] K.A. Nielsen, M. Solvang, S.B.L. Nielsen, A.R. Dinesen, D. Beeaff, P.H. Larsen, Glass composite seals for SOFC application. Journal of the European Ceramic Society 27 (2007) 1817-1822.

[Nie 2008] K. A. Nielsen, M. Solvang, S. B. L. Nielsen, D. Beeaff, Mechanical Behaviour of Glassy Composite Seals for IT-SOFC Application. Advances in Solid Oxide Fuel Cells II: Ceramic engineering and science proceedings 27 (4) (2008) 315-323.

[Nix 1941] F.C. Nix and D. Macnair, The thermal expansion of pure metals: copper, gold, aluminum, nickel and iron. Physical Review 60 (1941) 597-605.

[PAb 1997] A. De Pablos, A. Durán, and M. I. Nieto: *Adjusting of laboratory filature furnace for obtaining fiber glass*: Bol. Soc. Esp. Ceram. Vdr., 1997, **36** (5), 517 – 23.

[Pab 2013] U. Pabst, F 13001-P1 Rechnerische Untersuchung und Optimierung von Glaslot-Zugproben. Forschungszentrum Jülich, ZEA-1-KSA internal report, 2013.

[Pas 2001] M. J. Pascual, L. Pascual, A. Durán, Determination of the viscosity temperature curve for glasses on the basis of fixed viscosity points

determined by hot stage microscopy. Physics and Chemistry of Glasses 42 (1) (2001) 61-6.

[Pas 2005] M. J. Pascual and A. Durán, A new method for determining fixed viscosity points of Glasses. . Physics and Chemistry of Glasses 46 (5) (2005) 512-520.

[Pas 2007] M.J. Pascual, A. Guillet, A. Durán, Optimization of glass–ceramic sealant compositions in the system MgO–BaO–SiO2 for solid oxide fuel cells (SOFC). *Journal of Power Sources* 169 (2007) 40-46.

[Pay 2000] J.C. Payao, W. Schmidt, G. Schroeder, *Fundamentos de ensaio de vazamento e estanqueidade*. Forschungszentrum Juelich GmbH, Germany, 2000.

[Qi 2001] X. Qi, F.T. Akin, Y.S. Lin, Ceramic-glass composite high temperature seals for ionic-conducting ceramic membranes. Journal of Membrane Science 193 (2001) 185-193.

[Qui 1991] G. D. Quinn, Strength and Proof Testing. Engineered Materials Handbook vol. 4 Ceramics and Glasses, ASM International, USA (1991) 493-501.

[Rhe 2003] H. Rhee, K.N. Subramanian, A. Lee, J.G. Lee, Mechanical characterization of Sn-3.5Ag solder joints at various temperatures. Soldering & surface mount technology 15 (3) (2003) 21-26.

[Ric 2004] B. Riccardi, L. Giancarli, A. Hasegawa, Y. Katoh, A. Kahyama, R. H. Jones, L.L. Snead, Issues and advances in SiC_f/SiC composites development for fusion reactors. Journal of Nuclear Materials 329-333 (2004) 56-65.

[Rou 1999] M. Roulin, J. W. Luster, G. Karad En Iz, A. Mortensen, Strength and Structure of furnace-brazed joints between aluminum and stainless steel. Welding Research Supplement May (1999) 151-155.

[Sch 1962] H. Scholze, Influence of viscosity and surface tension on hot-stage microscopy measurements on glasses. Ver. Deutsche Keramische Gesellschaft 391 (1962) 63-8.

[Sch 1990] Scholze H.: "Glass, nature, structure and properties", translated by Lakin M. J., Springer-Verlag, Berlin, (1990).

[Sch 2002a] T. Schwickert, R. Sievering, P. Geasee and R. Conradt, Glass-ceramic materials as sealants for SOFC applications. Materialwissenschaft und Werkstofftechnik 33 (2002) 363-366.

[Sch 2002b] T. Schwickert, Fügen von Hochtemperatur-Brennstoffzellen. Dissertation RWTH Aachen, 2002.

[Set 1968] M.A. Stett, R.M. Fulrath, Strengthening by Chemical Bonding in Brittle Matrix Composite. Journal of the American Ceramic Society – Discussions and Notes 51 (10) (1968) 599-600.

[Sig 2012] Sigma Aldrich, Nano Minerals: Nanoclays. [Online] 2012 Available: http://www.sigmaaldrich.com/materials-science/nanomaterials/nanoclay-building.html

[Sme 2008a] F. Smeacetto, M. Salvo, M. Ferraris, J. Cho, A.R. Boccaccini, Glass-ceramic seal to join Crofer22APU alloy to YSZ ceramic in planar SOFCs. Journal of the European Ceramic Society 28 (2008) 61-68.

[Sme 2008b] F. Smeacetto, M. Salvo, M. Ferraris, V. Casalegno, P. Asinari, **A**. Chrysanthou, Characterization and performance of glass–ceramic sealant to join metallic interconnects to YSZ and anode-supported-electrolyte in planar SOFCs. Journal of the European Ceramic Society 28 (2008) 2521-2527.

[Sme 2010] F. Smeacetto, M. Salvo, F.D. D'Hérin Bytner, P. Leone, M. Ferraris, New glass and glass-ceramic sealants for planar solid oxide fuel cells. Journal of the European Ceramic Society 30 (2010) 933-940.

[Sri 1995] S. Sridharan, and M. Tomozawa, Toughening of glass-ceramics by both transformable and transformed zirconia. Journal of Non-Crystalline Solids 182 (1995) 262-270.

[Ste 1968] M.A. Stett, R.M. Fulrath, Strengthening by chemical bonding in brittle matrix composite. Journal of American Ceramic Society 51 (10) (1968) 599-600.

[Ste 2001] B. C. H. Steele and A. Heinzel, Materials for fuel-cell technologies. Nature, 414, 2001, 345-352.

[STe 2003] Steinberger-Wilckens R., de Haart L.G.J., Vinke I.C., Blum L., Cramer A., Remmel J., Blass G., Tietz F., Quadakkers W.J.. Recent results of stack development at Forschungszentrum Jülich. SOFC-VIII, Electrochemistry Society (2003) 98-104.

[Tam 1925] G. Tammann, Glasses as supercooled liquids. Journal of the Society of Glass Technology 9 (1925) 166-185.

[Tax 2013] Tax Free Gold, Silver live price. [Online] 2013 Available: http://www.taxfreegold.co.uk/preciousmetalpriceseuros.html

[Thy 2013] Thyssenkrupp, NiCr (80-20) prices. [Online] 2013 Available: http://www.thyssenkrupp-vdm.com/en/services/metal-surcharges/

[Tie 1999] F. Tietz, Thermal expansion of SOFC materials. Ionics 5 (1999) 129-139.

[Uhl 1983] Uhlmann D. R. and Kreidl N. J.: "Glass: Science and technology, vol. 1. Glass-forming systems", Academic press, London, (1983).

[Voe 1921] H. Vogel, Temperaturabhängigkeit der Viskosität von Flüssigkeiten. Zeitschrift für Physik 22 (1921) 645-646.

[Voe 1992] Vogel W.: "Glaschemie", 3 Auflage, Springer Verlag, Berlin, 1992.

[Wan 2007] E. Wanko, S. Groß, T. Koppitz, J. Remmel, U. Reisgen, W. Willsmann and R. Conradt, Glass-ceramic materials of the system Ba-MgO-SiO2 used as

sealant for solid oxide fuel cell (SOFC). Löt 2007 DVS Band, DVS Berichte 243 (1) (2007) 130-134.

[Wan 2010] E. Wanko, Entwincklung eines neuen Konzepts zur Steuerung der thermischen Ausdehnung von glaskeramischen Verbundwerkstoffen mit angepasster Fließfähigkeit am Beispiel der Hochtemperatur-Brennstoffzelle. Dissertation, RWTH Aachen University, 2010.

[Wei 2004] K.S. Weil, J.E. Deibler, J.S. Hardy, D.S. Kim, G.-G. Xia, L.A. Chick, C.A. Coyle, Rupture testing as a tool for developing planar solid oxide fuel cell seals. Journal of Materials Engineering and Performance **13** (3) (2004), pp. 316–326.

[Wei 2006] K. S. Weil, The State-of-the-Art in Sealing Technology for Solid Oxide Fuel Cells, J. of Minerals, 2006, 37-44.

[Wsj 2013] The Wall Street Journal, London Metal Exchange Price. [Online] 2013 Available: http://online.wsj.com/mdc/public/page/2_3021-londMetal.html

[Yeo 2008] J. A. Yeomans, Ductile particle ceramic matrix composites – Scientific curiosities or engineering materials?. Journal of the European Ceramic Society 28 (2008) 1543-1550.

[Zha 2009] T. Zhang, Q. Zhu and Z. Xie, Modeling of cracking of the glass-based seals for solid oxide fuel cell. Journal of Power Sources 188 (2009) 177-183.

[ZHa 2011] Y. Zhao, J. Malzbender, and S.M. Gross, The effect of room temperature and high temperature exposure on the elastic modulus, hardness and fracture toughness of glass ceramic sealants for solid oxide fuel cells. Journal of the European Ceramic Society 31 (2011) 541-548.

Band / Volume 241
Spannungsinduziertes Versagen in Hochtemperaturschichtsystemen
C. Nordhorn (2014), v, 118 pp
ISBN: 978-3-95806-016-6

Band / Volume 242
Änderungsdetektion digitaler Fernerkundungsdaten mittels objekt-basierter Bildanalyse
C. Listner (2014), 176 pp
ISBN: 978-3-95806-017-3

Band / Volume 243
Räumlich hoch aufgelöste Modellierung des Spaltproduktverhaltens in einem HTR-Core mit kugelförmigen oder prismatischen Brennelementen
A. Xhonneux (2014), viii, 239 pp
ISBN: 978-3-95806-020-3

Band / Volume 244
Effects of Cercospora leaf spot disease on sugar beet genotypes with contrasting disease susceptibility
S. Schmittgen (2015), 121 pp
ISBN: 978-3-95806-021-0

Band / Volume 245
Light scattering and trapping in thin film silicon solar cells with an n-i-p configuration
W. Böttler (2015), 132 pp
ISBN: 978-3-95806-023-4

Band / Volume 246
Nanostructured Si-alloys for silicon solar cells
K. Ding (2015), 210 pp
ISBN: 978-3-95806-024-1

Band / Volume 247
Electrochemical Texturing and Deposition of Transparent Conductive Oxide Layers for the Application in Silicon Thin-Film Solar Cells
J.-P. Becker (2015), ix, 156, XXIV pp
ISBN: 978-3-95806-027-2

Band / Volume 248
Stoffliche Charakterisierung radioaktiver Abfallprodukte durch ein Multi-Element-Analyseverfahren basierend auf der instrumentellen Neutronen-Aktivierungs-Analyse – MEDINA –
A. W. Havenith (2015), 311 pp
ISBN: 978-3-95806-033-3

Band / Volume 249
Quantitative Two-Layer Inversion and Customizable Sensor-Array Instrument for Electromagnetic Induction based Soil Conductivity Estimation
A. T. Mester (2015), viii, 119 pp
ISBN: 978-3-95806-035-7

Band / Volume 250
Partial Neutron Capture Cross Sections of Actinides using Cold Neutron Prompt Gamma Activation Analysis
C. Genreith (2015), vii, 166, XXXII pp
ISBN: 978-3-95806-036-4

Band / Volume 251
Long Term Aerosol Composition Measurements at the CESAR Tower at Cabauw, NL
P. Schlag (2015), iii, 228 pp
ISBN: 978-3-95806-037-1

Band / Volume 252
Modellbasierte Spezifikationsmethodik zur effizienten Systementwicklung von Brennstoffzellenantrieben
R. Biurrun Sotelo (2015), 255 pp
ISBN: 978-3-95806-038-8

Band / Volume 253
Three-dimensional ray-tracing simulations of convective gravity waves
S. Kalisch (2015), iii, 183 pp
ISBN: 978-3-95806-040-1

Band / Volume 254
First-Principles Study on Pyrites and Marcasites for Photovoltaic Application
T. Schena (2015), 206 pp
ISBN: 978-3-95806-041-8

Band / Volume 255
Glass-Ceramic Sealant Reinforcement for High-Temperature Applications
B. Cela Greven (2015), xi, 119 pp
ISBN: 978-3-95806-042-5

Energie & Umwelt /
Energy & Environment
Band / Volume 255
ISBN 978-3-95806-042-5